Isoform specific function of the metastatic formin FMNL2

Christine Péladeau

A Thesis submitted to the

Faculty of Graduate and Postdoctoral Studies

In partial fulfillment of the requirements for the

MSc degree in Cellular and Molecular Medicine

Cellular and Molecular Medicine

Faculty of Medicine

University of Ottawa

© Christine Péladeau, Ottawa, Canada 2013

Table of Contents

Table of Contents ..... **ii**
List of Tables ..... **iv**
List of figures ..... **v**
List of Abbreviations ..... **vi**
Abstract ..... **viii**
Acknowledgements ..... **ix**
Introduction **1**
1.1 Cancer and metastasis 2
1.2 Modes of single cell metastatic invasion 4
1.3 The cytoskeleton 5
1.4 Actin dynamics 7
1.5 Actin binding proteins 8
1.5.1 Profilin, Thymosin and ADF/cofilin 8
1.5.2 Capping proteins 9
1.5.3 Ena/VASP 9
1.5.4 Cross-linking proteins 10
1.6 Rho-GTPase and effectors 11
1.7 Actin drives cell motility 12
1.7.1 Filopodia formation 13
1.7.2 Lamellipodia formation 16
1.7.3 Stress fiber formation 17
1.7.4 Invadopodia formation 18
1.7.5 Plasma membrane blebbing 21
1.8 Formin Homology Domain Proteins 24
1.8.1 Formins and microtubule dynamics 30
1.9 FMNL2 31
1.9.1 Role of FMNL2 in invasion and metastasis 31
1.9.2 FMNL2 protein 32
1.9.3 FMNL2 isoforms 37
1.10 Hypothesis 40
Material and Methods **41**
2.1 Cell culture 42
2.2 RNA extraction 43
2.3 cDNA preparation 44

2.4 RT-PCR analysis....44
2.5 Cloning....45
2.6 Real-time PCR (qPCR)....49
2.7 Immunofluorescence....50
2.8 Serum Response Factor (SRF) assay....52
2.9 Western blotting....53
2.10 FMNL2 knockdown....54
2.11 Migration assay....55
2.12 Virus production....56
2.13 FMNL2 rescue assay....56
2.14 Transwell invasion assay....57
Results....61
3.1 Identification of four FMNL2 isoforms in SW620, SW480 and A375 cancer cell lines....62
3.2 FMNL2 TQS isoform is highly expressed in invasive human cancer cell-lines....67
3.3 Full length FMNL2 splice variants localize at the plasma membrane....71
3.4 Active derivatives of FMNL2 isoforms induce stress fiber formation....76
3.5 FMNL2 isoforms differ in activity and regulation....76
3.6 FMNL2 knockdown, rescue and overexpression affects A375 melanoma cell morphology....79
3.7 FMNL2 knockdown inhibits A375 melanoma cell migration....89
3.8 FMNL2 knockdown reduces melanoma amoeboid style invasion....89
3.9 FMNL2 isoforms rescue and potentiate A375 melanoma cell amoeboid style invasion....92
Discussion....100
4.1 Depletion of FMNL2 in melanoma cell lines inhibits amoeboid style motility....101
4.2 FMNL2 splice variants....102
4.2.1 FMNL2 TQS is preferentially expressed in invasive cancer cell lines....102
4.3 Functional characterisation of FMNL2 isoforms....104
4.3.1 FMNL2 isoforms vary in their regulation and activity....104
4.3.2 Full length FMNL2 splice variants localize to the plasma membrane....107
4.4. FMNL2 isoforms effect on cell motility....108
4.4.1 FMNL2 knockdown and overexpression affects A375 melanoma cell morphology....108
4.4.2 FMNL2 TQS drives plasma membrane extension....109
4.4.3 FMNL2 isoforms rescue and potentiate A375 melanoma cell amoeboid style invasion....110
4.5 Future directions....113
4.6 Conclusion....114
Appendices....115
References....118

List of Tables

Chapter 2: Material and Methods

Table 2.1: Cell lines used in this thesis. 42
Table 2.2: Primers produced for cancer cell line RT-PCR analysis. 45
Table 2.3: Primers created for the assembly of FMNL2 FL pEF-Plink2 cherry constructs. 48
Table 2.4: Primers produced for qPCR analysis. 49
Table 2.5: Antibodies used for immunofluorescence assays. 52
Table 2.6: Duplex sequences generated by Integrated DNA Technologies for knockdown assay 55

Chapter 3: Results

Table 3.1: Human cell lines for qPCR analysis 68

Appendices:

Table 5.1: FMNL2 constructs generated for the different experiments in this work. 115
Table 5.2: FMNL2 isoform derivative constructs generated for our collaborator (Dr. Higgs). 117

List of figures

Chapter 1: Introduction

Figure 1.1: Actin dynamics throughout lamellipodia and filopodia formation 14
Figure 1.2: Actin dynamics during invadopodia formation 19
Figure 1.3: Actin dynamics throughout plasma membrane blebbing 22
Figure 1.4: Schematic of the fifteen Human Formin Homology Proteins 25
Figure 1.5: FH2 dimerization and activity 27
Figure 1.6: FMNL2 is regulated by autoinhibition 33
Figure 1.7: FMNL proteins are myristoylated at their N-terminal domain 35
Figure 1.8: FMNL2 predicted splice variants 38

Chapter 2: Material and Methods

Figure 2.1: Full length FMNL2 isoform cloning 46
Figure 2.2: Inverse transwell invasion assay 59

Chapter 3: Results

Figure 3.1: RT-PCR analysis of FMNL2 isoform expression in SW480, SW620 CRC cells and A375 melanoma cells 63
Figure 3.2: FMNL2 isoform sequence alignment 65
Figure 3.3: Up regulation of FMNL2 in different cell lines 69
Figure 3.4: N-terminal tags on FMNL2 interfere with membrane targeting 72
Figure 3.5: Subcellular localization of FMNL2 isoforms 74
Figure 3.6: Stress fiber induction by C-terminal derivatives of FMNL2 isoforms 77
Figure 3.7: FMNL2 TQS is a potent activator of the SRF pathway 80
Figure 3.8: C-terminal derivatives of FMNL2 isoforms induce microtubule acetylation 82
Figure 3.9: FMNL2 knockdown affects A375 melanoma cell morphology 85
Figure 3.10: FMNL2 rescue and overexpression affects A375 melanoma cell morphology 87
Figure 3.11: FMNL2 knockdown inhibits A375 melanoma cell migration 90
Figure 3.12: FMNL2 knockdown decreases WM266.4 melanoma amoeboid style invasion 93
Figure 3.13: FMNL2 knockdown decreases A375 melanoma amoeboid style invasion 95
Figure 3.14: FMNL2 isoforms rescue and potentiate A375 invasion 97

Appendix 2

Figure 5.1: FMNL2 expression levels in A375 melanoma cells after knockdown, rescue and overexpression 116

List of Abbreviations

AA.....Amino acid
ADP..... Adenosine diphosphate
ATP.....Adenosine triphosphate
CA..... Constitutively active
CPRG.....Chlorophenol red-β-D-galactopyranoside
CRC.....Colorectal cancer
CSK.....Cytoskeletal
Ct.....Threshold cycle
DAAM ..... Dishevelled-associated activator of morphogenesis
DAD.....Diaphanous Autoinhibitory Domain
DAPI ..... 4’,6-diamidino-2-phenylindole
DBS..... Donor Bovine Serum
Dia.....Diaphanous
DD.....Dimerization Domain
DID .....Diaphanous Inhibitory Domain
DMEM .....Dulbecco’s Modified Eagle Medium
DRF.....Diaphanous-related Formin
ECM.....Extracellular matrix
EMEM..... Eagle's Minimum Essential Medium
EMT .....Epithelial-mesenchymal transition
Ena/VASP ..... Enabled/vasodilator-stimulated phosphoproteins
F-actin ..... Filamentous actin
FMN.....Formin
FMNL1 ..... Formin-like-1
FMNL2 ..... Formin-like-2
FMNL3 ..... Formin-like-3
FBS .....Fetal Bovine Serum
FH1 .....Formin Homology 1
FH2 .....Formin Homology 2
FHOD..... Formin homology domain-containing protein
G-actin.....Globular actin
GAP.....GTPase activating protein
GBD ..... GTPase Binding Domain
GDP..... Guanosine diphosphate
GEF.....Guanine nucleotide exchange factor
GTP.....Guanosine triphosphate
HRP.....Horseradish-peroxidase
INF ..... Inverted formin

IRES ..... Internal Ribosome Entry Site
L-15 ..... Leibovitz's L-15 Medium
MET ..... Mesenchymal to epithelial transition
MLC ..... Myosin regulatory light chain
MT1-MMP ..... Membrane type 1 metalloprotease
MTOC ..... Microtubule-organizing center
N.S ..... No significant differences
PAK ..... p21-activated kinases
PBS ..... Phosphate Buffered Saline
PDZ Psd-95/Dlg/Zo-1
PEI ..... Polyethylenimine
PFA ..... Paraformaldehyde
PI ..... Propidium Iodide
qPCR ..... Real-time polymerase chain reaction
ROCK ..... Rho-associated coiled-coil-forming kinases
RT-PCR ..... Reverse transcription polymerase chain reaction
SH3 ..... Src homology 3
SRF ..... Serum Response Factor
TEV ..... Tobacco Etch Virus
UTR ..... Untranslated region
WASP ..... Wiskott–Aldrich syndrome protein
WAVE ..... Wiskott-Aldrich syndrome protein family verprolin-homologous protein
WH2 ..... WASP Homology two

Abstract

Cancer cell metastasis is induced by actin-dependent cell migration and is affected by cytoskeletal remodelling proteins. FMNL2 is one such protein which promotes colorectal cancer (CRC) cell metastasis and amoeboid style invasion of melanoma cells. FMNL2 mRNA is subject to alternative splicing and studies suggest that the resulting encoded proteins are likely to differ in their regulation, subcellular localization and activity. We identified four FMNL2 isoforms (ITM, YHY, PMR and TQS) expressed in non-invasive (SW480) and invasive (SW620) CRC cells, as well as in highly invasive A375 amoeboid melanoma cells. qPCR data suggests that an "invasive" isoform (TQS) may be preferentially expressed in highly invasive and amoeboid cell lines. Boyden chamber invasion assay results show that FMNL2 knockdown inhibits amoeboid style invasion in two melanoma cell lines and that TQS is the most efficient isoform at rescuing the invasive phenotype. This study provides a further understanding of FMNL2's role in invasion and metastasis and identifies specific targets for the development of future antimetastatic therapies.

Acknowledgements

I wish to address my sincere thanks to all the people who have contributed to the realisation of this work:

I would like to start by thanking my supervisor Dr. John Copeland for his guidance, for sharing his knowledge with me and giving me the opportunity to work in his laboratory. To my committee members: Dr. Stephen Lee and Dr. Jonathan Lee for their input all through my project.

I would like to thank Chelsea Smallwood as well as Sarah Copeland for training me as well as giving me all the tools that I needed to succeed throughout this journey. A big thank you to Maria Ma and Gabriela Lahaie for their constant help and companionship. A special thanks to Allan Heibein for answering my countless questions and for the helping hand. To Raed Hanania for the microscopy training and assistance throughout my final experiments and to Dr. Trinkle-Mulcahy for helping me with the protrusion assay. In addition, I would like to thank Wojciech Kulacz, Christine Tenneson and Caroline Beauregard for their friendship while working alongside me in the lab. I could not have asked for better coworkers.

To the fellow laboratories: Laura Trinkle-Mulcahy lab, S. Lee lab and Jasmin lab. Thank you for the equipment, for the much needed materials as well as the useful comments and advice. A special thanks to Gabriel Lachance for the words of encouragement and friendship.

Finally, I would like to dedicate this thesis to my parents and my sister for their patience and support throughout the ups and downs of my studies. I could not have done it without you. I am grateful for all my friends, especially Stephane Laviolette, Robert Bennett and Isabelle Strickland for their support and encouragement along the way.

Chapter 1

Introduction

1.0 Introduction

Metastasis and invasion of tumor cells are key hallmarks of cancer and are the primary cause of cancer-related deaths (Hanahan and Weinberg 2000; 2011). Metastasis, by definition, is a cell motility driven process that requires cytoskeletal remodeling and regulation of actin dynamics. To better comprehend this process, it is important to understand the mechanisms driving motility as well as the actin-binding proteins regulating this process.

Formins are a significant class of Rho GTPase effector proteins which govern actin cytoskeletal dynamics and are thought to drive malignant cell motility (Kitzing *et al.* 2007; DeWard *et al.* 2010; Nürnberg *et al.* 2011; Hager *et al.* 2012). Formin-like 2 (FMNL2), is highly expressed in a variety of cancer cell lines and can drive metastasis as well as amoeboid invasion *in vivo* (Kitzing *et al.* 2007; Parsons *et al.* 2008; Zhu *et al.* 2011). Alternative splicing of the FMNL2 mRNA results in proteins that vary at the C-terminus, a region thought to govern FMNL2 activity, auto-regulation and sub-cellular localization (Katoh and Katoh 2003; Vaillant *et al.* 2008; Heimsath and Higgs 2012).

1.1 Cancer and metastasis

Tumorigenesis is a multistep process involving genetic alterations that drive normal human cell transformation. There are six main hallmarks of cancer: proliferative signal promotion, growth suppressor evasion, replicative immortality, apoptosis resistance, angiogenic stimulation and invasive metastasis. Two additional hallmarks have also been put forth: reprogramming of energy metabolism and avoiding immunity (Hanahan and Weinberg 2000, 2011). Cell invasion and metastasis are present at an advanced stage of malignancy and account for over 90% of all cancer-related deaths.

Metastasis is a complex process where tumor cells dissociate from a primary tumor, disseminate throughout the body and colonize distant organs. Thus, it is imperative to study the mechanisms that promote motility and invasion of tumor cells to better comprehend this process (Valastyan and Weinberg 2011; Bravo-Cordero *et al.* 2012).

Cell migration and invasion is a multistep process involving modulation of the cytoskeleton, formation of cytoskeleton structures, contractile forces, cell-substrate adhesions and mechanisms permitting passage through the extracellular matrix – either proteolytically or through amoeboid migration (Gimona *et al.* 2008). Invading cells are able to migrate through the ECM either collectively or individually. Single cell migration requires dissociation from the surrounding cells and allows localization in tissues and invasion of nearby stroma, similar to what occurs throughout morphogenesis and the immune response. Alternatively, collective migration necessitates that cells remain connected as they travel, resulting in the migration of cell aggregates or sheets of tissues (Friedl and Wolf 2003). The work in my thesis is mostly concerned with single cell migration.

A critical element for single-cell invasion is the dissociation of individual cells from epithelial cell sheets. In order to do so, cancer cells adopt a specific biological program referred to as epithelial-mesenchymal transition (EMT), coordinated by a combination of transcription factors (Snail, Twist, Slug, Zeb 1 and 2). These transcription factors initiate a genetic program associated with the progression of invasion and metastasis including the release of matrix-degrading enzymes and repression of E-cadherin expression, resulting in dissociation of tight and adherens cell junctions and the

rise of resistance to anoikis. Thus, this process sets the stage to allow cells to escape from the primary tumor. (Thiery *et al.* 2009).

1.2 Modes of single cell metastatic invasion

Different cell lines will vary in their morphology when migrating on a two-dimensional (2D) versus a three-dimensional (3D) matrix. For example, invasive A375 melanomas have a more elongated morphology when migrating on a 2D surface, but will be rounded when invading a 3D gel (Sahai and Marshall 2003). Furthermore, cells will alter their morphology in order to adopt a specific mode of invasion when traveling through a 3D milieu. There are two different methods of tumor-cell invasion in a 3D environment: mesenchymal and amoeboid. The mesenchymal mode involves F-actin driven lamellipodia and invadopodia formation governed by the Rho GTPase Rac1. This promotes an elongated morphology of the cell and increased cell-substrate adhesions. In this context, mesenchymal invasion requires the presence of matrix-degrading proteases and lower actomyosin contractility, and is associated with low levels of RhoA/C activity (Sahai and Marshall 2003; Lämmermann and Sixt 2009; Petrie and Yamada 2012).

Amoeboid invasion consists of increased activity of RhoA or RhoC, signalling through Rho-associated coiled-coil-forming kinases (ROCK), resulting in a rounded, blebbing cell morphology. This mode of invasion requires lowered expression levels of Rac1, necessitates high contractility, little adhesion to the cell matrix and is protease-independent (Sahai and Marshall 2003; Petrie and Yamada 2012). How amoeboid cells actually make their way through the ECM is still unknown (Wolf *et al.* 2003).

Even though a given cell-type will adopt a specific mode of invasion, they will switch from mesenchymal to amoeboid migration when Rho is upregulated and Rac1 decreased. This process is known as the mesenchymal-to-amoeboid transition (MAT) (Sahai and Marshall 2003; Wolf *et al*. 2003). Also, cell lines using a mesenchymal mode of invasion, including HT-1080 fibrosarcoma and MDA-MB-231 breast cancer cells, will switch to amoeboid style invasion after protease inhibition (Sahai and Marshall 2003; Wolf *et al*. 2003; Zaman *et al*. 2006). In contrast, protease inhibition in amoeboid cells such as WM266.4 melanoma does not affect morphology or mode of invasion (Wyckoff *et al.* 2006). Despite the differing factors driving their migration, in both cases invasive motility is an actin driven process controlled by actin cytoskeleton remodelling proteins.

1.3 The cytoskeleton

The cytoskeleton plays an important role in a variety of dynamic cellular processes including cell division, intracellular transport, cell migration, cell morphology and tumor metastasis (Chesarone *et al.* 2010). There are three major cytoskeletal filament classes: intermediate filaments, microtubules and actin filaments. Intermediate filaments are essential in providing mechanical strength and maintaining cell integrity. Unlike microtubules and actin filaments, the intermediate filaments are composed of many kinds of proteins depending on the cell type, including keratin, vimentin and desmin (Pruss *et al.* 1981; Cooper 2000). These filaments play a role in organelle positioning and protein targeting towards their specific subcellular compartments (Toivola *et al.* 2005).

Microtubules are large dynamic polymers composed of dimerized α and β tubulin subunits that assemble head-to-tail to create a hollow tubule. This tubule has an intrinsic

structural polarity with α tubulin exposed at the minus end and β tubulin at the plus end (Desai and Mitchison 1997). Each tubulin subunit binds GTP which permits them to assemble into the growing microtubule. Only the GTP bound to β tubulin, however, is subjected to hydrolysis to GDP. It is GTP hydrolysis that can destabilize the microtubule leading to their depolymerisation or "catastrophe". Microtubules form cilia and flagella which projects from the cell surface to serve as sensory and motor organelles (Dentler 1981; Bartolini and Gundersen 2010; Bloodgood 2010). Microtubules also play a role in cell division, cell anchoring, cell morphogenesis, intracellular vesicle transport and organisation of organelles (Schulze and Kirschner 1987; Desai and Mitchison 1997; Doherty and McMahon 2008).

Microtubules are attached by their minus ends to the microtubule-organizing center (MTOC) or centrosome. When a cell is migrating, the centrosome, the golgi apparatus and the positive end of the microtubules will reorient towards the leading edge of the cell. It is thought that this re-orientation of organelles acts in conjunction with a stabilized microtubule network. Stability of microtubules increases the interaction with the motor protein kinesin that walks along the microtubules to reorient the organelles and to facilitate vesicular transport to the leading edge to promote directed cell (Watanabe *et al.* 2005; Reed *et al.* 2006; Bartolini and Gundersen 2010). In this context, the microtubule network can be thought to act as the guidance system of the cell whose migration is driven by the actin cytoskeleton (Olson and Sahai 2009).

1.4 Actin dynamics

The 42 kDa actin protein is one of the most abundant proteins in eukaryotic cells (Gettemans *et al.* 2005). Polymeric filamentous actin (F-actin) is formed from monomeric globular actin (G-actin). Actin filament assembly is a multi-step process. Filament nucleation is initiated when an unstable dimer of G-actin subunits is formed followed by the addition of a third actin monomer to create a stable trimer. Nucleating factors such as the ARP2/3 complex, formins and spire have the ability to increase the rate of nucleation (see below) (Pruyne *et al.* 2002; Pring *et al.* 2003; Zigmond 2004; Bussell 2005; Kovar *et al.* 2006). Once nucleated the polymerization of the actin filament proceeds rapidly and is directly proportional to the concentration of available monomeric G-actin.

Actin filaments are assembled at the positive "barbed end" and disassembled at the negative "pointed end". Monomeric actin can be added and removed at both ends of the filament; yet, the polymerization is more efficient at the barbed end due to higher local concentration of G-actin monomers (Neuhaus *et al.* 1983). This results in the depolymerization of the actin filament. Actin can switch between an ATP-bound state and ADP-bound state. Even though both ATP and ADP-bound actin can be polymerized, ATP-bound actin has a higher affinity for the growing filament than ADP-bound actin (Pollard 1984). ADP-bound G-actin monomers dissociate from the pointed end of the filament and can then exchange ADP for ATP allowing for barbed end binding. This cycle is called actin treadmilling (Neuhaus *et al.* 1983; Korn *et al.* 1987; Staiger and Blanchoin 2006). The actin polymerization and bundling process is regulated by many

actin-binding proteins such as profilin, cofilin, Ena/VASP, capping proteins and cross-linking proteins.

1.5 Actin binding proteins

1.5.1 Profilin, Thymosin and ADF/cofilin

Profilin is a small G-actin binding protein that promotes the exchange of actin-ADP to actin-ATP. Profilin is also able to bind proline-rich sequences such as formin homology domain 1 (FH1) which promotes delivery of profilin-actin complexes to the growing barbed end (Paavilainen *et al.* 2004; Higgs 2005; Staiger and Blanchoin 2006).

Profilin competes with another actin-binding protein, thymosin β4, for binding to monomeric G-actin. Thymosin β4 prevents the assembly of filaments by creating a 1:1 complex with actin monomers to keep them in a locked state blocking the ability of profilin to hydrolyse or exchange their bound nucleotide (Goldschmidt-Clermont *et al.* 1992; Paavilainen *et al.* 2004).

The ADF/cofilin family of small actin binding proteins possess the ability to bind both actin-filaments and monomeric actin. Cofilin's affinity is higher for ADP-bound actin than ATP-bound actin; thus, inducing dissociation of ADP-actin from the pointed end of F-actin. Cofilin can also bind along the side of F-actin to induce filament twisting. This creates mechanical stress and changes the thermodynamic stability of the filaments resulting in depolymerisation. Severed G-actin monomers can subsequently be recycled for creation of new actin polymerisation (McGough *et al.* 1997; Paavilainen *et al.* 2004).

1.5.2 Capping proteins

Capping proteins, such as CapZ, are heterodimeric proteins composed of α and β subunits, which have the ability to bind actin filament's barbed end (Yamashita *et al.* 2003). Barbed-end capping of F-actin is required for the regulation of lamellipodia in order to terminate filament elongation driving cell motility and essentially to cap actin filaments that are no longer participating in cell movement, creating a dendritic network of short actin filaments (Pollard and Borisy 2003). During filopodia formation, barbed-end capping needs to be prevented to permit filament elongation (Mallavarapu and Mitchison 1999; Breitsprecher *et al.* 2008). Depletion of CapZ protein results in a loss of lamellipodia formation and a rise in filopodia formation (Mejillano *et al.* 2004) (Lamellipodia and filopodia structures will be better described below).

1.5.3 Ena/VASP

Enabled/vasodilator-stimulated phosphoproteins (Ena/VASP) have been shown to play a role in actin filament elongation and localize at stress fibers, focal adhesions, lamellipodial and filopodial leading edge (Rottner *et al.* 1999; Mellor 2010). There are three different members of the Ena/VASP family found in vertebrates: Mena, Evl and VASP. The Ena/VASP proteins share conserved domains: the N-terminal EVH1-domain for subcellular localization, the proline-rich domain, which can interact with profilin, and the functional C-terminal EVH2 domain permitting binding to actin (Krause *et al.* 2003). Ena/VASP generates filament elongation by delivering G-actin monomers to the growing barbed end which pushes the plasma membrane forward, creating filopodia (Gupton and Gertler 2007; Breitsprecher *et al.* 2008; Mellor 2010). Furthermore, Ena/VASP proteins

have the ability to bundle actin filaments which is critical for filopodia formation (Bachmann *et al.* 1999).

1.5.4 Cross-linking proteins

Many different F-actin cross-linking proteins have been identified and play a role in specific actin structures. Cross-linking proteins can promote the assembly of F-actin networks as well as tightly or loosely bundled actin (Matsudalra 1991; Otto 1994; Vignjevic *et al.* 2006). An F-actin network is a flexible arrangement of filaments separated by large cross-linking proteins such as Filamin. These networks create a flexible cytoplasmic skeleton for the cell. Filamin is also required for lamellipodia formation (Pudas *et al.* 2005). Depletion of Filamin in cells decreases their ability to migrate and lack proper lamellipodia formation (Cunningham *et al.* 1992).

It is thought that bundling proteins are important for organizing actin filaments in parallel by tightly packing them, thus preventing myosin II from entering the bundle. For example, fimbrin and villin crosslinking proteins both tightly bundle actin filaments in microvilli and also reinforce cell adhesions to the ECM (Matsudaira 1994; Alberts *et al.* 2002).

Bundling proteins such as α-actinin and fascin contain two actin-binding domains that are further apart, separating filaments by approximately 30nm. These proteins cross-link actin filaments into loose bundles allowing the motor protein myosin II to create contractile stress fibers during cell movement (Ishikawa *et al.* 2003). These bundled filaments are also commonly found in filopodia and invadopodia structures, hence, α-

actinin and fascin are implicated in maintenance of cell adhesions to the ECM and cell motility (Vignjevic *et al.* 2006; Gupton and Gertler 2007; Machesky and Li 2010).

1.6 Rho-GTPase and effectors

Rho GTPases also known as Ras-related GTPases, are important signal transducers that regulate the formation of many actin structures such as adhesion junctions, stress fibers and plasma membrane protrusions (Nobes and Hall 1995; Goode and Eck 2007). These proteins can switch between an active guanosine triphosphate (GTP)-bound state and an inactive guanosine diphosphate (GDP)-bound state. Rho proteins are kept in the inactive GDP-bound conformation when associated with Rho GDP-dissociation inhibitor protein (RhoGDIs). Guanine nucleotide exchange factor (GEFs) induces the exchange from GDP to GTP in order to activate Rho GTPase where it can bind its downstream effector proteins (e.g. formins). GTPase activating proteins (GAP) catalyse GTP hydrolysis resulting in RhoGTPase inactivation (Bächner *et al.* 1995; Sahai and Marshall 2002a; Ridley 2011).

Rho GTPases, can be subdivided into four groups: Rho, Rac, cdc42, and a distinct class that lack GTPase activity (Nobes and Hall 1995; Sahai and Marshall 2002a). Rho, Rac and cdc42 proteins are the best understood and are implicated in specific actin structure formation. Rac induces lamellipodia formation through its effectors such as the nucleation promoting factors Wiskott–Aldrich syndrome protein (WASp) and WASp protein family member verprolin-homologous protein (WAVE) which activate Arp2/3 (Leung and Rosen 2005; Takenawa and Suetsugu 2007). Cdc42 induces filopodia and invadopodia formation also through activation of WASp and ARP2/3. Rac1 and cdc42

both interact with p21-activated kinases (PAKs) to activate LIM kinase, which phosphorylates cofilin, with the aim of inhibiting its activity on severing and depolymerizing the actin filament, as well as decreasing its ability to modulate lamellipodia and filopodia dynamics (Delorme *et al.* 2007; Rheenen *et al.* 2009).

Rho interacts with ROCK and the formin mammalian Diaphanous homologue 1 (mDia1) to make stress fibers (Sahai and Marshall 2002b). ROCK is part of the serine/threonine kinase family and is activated when released from its auto-inhibition by GTP-bound Rho. Similar to PAK, ROCK functions downstream of RhoA to phosphorylate LIM kinase which then inactivates cofilin to block F-actin depolymerization (Maekawa *et al.* 1999). ROCK governs several aspects of RhoA/C-mediated actin reorganization, including plasma membrane blebbing (Sahai and Marshall 2003; Charras 2008; Olson and Sahai 2009). Rho proteins are also key regulators of many formin family members. They are thought to bind a specific GTPase binding domain to relieve them from their auto-inhibition, permitting them to bind the barbed end of actin filaments. mDia1 has the ability to nucleate actin polymerization at the barbed end of F-actin. Its activity correlates with RhoA and ROCK induced contractile stress fiber formation and focal adhesions (Watanabe *et al.* 1999; Sahai and Marshall 2002b). The actin structures generated by the Rho GTPase family members and their effectors are required for cell motility and are described in more details in the following sections.

1.7 Actin drives cell motility

Cell motility depends upon the coordinated formation of lamellipodia, filopodia, invadopodia, stress fibers and blebs. Lamellipodial extension promotes cell spreading and

migration (Goode and Eck 2007). Filopodia assist cells to sense their external environment and guide them toward chemoattractants (Pellegrin and Mellor 2005; Gupton and Gertler 2007). Invadopodia degrade the ECM and promote invasion through surrounding tissues (Buccione *et al.* 2009). Finally, plasma membrane blebbing can drive cell motility without the use of lamellipodia as seen in amoeboid style movement (Charras and Paluch 2008; Kitzing *et al.* 2010). Nonetheless, cells use these membrane remodeling methods in order to move into surrounding tissues and blood vessels throughout tumor cell invasion and metastasis (Condeelis *et al.* 2001; Weaver 2006; Buccione *et al.* 2009; Kitzing *et al.* 2010).

1.7.1 Filopodia formation

Filopodia are finger-like membrane protrusions containing bundles of straight parallel actin filaments that have the ability to extend and retract. These structures are essential for guidance throughout cell migration, wound healing closure and adhesion to the extracellular matrix (Gupton and Gertler 2007). Filopodia protrusions are induced by barbed-end actin polymerization and actin retrograde flow pushing towards the leading edge (figure 1.1). There are two models of filopodia formation. In the first model, filopodia emerge from the lamellipodial F-actin network as an existing actin-filament nucleated by Arp2/3 and elongated by Ena/VASP. Ena/VASP provides monomeric G-actin at the filopodia growing tip while protecting the actin filament from capping proteins (Breitsprecher *et al.* 2008). The actin cross-linking protein fascin is able to bind β-catenin (part of the adherens junction protein complex), to localize at the leading edge

Figure 1.1: Actin dynamics throughout lamellipodia and filopodia formation. During lamellipodia formation, the Arp 2/3 complex and WASP create branched F-actin networks. Barbed ends of the actin filaments are bound by formins and Spire during F-actin elongation. WAVE protein, regulated by Rac1, promotes lamellipodium extension by binding Arp2/3 complex and localizing to the plasma membrane. The severing protein cofilin is inhibited by PAK through LIM-kinase. Filopodia generally originate from the lamellipodia branched networks. These protrusions are made of elongated actin bundles generated by Ena/VASP, fascin and formins activated by cdc42.

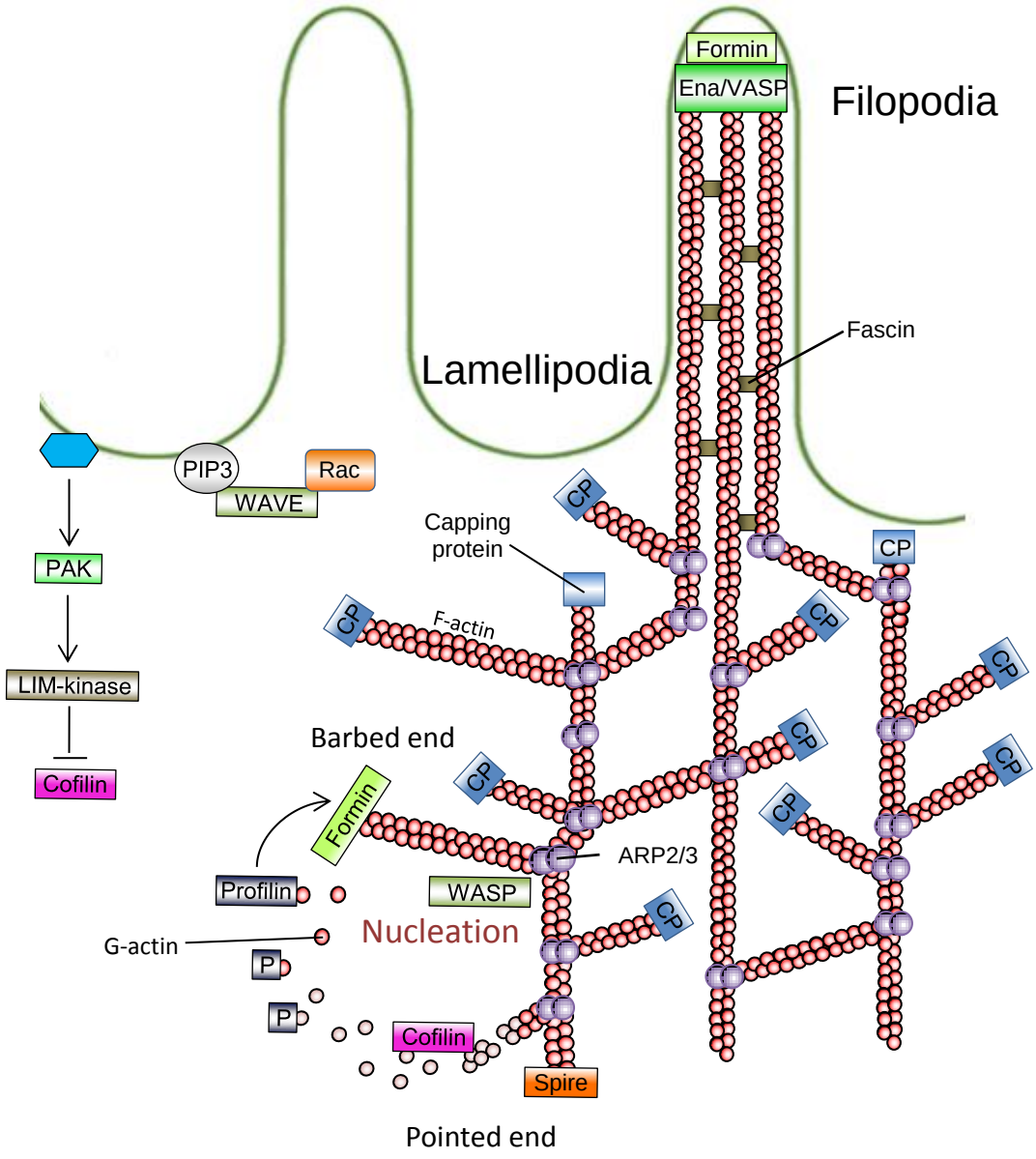

Adapted from Miyoshi 2008

of moving cells and is important in actin bundling, assembly and stability of the filopodia (Otto 1994; Machesky and Li 2010). Formins have also been shown to be implicated in filopodia formation. The Diaphanous-related formin (DRF), Dia2, is believed to be released from its autoinhibition by cdc42 in order to nucleate straight F-actin, induce actin polymerization, bundle actin filaments, and shield the barbed end from capping proteins. The growing barbed end pushes the plasma membrane forward creating filopodia (Li and Higgs 2003; Kovar and Pollard 2004; Pellegrin and Mellor 2005). Other DRF proteins have been recently shown to induce filopodia formation, including FMNL3. Despite very similar properties and characteristics between the DRF family members, some of these formins, such as FMNL1, lack the ability to assemble filopodia (Harris *et al.* 2010)

1.7.2 Lamellipodia formation

Actin polymerization has been shown to drive protrusion of the plasma membrane in lamellipodia, regulated by a variety of actin remodeling proteins (Ridley *et al.* 2003) (figure 1.1). Briefly, the fast growing barbed end of the actin filament is orientated in the direction of the leading edge, pushing the plasma membrane forward by the addition of monomeric G-actin at the barbed end. Three groups of actin nucleation factors are implicated in lamellipodia formation: the Arp2/3 complex, spire and formins (Nürnberg *et al.* 2011). The Arp2/3 complex nucleates polymerization at a 70^{o} angle from the side of mother actin filaments and induces the formation of a branched "dendritic" actin filament network (Campellone and Welch, 2010). Nucleation promoting factor WASp activates Arp2/3 complex by generating a conformational modification by bringing Arp2 and Arp3

in a closed state to promote filament nucleation (Rodal *et al.* 2005). The nucleation promoting factor WAVE, regulated by Rac1, promotes lamellipodium extension by binding the Arp2/3 complex and localizing it to the plasma membrane (Chen *et al.* 2010).

The two other actin nucleators, Spire and formins, contribute to lamellipodia extension by protecting the growing barbed end from capping proteins and inducing filament elongation of the branched filaments (Campellone and Welch 2010; Ridley 2011). Spire nucleation factor proteins contain four WASp homology 2 (WH2) domains which nucleate polymerization and stay bound at the pointed end of the actin filament (Rosales-Nieves *et al.* 2006). The Rho GTPase effector formins nucleate the actin polymer at the barbed end and stay bound during the elongation of the actin filament in order to block capping proteins (Pruyne *et al.* 2002). This process will be further elaborated in section 1.8.

Lamellipodial extension can generate cell migration when the growing leading edge protrusions bind the ECM via adhesion molecules such as transmembrane receptors of the integrin family. This creates focal adhesions. Actomyosin contractility needs to be accomplished in order to project the cell forward and promote cell migration. Stress fibers will then promote retraction of the cell's trailing end (Friedl and Wolf 2003).

1.7.3 Stress fiber formation

Stress fibers are thick unbranched actin filament bundles, held together by actin-crosslinking proteins that create contractile forces during cell motility while maintaining structural integrity (Lazarides and Burridge 1975; Russell *et al.* 2009). Overexpression of RhoA, RhoB, or RhoC will produce stress fibers (Wheeler and Ridley 2004). RhoA

activates the formin mDia1, resulting in actin filament nucleation and elongation (Watanabe *et al.* 1999; Sahai and Marshall 2002b). Filaments are loosely bundled and held together by crosslinking proteins such as α-actinin and fascin permitting myosin II to create contractile stress fibers. Stress-fiber contractility is generated by the RhoA effector ROCK which has the ability to phosphorylate the myosin regulatory light chain (MLC) of myosin II (Katoh *et al.* 2001; Sahai and Marshall 2003). The phosphorylation of MLC enhances ATPase activity of myosin II, permitting it to bind the actin filament to promote contraction (Katoh *et al.* 2001). Actomyosin contractility projects the cell forward as focal adhesions at the rear of the cell disassemble (Friedl and Wolf 2003).

1.7.4 Invadopodia formation

Invadopodia play a key role in attachment and degradation of the ECM by invading cells (Sahai and Marshall 2003; Weaver 2006; Lämmermann and Sixt 2009). Invadopodia are formed in a 3D milieu and require force driven by actin polymerization (Friedl and Gilmour 2009). Many of the actin-regulatory proteins used throughout invadopodia formation are also found in lamellipodia and filopodia (figure 1.2). However, invadopodia degrade the ECM, and a supply of vesicles containing matrix-degrading proteases are transported on microtubules to the end of the invadopodia (Schoumacher *et al.* 2010). It is thought that actin polymerization and filament elongation is induced by the formin mDia1 and further branching of the mother filament is generated by cdc42-mediated WASp activation of the Arp2/3 complex. Actin filaments are then bundled by fascin proteins into stress fibers (Lizárraga *et al.* 2009; Buccione *et al.* 2009).

Figure 1.2: Actin dynamics during invadopodia formation. Invadopodia formation starts by actin polymerization and filament elongation induced by mDia1 and further branching of the mother filament is mediated by cdc42-mediated WASP activation of the Arp2/3 complex. Cofilin severs F-actin providing new sites for actin nucleation. Actin is bundled by fascin proteins. Invapodias are formed in a 3D milieu and necessitate the supply of vesicles containing MT1-MMP transported on microtubules to degrade the ECM.

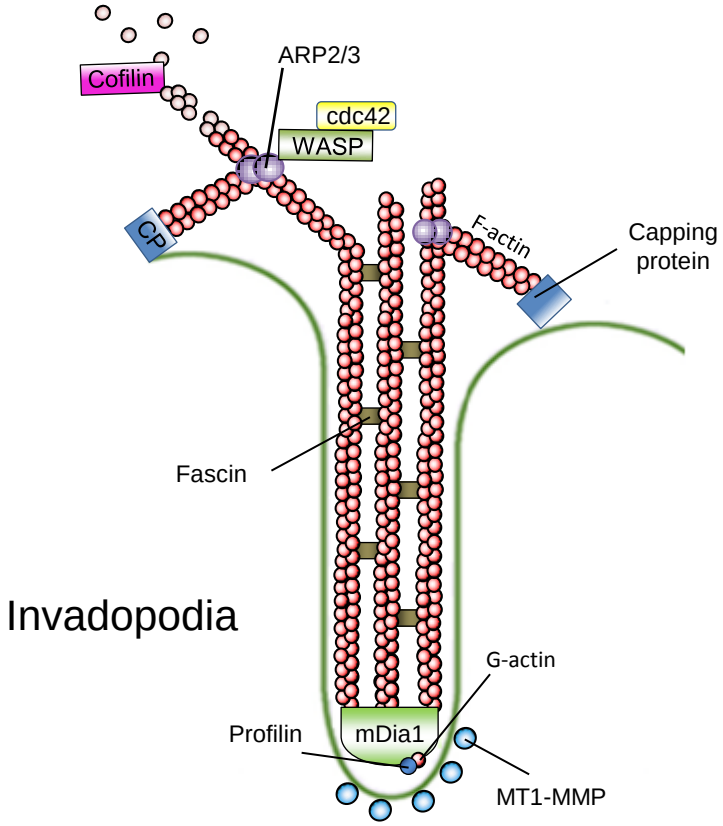

Adapted from Ridley 2011

The growing barbed ends of the bundled actin filaments push towards the plasma membrane, creating invadopodial protrusion. The invadopodia adhere to (via integrins) and degrade the ECM in order to invade the surrounding tissues (Weaver 2006)

1.7.5 Plasma membrane blebbing

In addition to lamellipodia and filopodia, protrusions can also be produced by actin-network contractions generating hydrostatic pressure on the leading edge, which results in membrane "blebbing" (Lämmermann and Sixt 2009) (figure 1.3). Blebbing also occurs through a similar process during cell spreading, cytokinesis, and apoptosis (Charras 2008). Contractions by myosin II with Rho and ROCK creates an increase in hydrostatic pressure, resulting in rupture of the actin cortex or detachment of the cell membrane from the actin cortex (Paluch *et al*. 2005). At the same time, the pressure produced by the contractions generates bleb expansion as the cytosol streams out of the cell body to inflate the new bleb. Once the pressure equilibrates and the expansion of the bleb ceases, actin binding proteins are recruited to the bleb to reassemble the cell membrane cortex, resulting in bleb retraction (Sahai and Marshall 2003; Charras 2008; Olson and Sahai 2009). In migrating cells, a new bleb forms quickly after the retraction. This sequential blebbing is thought to explain amoeboid motility (Charras and Paluch 2008).

Figure 1.3: Actin dynamics throughout plasma membrane blebbing. Membrane blebs are generated by actomyosin contractions with Rho and ROCK creating an increase of hydrostatic pressure resulting in rupture in the actin cortex or detachment of the cell membrane from the actin cortex. This leads to fluid flow pushing the membrane outwards locally. The cytosol flow will then push the membrane outwards, resulting in bleb inflation. Retraction of the bleb occurs due to myosin II activity and actin polymerization on the membrane by formins.

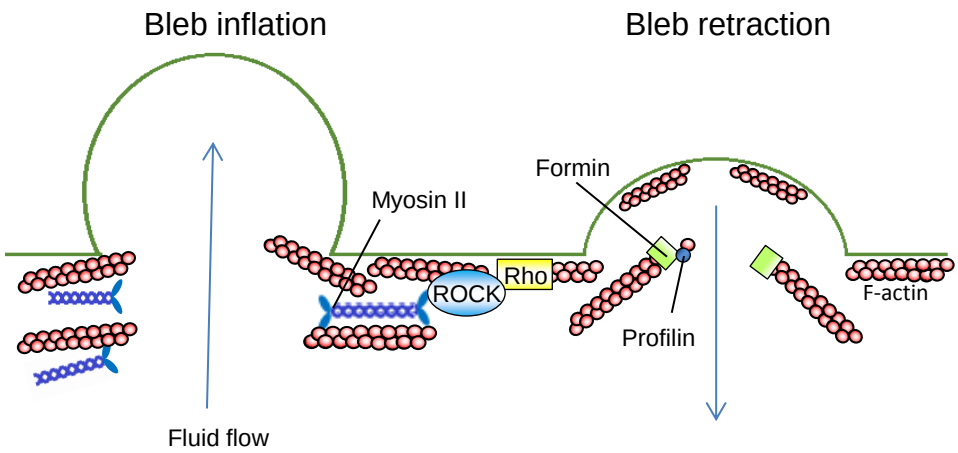

Adapted from Ridley 2011

1.8 Formin Homology Domain Proteins

Formins are large multidomain proteins expressed in all eukaryotes from fruit flies to plants to mice and humans. 15 formins are found in vertebrates which can be further sub-divided into seven groups, based on homology and domain architecture (Higgs 2005) (figure 1.4). Formins can regulate a variety of actin-based processes, including cell motility, cell invasion, cell-cell junction assembly, cell division, cell polarity and cell shape (Goode and Eck 2007; Vaillant *et al.* 2008). As previously described, these proteins also play a role in the formation of specific cellular structures such as unbranched actin filaments, stress fibers and plasma membrane protrusions (Goode and Eck 2007). Formins have the ability to stimulate actin polymerization through the activity of two conserved formin homology domains: FH1 and FH2. FH1 is composed of a series of proline residues, is proximal to FH2 and becomes a ligand for proteins containing a SH3 domain (like Ras GTPase) or other small actin-binding proteins like profilin (Chan *et al.* 1996). The 400 amino acid FH2 domain can bind the actin filament barbed end throughout the elongation process while protecting it from capping proteins (Copeland and Treisman 2002; Pring *et al.* 2003; Pruyne *et al.* 2002; Zigmond 2004).

Formins are able to nucleate a new filament and remain bound to the elongating barbed end (Pruyne *et al.* 2002) (figure 1.5a). For an actin filament to form, the G-actin monomers spontaneously collide and nucleate to form a dimer and subsequently a trimer (Goode and Eck 2007). Nucleation can be aided by proteins like formins to associate with the monomers, stabilize the dimer and facilitate the formation of the trimer

Figure 1.4: Schematic of the fifteen Human Formin Homology Proteins. Formins can be divided into seven sub-families: Diaphanous (Dia), Formin-like (FMNL), Dishevelled-associated activator of morphogenesis (DAAM), Inverted formin (INF), Formin homology domain-containing protein (FHOD), Formin (FMN), and Delphilin. Each formin contains the functional domains: Formin Homology 1 (yellow) and Formin Homology 2 (blue). Most of these proteins also comprise of regulatory domains: Diaphanous Inhibitory Domain (DID) (red), coiled-coiled Domain (CC) (grey) and Diaphanous Autoregulatory Domain (DAD) (green). Certain formins also have a GTPase-binding domain (violet) or PDZ domain (Psd-95/Dlg/Zo-1) at the N-terminus. The DRF subgroup comprise of the Dias, FMNLs and DAAMs proteins.

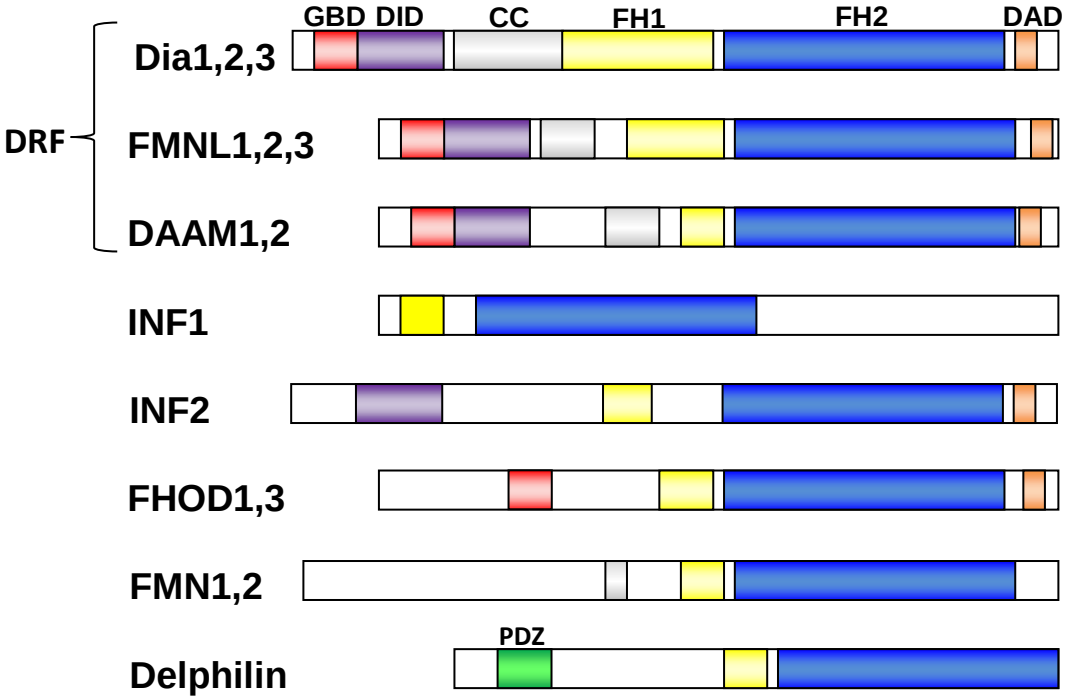
GBD DID
CC
FH1
FH2
DAD
DRF
Dia1,2,3
FMNL1,2,3
DAAM1,2
INF1
INF2
FHOD1,3
FMN1,2
PDZ
Delphilin

Figure 1.5: FH2 dimerization and activity. (A) The FH2 homodimers are able to induce actin filament elongation while staying bound to the barbed end. Throughout filament elongation, the ATP from the ATP-bound actin subunit is hydrolyzed to an ADP-bound actin state with a release of a free inorganic phosphate. Cofilin severs the pointed end of the F-actin creating new monomeric G-actin. Profilin binds the G-actin monomer and helps the exchange from ADP to ATP and bind the FH1 domain to bring the new ATP-bound G-actin to the barbed end. (B) The FH2 dimerization is accomplished by the interaction between the N-terminal "lasso" of the first FH2 subunit to the C-terminal "post" of the other FH2 subunit.

A

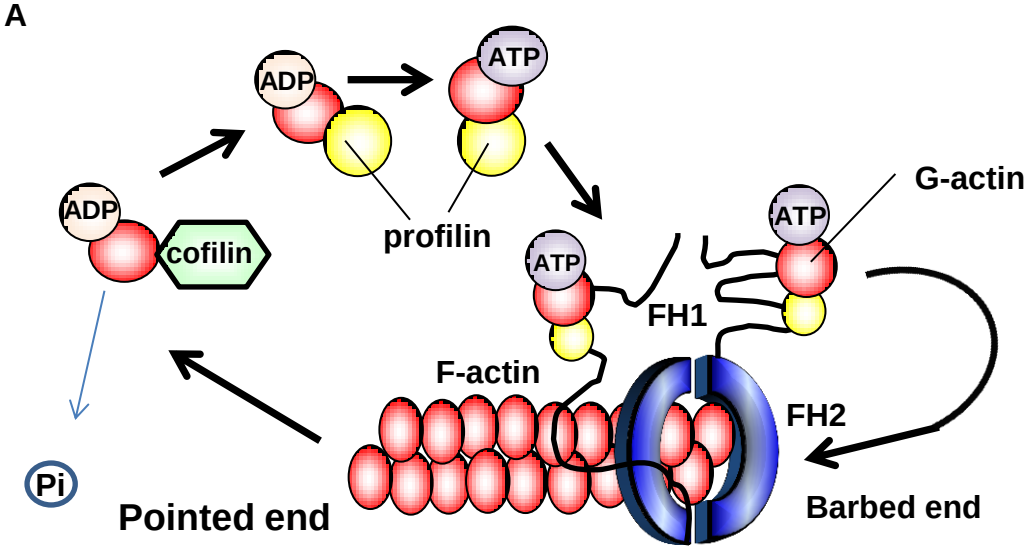
ADP
ATP
ADP
cofilin
profilin
ATP
G-actin
ATP
FH1
F-actin
FH2
Pi
Pointed end
Barbed end

B

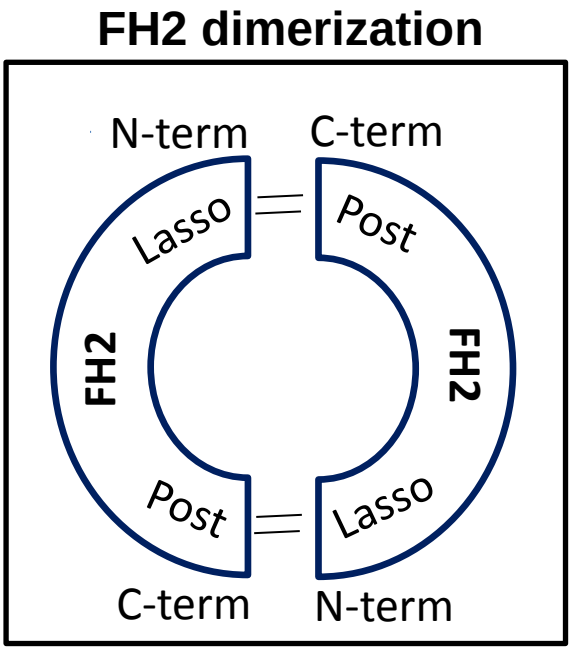
FH2 dimerization
N-term
C-term
Lasso
Post
FH2
FH2
Post
Lasso
C-term
N-term

(Pruyne *et al*. 2002; Goode and Eck 2007). However, there is great variability in nucleation potency between one formin to another. For example, mDia1 is an efficient nucleator (Li and Higgs 2003) whereas FMNL1 (Harris *et al.* 2004) and Bni1 (Pring *et al*. 2003) are weak nucleators. The FH2 domain has been shown to mediate actin nucleation and binds the barbed end of the filament as a homodimer as in the case of Bn1 and DRF mDia1 upon activation (Pruyne *et al.* 2002; Copeland *et al.* 2004; Moseley *et al.* 2004) Structural evidence provided by a crystallography analysis of the Bni1p FH2 dimer shows a donut-like state where the head (lasso) of the first FH2 interacts with the tail (post) of the other (Otomo *et al.* 2005; Xu *et al.* 2004) (figure 1.5b).

FH2 homodimers function as leaky cappers that induce actin filament elongation while staying bound to the barbed end (Zigmond *et al.* 2003). Many models have suggested that the FH2 stays at the barbed end in an "open" or "closed" state (Kovar 2006; Paul and Pollard 2009). It is believed that, throughout the closed conformation, the FH2 homodimer associates with the three actin subunits at the barbed end of the actin filament. The open state consists of one FH2 domain bound to an actin subunit while the other FH2 domain partially unfastens from the trailing actin subunit. The next free actin monomer is then accepted into the growing filament in a step-like manner. (Xu *et al.* 2004; Higgs 2005; Paul and Pollard 2008; 2009).

Formins have been shown to be able to bind the sides of F-actin and mediate filament bundling (Michelot *et al.* 2005; Harris *et al.* 2006; Esue *et al.* 2008). Bundling is dependent upon the FH2 domain as well as a WH2 domain found C-terminal to FH2. In FMNL3, the WH2 domain also plays a role in binding the barbed end and stabilizing the actin filament nucleus (Heimsath and Higgs 2012; Thompson *et al.* 2013)

1.8.1 Formins and microtubule dynamics

Previous work from our lab and others suggests that formins are able to regulate microtubule dynamics in an FH2-dependent manner (Ishizaki *et al.* 2001; Bartolini *et al.* 2008; Thurston *et al*. 2012). Formins, such as mDia1, induce reorganisation and alignment in parallel of both bundled actin filaments and microtubules (Ishizaki *et al.* 2001). Formins can also regulate microtubule stabilization; mDia co-localizes and binds stable detyrosinated microtubules *in vitro* (Palazzo *et al.* 2001). Previous work from our lab confirms these data by reporting that formins can induce microtubule acetylation, a marker of microtubule stabilization. However, it is still unknown which modification takes place throughout formin-induced microtubule stabilization: acetylation or de-tyrosination (Bartolini and Gundersen 2010).

Stable microtubules are critical for cell polarization and are oriented towards the leading edge of the migrating cell. Formins can be classified into strong : (DAAM1, DAAM2, Dia1, Dia2, Dia3, FMNL1 and INF1), and weak inducers of microtubule acetylation (FMNL2,3 and INF2) (Thurston *et al.* 2012). Cell polarity is controlled by both microtubule and actin cytoskeleton dynamics, which suggests that formins might be a unique group of cytoskeletal cross linking proteins that play a role in regulating both F-actin and microtubule networks during cell motility (Bartolini and Gundersen 2010; Thurston *et al*. 2012).

Formin-regulated cytoskeletal dynamics are thought to be involved in the progression of cancer cell metastasis (Olson and Sahai 2009; DeWard *et al.* 2010). DRFs have been shown to be highly expressed in cancer cells; Dia 1 drives invasion (Kitzing *et al.* 2007), FMNL1 is upregulated in lymphoid cancer (Favaro *et al.* 2006), FMNL3 is up

in prostate cancer (Tanji *et al.* 2010; Vega *et al.* 2011); FMNL2 is up regulated in metastatic colorectal cancer (CRC) cells and is required for amoeboid invasion (Zhu, Liang, and Ding 2008; Kitzing *et al.* 2010; Li *et al.* 2010; Zhu *et al.* 2011).

1.9 FMNL2

1.9.1 Role of FMNL2 in invasion and metastasis

FMNL2 mRNA is expressed in several normal and cancerous tissues (Katoh and Katoh 2003; Parsons *et al.* 2008; Kitzing *et al.* 2010). The human protein atlas reports that FMNL2 is overexpressed in a variety of malignant cell lines such as gliomas, ovarian, endometrial, urothelial, testicular, thyroid cancers as well as head and neck cancers. (Human Protein Atlas, http://www.proteinatlas.org). FMNL2 expression levels have been shown to be elevated in invasive CRC and increased FMNL2 expression is directly correlated with increased CRC cell metastasis in patient samples (Zhu, Liang, and Ding 2008, Li *et al.* 2010; Zhu *et al.* 2011). This is thought to be mediated in part by FMNL2 regulated cytoskeletal dynamics in conjunction with regulation of growth factor TGF-β dependent EMT. FMNL2 depletion in invasive CRC cells decreases the ability of TGF-β to promote EMT and induces a change in cell morphology from a spindle mesenchymal shape to a cobblestone epithelial shape (Li *et al.* 2010).

FMNL2 has been identified as a specific RhoC effector in the progression of amoeboid style invasion. FMNL2 is the most highly expressed formin in invasive MDA-MB-435 amoeboid melanoma cells. Knockdown of FMNL2 expression in MDA-MB-435 cells inhibited cell invasion (Kitzing *et al.* 2010). In these cells, FMNL2 showed selective

interaction with RhoC, but not RhoA or RhoB, suggesting that RhoC is mediated through FMNL2 for rounded invasive cell migration (Kitzing *et al.* 2010).

Although FMNL2 upregulation is associated with increased invasiveness in a variety of cancer cell lines this is not the case for all cancerous cells. FMNL2 expression levels are lowered in hepatocellular carcinoma cells and FMNL2 transfection suppresses their motility and invasion (Liang *et al*. 2011).

1.9.2 FMNL2 protein

Formin-like 2 (FMNL2), also known as FRL3 or FHOD2, is a member of the DRF sub family. As with all formins, FMNL2 contains the functional FH1 and FH2 domains as well as a WH2 domain required for FMNL2-dependent actin bundling (Vaillant *et al.* 2008). Like other DRFs it has a regulatory Rho GTPase-binding domain (GBD), a diaphanous-inhibitory domain (DID), an N-terminal dimerization domain (DD) and a C-terminal diaphanous autoregulatory domain (DAD).

FMNL2 is autoregulated through the DAD and DID interaction (figure 1.6) and deletion of either DID or DAD is sufficient to render FMNL2 constitutively active (Vaillant *et al.* 2008). Based on analogy to FMNL3 and FHOD1, it has been proposed that the DID/DAD interaction can be affected by residues C-terminal to DAD. For example, FMNL3, which contains nearly identical DID/DAD regulatory domains as FMNL2, is not efficiently auto-inhibited (Vaillant *et al.* 2008).

FMNL1, FMNL2 and FMNL3 are myristoylated at glycine residue 2 in the N-terminus (Han *et al.* 2009; Moriya *et al.* 2012) (figure 1.7). N-terminal myristoylation can induce binding of proteins to the lipid membrane by hydrophobic interaction with the

Figure 1.6: FMNL2 is regulated by autoinhibition. FMNL2 is inactive when the N-terminal DID binds the C-terminal DAD. Rho GTPase binds the GTPase binding domain relieving the DID/DAD interaction and unmasking the FH2 domain. This active conformation permits the FH2 to bind the F-actin at the barbed end to generate actin filament elongation. Profilin protein binds the FH1 domain and helps to bring GTP-bound actin monomers to the growing barbed end.

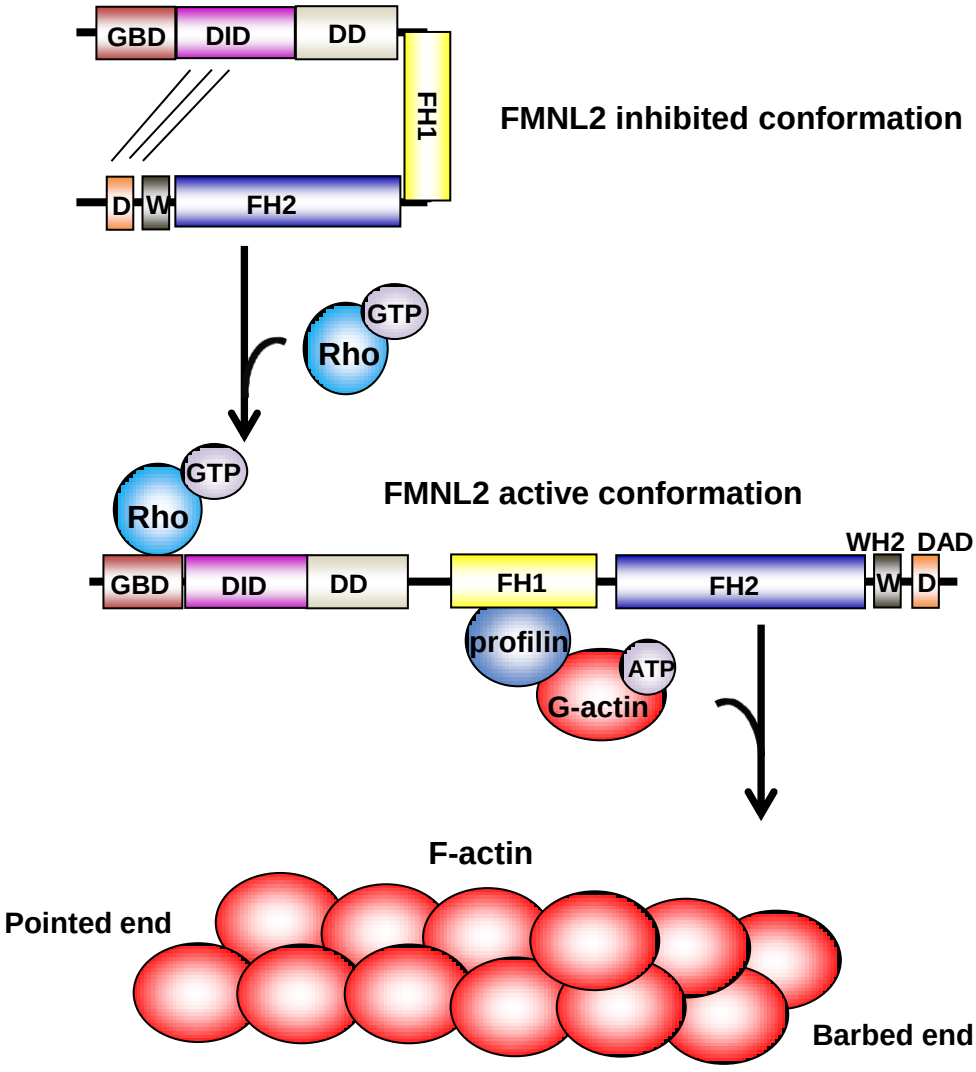
GBD
DID
DD
FH1
D
W
FH2
FMNL2 inhibited conformation
GTP
Rho
GTP
Rho
FMNL2 active conformation
WH2
DAD
GBD
DID
DD
FH1
FH2
W
D
profilin
ATP
G-actin
F-actin
Pointed end
Barbed end

Figure 1.7: FMNL proteins are myristoylated at their N-terminal domain. N-terminal myristoylation on glycine at position 2 can drive binding of proteins to the lipid membranes by hydrophobic interaction with the membrane bilayer. The myristoylation site is conserved between proteins FMNL1, FMNL2 and FMNL3, at the N-terminus upstream of the GTPase binding site.

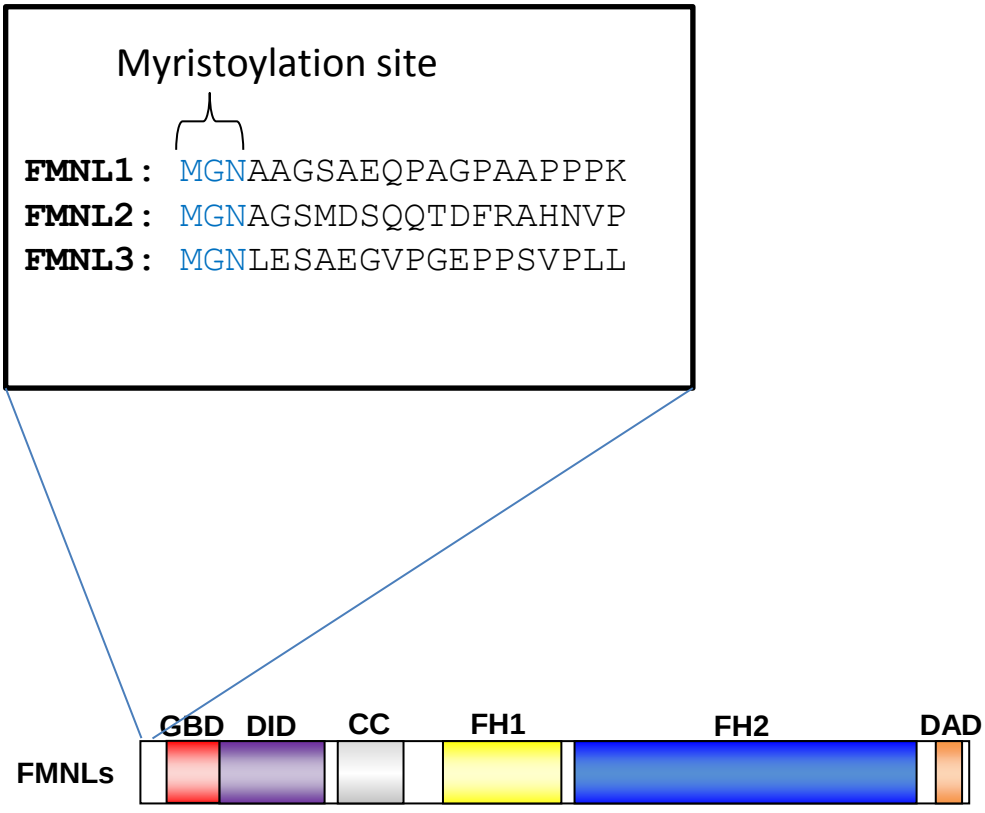
Myristoylation site
FMNL1 : MGNAAGSAEQPAGPAAPPPK
FMNL2 : MGNAGSMDSQQTDFRAHNVP
FMNL3 : MGNLESAEGVPGEPPSVPLL
GBD
DID
CC
FH1
FH2
DAD
FMNLs

membrane bilayer, which is necessary for protrusion induction at the lamellipodia tip. (Moriya *et al.* 2012; Block *et al.* 2012).

1.9.3 FMNL2 isoforms

FMNL2 mRNA is subject to alternative splicing and, based on the regions affected; it is likely that the encoded proteins will differ in their regulation, subcellular localization and activity. At least seven FMNL2 isoforms are predicted in the NCBI database, many of which are conserved between chimps, humans and mice (figure 1.8) Only two of these isoforms have been described in the literature prior to this work: the 1092 amino acids (AA) FMNL2 isoform (designated FMNL2 ITM) and the 1052 residue variant designated FMNL2 YHY (Katoh and Katoh 2003). These two isoforms are identical save for the last 28-36 AA residues C-terminal to the DAD domain. Similarly, two additional predicted FMNL2 isoforms, altered in their C-terminal domain have been described: FMNL2 PMR (1084 AA) and FMNL2 TQS (1087 AA).

Three other predicted short FMNL2 splice forms are altered at the C-terminal domain and vary in their N-terminal domain: a short FMNL2 TQS (569 amino acid) splice variant as well as short FMNL2 ITM and YHY isoforms called craA and craB that lack the N-terminal motif before the GTPase binding domain.

Actin-associated protein isoforms have been shown to be preferably expressed in tumor cell lines and have been directly correlated with tumor cell invasion and metastasis (Philippar *et al.* 2008; Goicoechea *et al.* 2010). For example, the palladin protein has two main splice variants, one that is expressed in normal epithelial cells while the second isoform is highly expressed in tumor-associated fibroblasts (Goicoechea *et al.* 2010).

Figure 1.8: FMNL2 predicted splice variants. Many FMNL2 splice forms are conserved between chimps, humans and in mice. Two different human FMNL2 isoforms are reported in the literature: FMNL2 ITM and FMNL2 YHY that varies in its C-terminal motif following the DAD domain. Two additional splice forms altered in their C-terminal domain are predicted (FMNL2 PMR and FMNL2 TQS). Three short splice variants are also predicted varying in their N-terminal and C-terminal domains: short FMNL2 TQS, short FMNL2 ITM (craA) and short YHY (craB)

Predicted FMNL2 isoforms

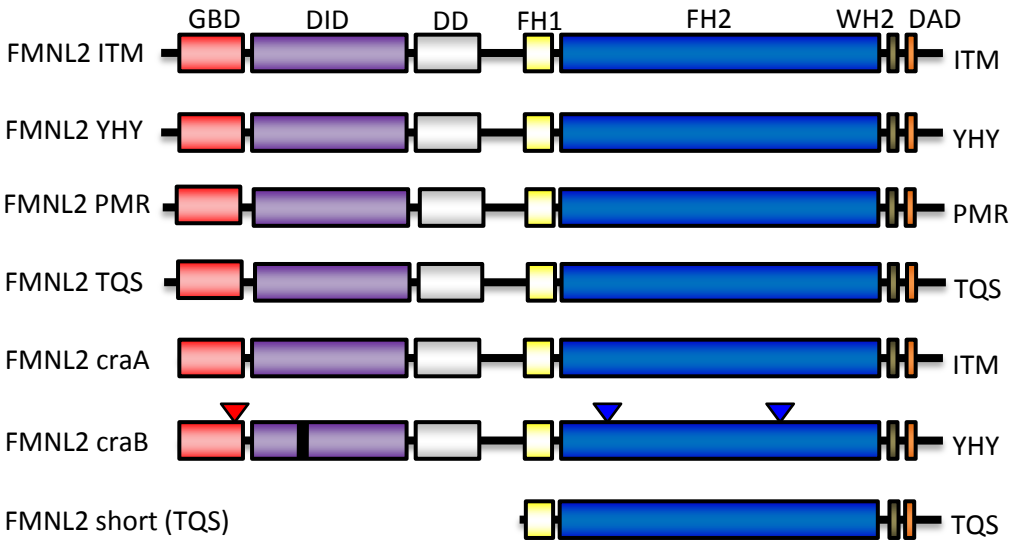

Furthermore, an invasive isoform of Mena promotes carcinoma cell motility and invasiveness *in vivo* and *in vitro* as well as increasing lung metastasis (Philippar *et al.* 2008). Since FMNL2 has been shown to drive metastasis and invasion in certain cancer cell lines (Kitzing *et al.* 2010; Li *et al.* 2010; Zhu *et al.* 2011), it is of great interest to determine if a specific isoform predominates in this role.

1.10 Hypothesis

The objective of this work is to test the hypothesis that a specific isoform of FMNL2 is essential for amoeboid style invasion as well as to determine the effect of alternative splicing of FMNL2 on the regulation, subcellular localization and activity of the encoded proteins.

Chapter 2

Material and Methods

2.0 Material and Methods

2.1 Cell culture

Table 2.1: Cell lines used in this thesis.

Cell line	Company	Cell type	Organism	Medium	Conditions
NIH3T3	ATCC	Fibroblast	*Mus musculus*	10% DBS (ATCC) in DMEM (ATCC)	37°C, 5% CO_2
A375	ATCC	Melanoma	*Homo sapiens*	10% FBS (Wisent) in DMEM	37°C, 5% CO_2
A431	ATCC	Epidermoid carcinoma	*Homo sapiens*	10% FBS in DMEM	37°C, 5% CO_2
HTB107	ATCC	Thyroid, squamous cell carcinoma	*Homo sapiens*	10% FBS in L-15 (ATCC)	37°C,100% air
HUVEC	ATCC	Umbilical Vein Endothelial Cells	*Homo sapiens*	Endothelial basal medium + growth factors (EGM2) (Lonza)	37°C, 5% CO_2
LS174T	ATCC	Colorectal adenocarcinoma	*Homo sapiens*	EMEM (ATCC) 10% FBS	37°C, 5% CO_2
Melanocytes	ATCC	Primary epidermis cells (basal layer)	*Homo sapiens*	Dermal Cell Basal Medium + Adult Melanocyte Growth Kit (ATCC)	37°C, 5% CO_2
SW480	ATCC	Colorectal adenocarcinoma	*Homo sapiens*	10% FBS in L-15	37°C,100% air
SW620	ATCC	Colorectal adenocarcinoma - Derived from metastatic site: (lymph node)	*Homo sapiens*	10% FBS in L-15	37°C,100% air
U2OS*	ATCC	Osteosarcoma	*Homo sapiens*	10% FBS in DMEM	37°C, 5% CO_2
WM266.4	ATCC	Melanoma	*Homo sapiens*	10% FBS in EMEM	37°C, 5% CO_2

* Obtained from the laboratory of Dr. Laura-Trinkle Mulcahy

Cells were thawed and expanded in the appropriate media (table 2.1). For cryopreservation, cells were stored in the liquid N_2 vapour phase in media + 10% DMSO (Sigma). All cells were passaged the same way with the exception of the HUVECS and Melanocytes. Briefly, cells were washed with 1X PBS and trypsinized in 0.25% Trypsin-0.53 mM EDTA (Gibco) until the cell layer was dispersed. Trypsinization was stopped with the addition of growth media. The appropriate number of cells was resuspended in growth media, and transferred to a new culture dish (Corning) (approximately 3-5x10^3

cells/cm^2). For primary Melanocytes, cells were washed with 1XPBS and trypsinized using Trypsin-EDTA for Primary Cells (ATCC). Trypsinization was stopped with Trypsin Neutralizing Solution (ATCC). Cells were transferred to a sterile centrifuge tube (Sarstedt) and centrifuged at 150 x g for 5 minutes. The supernatant was gently aspirated and the pellet resuspended in its media. Cells were counted on a hemocytometer and seeded in a new dish at a density of 2,500 to 5,000 cells per cm^2. HUVEC cells were washed with 1X PBS and trypsinized with 0.25% Trypsin-0.53 mM EDTA; trypsinization was terminated using Hank's Balanced Salt Solution 1X (Wisent). The cells were transferred to a sterile centrifuge tube and spun down at 300 x g for 5 minutes. Cells were counted and seeded in a new petri dish at a density of 2,500 to 5,000 cells per cm^2.

2.2 RNA extraction

Cells were grown to 70-80% confluence in a 10cm petri dish. Total RNA was harvested using an RNeasy mini kit (Qiagen) according to the manufacturer's instructions. Briefly, the cells were washed with 1XPBS, trypsinized and counted using a hemocytometer as above. In order to use the RNeasy mini kit, it is important that the number of cells does not surpass $7x10^6$ otherwise the RNA binding column capacity will be exceeded. Cells were lysed using the RLT buffer provided with 1% β-mercaptoethanol. The lysate was homogenized using a 20-gauge needle and and total RNA was captured by passage through a silica gel column. The column was washed with Buffer RDD containing DNase1 in order to digest the genomic DNA. Total RNA was eluted using RNase-free DEPC-treated water. RNA concentration was determined with

an eppendorf Biophotometer. The $OD_{260/280}$ ratio provides an estimate of the purity of RNA and A_{260} x 40 determines single-stranded RNA quantity in μg/μL. RNA quality and purity was assessed on a denaturing formaldehyde/agarose MOPS gel.

2.3 cDNA preparation

Total RNA extracted from specific cancer cell lines was used as a template for cDNA production using the GeneAmp RNA PCR kit (Applied Biosystems). Briefly, each 20μl cDNA reaction consisted of 5mM $MgCl_2$, 1x PCR buffer II, 1mM dNTPs, 1U/μl RNase Inhibitor, 2.5μM Random Hexamers, 2.5U/μl MuLV Reverse Transcriptase and 1μg RNA. PAW109 RNA served as a positive RT-PCR control and no RNA (ddH_20) served as a negative control. The cDNA reaction was performed in a Biometra Thermocycler (see the GeneAmp RNA PCR kit protocol for thermocycler conditions). The reactions were stored at -20^oC for future use.

2.4 RT-PCR analysis

FMNL2 isoforms found in A375, SW620 and SW480 cancer cell lines were identified by reverse transcription polymerase chain reaction (RT-PCR) analysis. A 100μl PCR reaction consisted of 2mM $MgCL_2$ solution, 1x PCR buffer I, ddH2O, 2.5U/100μl AmpliTaq DNA Polymerase, 20μl cDNA reaction produced from the specific cell line as well as 0.15 μM of both forward and reverse FMNL2 or control specific primers (table 2.2). The PCR reaction was performed in a Biometra Thermocycler (see the GeneAmp RNA PCR kit protocol for full PCR details and for the thermocycler conditions).

Table 2.2: Primers produced for cancer cell line RT-PCR analysis.

Name	Primer direction	Primer sequence	Amplicon length	Primer position (bp)
FMNL2 ITM	Forward	5'-CCTGTCTTTGTCCGGTTTGTGAAAGC-3'	362	2914
	Reverse	5'-CGTTCTGTTAATGGTGCCGAAATAACA ATG-3'		3276
FMNL2 YHY	Forward	5'-CCTGTCTTTGTCCGGTTTGTGAAAGC-3'	345	2914
	Reverse	5'-CTGTTCTCACTGAGGAATACCATTAC-3'		3258
RTPCR control IL-1α (RNA PAW109)	Forward	5'-GTCTCTGAATCAGAAATCCTTCTATC-3'	309	1044
	Reverse	5'-CATGTCAAATTTCACTGCTTCAATCC-3'		1352

A 1% agarose gel was loaded with 10µl of 1:1 PCR reaction: loading dye. Bands were visualized with ethidium bromide, excised and extracted (Sigma Genelute Gel extraction kit). The isolated amplified fragments were sequenced and their identity determined using the BLAST homology search engine. Splice form specific primers were designed (same as qPCR primers – see table 2.4) in order to confirm the presence of endogenous isoforms in SW620s, SW480s and A375.

2.5 Cloning

A variety of FMNL2 constructs were created for this work (see appendix 1 – Table 5.1). Full length (FL) FMNL2 constructs were cloned into pEF-plink2 encoding a C-terminal cherry tag (figure 2.1). Briefly, the 3'ends of each FMNL2 isoform was amplified by PCR directly from SW620 cDNA (table 2.3 for cloning primers). The conserved 5' portion of FMNL2 was digested out of FMNL2 full length pEF Flag construct (Vaillant et al 2008). Plasmids were purified using Genelute plasmid miniprep kit (Sigma) and Gen elute HP Plasmid Maxiprep kit (Sigma). FMNL2 FH1 FH2 C-terminal derivatives (cherry or myc-tagged) of each splice form were subcloned into

Figure 2.1: Full length FMNL2 isoform cloning. Full length FMNL2 isoforms were cloned in a C-terminal cherry-tagged pEF Plink2 plasmid in three different steps. The first and second parts of the FL construct were both digested (1-260 with *NCO1-BamH1* and 260-1952 with *BamH1 and EcoR1*) from a Full length FMNL2 pEF Flag template. These were ligated in a C-terminal cherry-tagged pEF Plink2 plasmid in a step-wise fashion due to another *NCO1* restriction site at 1508bp. The C-terminal varying ends of the FMNL2 isoforms were amplified by PCR directly from the endogenous cDNA generated by SW620 cells. These were digested with *EcoR1* and *Spe1* enzymes and ligated in at position 3 in the C-terminal cherry-tagged pEF Plink2 plasmid.

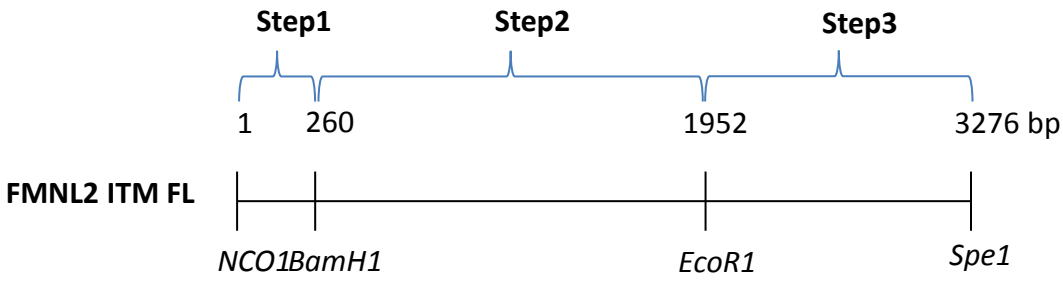
Step1
Step2
Step3
1
260
1952
3276 bp
FMNL2 ITM FL
NCO1BamH1
EcoR1
Spe1

1
260
1952
3258 bp
FMNL2 YHY FL
NCO1BamH1
EcoR1
Spe1

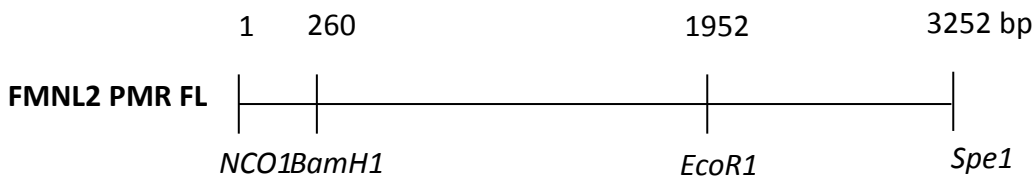
1
260
1952
3252 bp
FMNL2 PMR FL
NCO1BamH1
EcoR1
Spe1

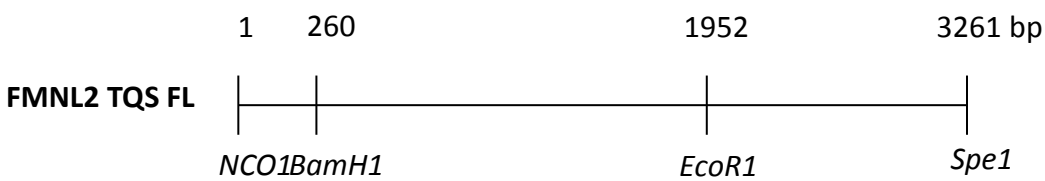
1
260
1952
3261 bp
FMNL2 TQS FL
NCO1BamH1
EcoR1
Spe1

pEF-NBRSS. FMNL2 1-503 and FMNL2 140-503 were subcloned into pEF Plink2 encoding a C-terminal cherry-tag. For lentiviral vector production FMNL2 full-length isoforms were sub-cloned into pLVX-IRES-mCherry and included a ribosome binding site introduced at the 5'end of FMNL2.

Table 2.3: Primers created for the assembly of FMNL2 FL pEF-Plink2 cherry constructs.

Name	Primer direction	Primer sequence	Amplicon length	Primer position (bp)
FMNL2 ITM (1952-end)	Forward	5'-TAGAATTCTGGAGGATTTAAATGTGGATG-3'	1325	1952
	Reverse	5'-AATGGTGCCGAAATAACAATGACTAGTGC-3'		3276
FMNL2 YHY (1952-end)	Forward	5'-TAGAATTCTGGAGGATTTAAATGTGGATG-3'	1307	1952
	Reverse	5'-CTCACTGAGGAATACCATTACACTAGTGC-3'		3258
FMNL2 PMR (1952-end)	Forward	5'-TAGAATTCTGGAGGATTTAAATGTGGATG-3'	1301	1952
	Reverse	5'-CATACAGACGAGCCGATGCGGACTAGTGC-3'		3252
FMNL2 TQS (1952-end)	Forward	5'-TAGAATTCTGGAGGATTTAAATGTGGATG-3'	1310	1952
	Reverse	5'-GTGGTGGAGGATACACAGAGCACTAGTGC-3'		3261
FMNL2 1-503	Forward	5'-GTCCATGGATGGGCAACGCAGGGAGCATG-3'	1509	1
	Reverse	5'-CGCCATACTGCCAGTTGTGGCTTCTGGCACA TTGTCCACTAGTGC-3'		1509
FMNL2 140-503	Forward	5'-GCCCATGGATGCTCTCATTTGCACAGTACGC G-3'	1092	418
	Reverse	5'-CGCCATACTGCCAGTTGTGGCTTCTGGCACA TTGTCCACTAGTGC-3'		1509
FMNL2 ITM FL + ribosome binding site	Forward	5'- GCGCCTCGAGGCCGCCGCCATGGGCAACG CAGGGAGCATG-3'	3276	1
	Reverse	5'- AATGGTGCCGAAATAACAATGTGAGCGGCC GCAT-3'		3276
FMNL2 YHY FL + ribosome binding site	Forward	5'-GCGCCTCGAGGCCGCCGCCATGGGCAACGC AGGGAGCATG-3'	3258	1
	Reverse	5'- CTCACTGAGGAATACCATTACTGAGCGGCC GCAT-3'		3258
FMNL2 PMR FL + ribosome binding site	Forward	5'-GCACTAGTGCCGCCGCCATGGGCAACGCAG GGAGCATG-3'	3252	1
	Reverse	5'- CATACAGACGAGCCGATGCGGTGAGCGGCC GCAT-3'		3252
FMNL2 TQS FL + ribosome binding site	Forward	5'-GCGCCTCGAGGCCGCCGCCATGGGCAACGC AGGGAGCATG-3'	3261	1
	Reverse	5'- GTGGTGGAGGATACACAGAGCTGAGCGGCC GCAT-3'		3261

2.6 Real-time PCR (qPCR)

Absolute expression levels of each FMNL2 isoform was determined by real-time PCR (qPCR). Standard curves were generated using a dilution series of plasmid templates corresponding to each isoform (10^2, 10^3, 10^4, 10^5, 10^6 copies per tube). QPCR conditions were optimized to obtain a standard curve starting no earlier than 15 CTs and finishing no later than 35 CTs. Note that a standard curve was also established with a β-actin template to serve as a "loading" standard. Each experiment included standards, no template controls and unknowns and each sample was assayed in triplicate. Standard reactions contained 5µl of a specific FMNL2 isoform template dilution, 5µl of FMNL2 isoform primer (final concentration: 300ng/well/primer) (table 2.4) and 10µl or the SYBR Advantage qPCR Premix (Clontech). Unknowns reactions were 5µl cDNA (0.05µg/tube), 5µl primers and 10µl SYBR Advantage qPCR Premix. No template reactions were 5µl primers, 10µl of SYBR Green mix and 5µl ddH2O. 5-carboxy-X-Rhodamine (ROX) was also included in the SYBR Green Advantage qPCR Premix and served as a passive loading reference dye.

Table 2.4 Primers produced for qPCR analysis.

Name	Primer direction	Primer sequence	Ampli-con length	Primer position (bp)
FMNL2 ITM	Forward	5'-GCCATTGAAGATATTATCACAGATC-3'	115	3148
	Reverse	5'-AACTTGCGTTCTGTTAATGGTG-3'		3262
FMNL2 YHY	Forward	5'-CTGAAGACTGTGCCCTTTACTGCT-3'	87	3172
	Reverse	5'-CCTGTTCTCACTGAGGAATACCATTAC-3'		3258
FMNL2 PMR	Forward	5'-CATTGAAGATATTATCACAGCCTTA-3'	87	3150
	Reverse	5'-GAGGATCTTAGAAACCAACCATA-3'		3235
FMNL2 TQS	Forward	5'-GATATTATCACAGCCTTAAAGAAGAAT-3'	106	3157
	Reverse	5'-TGGTGGAGGATACACAGAGCT-3'		3262
FMNL2 total isoforms	Forward	5'-GCTCCTCCCTTAGCACCT-3'	127	1750
	Reverse	5'-GCCAATCAAGACGAAGTTCAGA-3'		1875
β-actin	Forward	5'-GCACCACACCTTCTACAATGAG-3'	122	258
	Reverse	5'-GACCCAGATCATGTTTGAGACC-3'		378

The qPCR reactions were performed on an Mx 3005P qPCR machine (Stratagene). The Mx3005P plots the detected fluorescence emitted by SYBR Green against the number of cycles on a logarithmic scale. A threshold is detected for the background fluorescence. The number of cycles when the fluorescence detected surpasses this base-threshold is termed the threshold cycle (Ct). The real-time cycler conditions consisted of 3 different segments: 1) Enzyme activation for 15 minutes at 95^{o}C, 2) 40 cycles of 15 seconds denaturation (94^{o}C), 30 seconds annealing (55^{o}C) and 30 seconds extension (72^{o}C). The third segment consists of the melting curve (1 minute at 95^{o}C, 30 seconds at 55^{o}C and 95^{o}C for 30 seconds). Briefly, dsDNA is denatured by a stepwise rise in temperature with fluorescence emission being detected at each step. When the fluorescence intensity drops at a specific melting temperature, it is possible to attribute this melting temperature to the specific product of interest. In order to evaluate the absolute copy number of FMNL2 isoforms in each human cell lines, we used the standard curves obtained with the plasmid templates to determine the relationship between the fluorescent signal (the CT value) and FMNL2 mRNA copy number.

2.7 Immunofluorescence

Coverslips used for immunofluorescence were acid-treated with a 40% HCl, 60% ethanol solution for 5 hours. After multiple washes with distilled water, the coverslips (Fisher scientific) were left to soak in 70% ethanol. The next day, they were transferred to a fresh 70% ethanol solution. Once flamed, the coverslips were inserted in 6 well plates (Corning).

For immunofluorescence NIH-3T3 Fibroblasts were seeded at a density of 125 000 cells/well in 6-well plates containing acid-washed coverslips and 10% DBS DMEM media. On the following day the cells were transfected using polyethylenimine (PEI) and a total of 1.5µg DNA. Briefly, the appropriate DNA was added to Optimem and PEI and incubated 20 minutes at RT. Following incubation the DNA: PEI complexes were added to the cells in 1mL. After 5 hours at 37^{o}C (CO_2 5%), the media was replaced with 10 % DBS in DMEM (for FMNL2 localization assay) or replaced with starving media (0.5% DBS in DMEM) (for stress fibers and acetylated microtubules assays). After 24 hours, the cells were fixed with 4% Paraformaldehyde (PFA) in PBS for 15 minutes, washed 3 times with 1x PBS (5 min) and permeabilized for 30 minutes with 0.3% Triton X-100, plus 10% horse serum in 1XPBS. Note that in the acetylated microtubule assay, the cells are left in starving media after transfection for 48 hours (instead of 24 hours) and the cells were fixed with cold methanol for 10 minutes, washed and permeabilized as described.

Cells were incubated at room temperature with the appropriate primary antibody in 0.03% Triton X-100 plus 5% horse serum in 1X PBS. After 1 hour, cells were washed 3 times in 1X PBS and incubated with the appropriate secondary antibody in 0.03% Triton X-100 plus 5% horse serum in 1X PBS at room temperature for 1 hour (see table 2.5 for antibody details). The cells were washed 3 times in 1X PBS and once in ddH_2O. They were then mounted on slides (25x75x1.0 mm by Fisher scientific) with Vectashield mounting media (with DAPI) (Vectashield Vector Laboratories). Images were captured on a Zeiss Axio Imager Z1 fluorescence microscope using a 63X Plan Apochromat objective and an AxioCam HRm camera. Images were processed using Axiovision software. Optical sections were obtained with the apotome structured illumination slider.

Table 2.5: Antibodies used for immunofluorescence assays.

Primary/secondary antibody	Antibody	Dilution	Company
Secondary	Fluorescein-Phalloidin	1:100	Molecular Probes
Primary	Rabbit anti-Myc	1:500	Santa Cruz
Secondary	Donkey anti-Rabbit 594	1:200	Jackson Immunoresearch
Primary	Mouse acetyl-alpha-tubulin	1:1000	Sigma
Secondary	Donkey anti-Mouse 488	1:200	Jackson Immunoresearch

2.8 Serum Response Factor (SRF) assay

NIH 3T3 fibroblasts were seeded on a 6-well plate at a density of 125 000 cells/well one day prior to transfection. In each tube, 0.1µg of a FMNL2 FL Plink 2 cherry isoform or FMNL2 FH1 FH2 NBRSS myc tagged isoform was added to two reporter plasmids: p3D.A.Luc (50ng/well) and pMLVLacZ (250ng/well), in 50µl Optimem (Gibco). A separate sample served as a positive control containing pEF-SRFVP16 (50ng/well) + the two reporter constructs. Cells were transfected using PEI as described above. After 5 hours, the Optimem was replaced with starvation media (0.5% FBS in DMEM) and left to incubate at 37^{o}C (5% CO_2).

After 24 hours, the cells were gently washed with chilled 1XPBS and harvested in 0.5ml of 1XPBS. The cells were pelleted by centrifugation for 5 minutes at 5000rpm at 4^{o}C. The pellet was then resuspended with 150µl of 1x Reporter Lysis buffer (Promega) and frozen at -20^{o}C overnight. The next day, the cell lysate was thawed at 37^{o}C, vortexed thoroughly, and spun down at maximum speed for 10 minutes at 4^{o}C.

For the luciferase assay, 30µl of the cell lysate and 40µl of luciferin reagent (Luciferase assay system with reporter lysis buffer - Promega) were added to the wells of a white 96 well plate (Thermo Fisher Scientific). Luciferase activity was measured

immediately upon addition of luciferin and read on an LMAXII Luminometer (Molecular Devices). A β-galactosidase (β-gal) assay was performed in parallel to control for transfection efficiency. Briefly, 30µl of the cell lysate and 200µl of 0.4mg/mL CPRG mix [10X chlorophenol red β-D galactopyranoside (Calbiochem) diluted in 1X β-gal buffer (10mM MgSO4, 0.5% B-mercaptoethanol in PBS)] were added to the wells of a clear 96 well plate (Costar) and incubated at 37^{o}C for 1h. Absorbance at 595nm was measured on a SpectraMax M2 plate reader (Molecular Devices). FMNL2 expression levels were determined by immunoblotting.

2.9 Western blotting

Cancer cells were grown to 70-80% confluence in a 10cm petri dish or a 6 well plate (3.5 cm/well), washed with 1XPBS and harvested in 1xSDS buffer. Cell lysis was then subjected to an 8% SDS-PAGE (25% of 40% Acrylamide, 1.875M Tris/SDS mix, 10% Ammonium Persulfate, 0.2% Temed and ddH2O) and transferred to a PVDF membrane (BioRAD). The blot was blocked with 5% skim milk in 1XPBS + 0.1% tween 20 for 1 hour and then probed with 1:1000 Rabbit-anti-FMNL2 antibody for another hour. The blot was washed and probed with 1:5000 Donkey-anti-Rabbit secondary antibody conjugated to horseradish-peroxidase (HRP). Chemiluminescence was performed using the western HRP substrate reagent (Millipore). Visualization was achieved using the GE Image Quant LAS4010 Imaging System. Antibodies were stripped off with a 0.1M Glycine and 0.5% SDS solution, at pH2.5, for 1 hour. The blot was then blocked for an hour and probed with a mouse-anti-tubulin primary antibody for another hour. The blot was washed and probed with Donkey-anti-mouse secondary antibody

conjugated to horseradish-peroxidase (HRP). Chemiluminescence and visualization was performed as described previously.

2.10 FMNL2 knockdown

A375 or WM266.4 melanoma cells were seeded in a 6 well plate or in a 3.5 cm petri dish (Corning) with a coverslip, at a density of 125 000 cells/well. The following day, cells were transfected with siRNA duplexes using a FMNL2 siRNA TriFECTa Dicer-Substrate RNAi Kit (IDT). Briefly, in a 1.5ml tube, 8μM of FMNL2 siRNA duplex was added to a total of 200μl in Optimem. A second tube contained 8μM Scramble siRNA duplex in Optimem, a third tube enclosed 10μM of a Fluorescent-labbeled duplex (TYE 563) in Optimem and a final tube only contained the 200μl of Optimem (see table 2.6 for duplex sequences). In a separate 15ml ependorf tube, 6μl of transfection reagent DharmaFECT #1 (Thermo Scientific) was added to 194μl of Optimem for each reactions (knockdown, scramble and mock). After 5 minutes of incubation at ambient temperature, the 200μl DharmaFECT solution was added to each 1.5ml tube, vortexed, and was left to incubate for another 20 minutes at room temperature. The 400μl samples containing the siRNA duplexes and mock were individually added to each well of the 6 well plate filled with 1.6ml of fresh DMEM 10% FBS (A375) or EMEM 10% FBS (WM266.4). These plates were left to incubate at 37^{o}C (5% CO_2) for 48 hours. The fluorescent control was added to the petri dish with a coverslip filled with 1.6ml of fresh DMEM 10% FBS (A375) or EMEM 10% FBS (WM266.4). This dish was left to incubate for 24 hours. The coverslip was then fixed with cold methanol and mounted on a slide with vectasheild (with DAPI) (Vectasheild Vector Laboratories). The fluorescent-labeled duplex served as a transfection control, thus, when visualizing under the Zeiss Axio Imager Z1

fluorescence microscope, it is important to observe 90-100% transfection efficiency. After 48 hours incubation the cells are harvested and are subjected to SDS-PAGE and immunoblotted to detect FMNL2 expression levels.

Table 2.6: Duplex sequences generated by Integrated DNA Technologies for knockdown assay.

Duplex name	Direction	Sequence
FMNL2 siRNA (3'UTR region)	Forward	5'-CCUGUUCAGAUUAAUCAAAGCAATA-3'
	Reverse	5'-UAUUGCUUUGAUUAAUCUGAACAGGUA-3'
siRNA scramble	Forward	5'-CGUUAAUCGCGUAUAAUACGCGUAT-3'
	Reverse	5'-AUACGCGUAUUAUACGCGAUUAACGAC-3'
TYE 563 DS (fluorescent control)	Forward	5'-/5TYE563/TCCUUCCUCUCUUUCUCUCCCUUGUGA-3'
	Reverse	5'-/5TYE563/TCACAAGGGAGAGAAAGAGAGGAAGGA-3'

2.11 Migration assay

A375 melanoma cells were seeded in a 6 well plate (Corning), and in a 3.5 cm petri dish (Corning) with a coverslip, at a density of 125 000 cells/well. The following day, the cells were treated with siRNAs (see knockdown procedure). After 48 hours, A375 cells were washed with 1XPBS, trypsinized and counted with a hemocytometer as described previously. 70µl of DMEM 10% FBS containing 100 000 cells were added to each chamber of an ibidi insert contained in a 3.5 cm petri dish (Ibidi). This ibidi culture–insert is composed of two chambers separated by a 500 µm wide median. Cells can be seeded in both chambers and grown to confluency. The outside of the insert was filled with 1.5ml of DMEM 10% FBS. Cells were also seeded for immunoblotting in order to verify FMNL2 knockdown. The next day, the insert was carefully removed using sterile tweezers, leaving a gap between the cells from each chamber. The plate was gently washed with DMEM 10% FBS to remove any floating cells. Live imaging was performed with a Zeiss Pascal confocal microscope (10x phase 1 objective) under a controlled

environment (5% CO_2, 37^oC). This permitted us to visualize the closure of the "wound" for 48 hours.

2.12 Virus production

HIV-1-based, lentiviral expression vector pLVX-IRES-mCherry containing FMNL2 full-length isoforms of interests were used for virus production (virus production was done by Allan Heibein). Briefly, 10 plates (15cm) of 293T cells at a 70% confluence were transfected with 96.85µg of the FMNL2 pLVX-IRES-mCherry construct, 53.95µg of the envelop plasmid (pMD2G coding for VSV-G envelope), 99.15µg of the packaging plasmid psPAX2 and PEI transfection reagent. The newly created virus was collected by absorbing the media every day for the next 48 hours. The virus was concentrated and titrated in order to determine the ratio of infectious virus particles to the number of cells, also called multiplicity of infection (MOI).

2.13 FMNL2 rescue assay

A375 melanoma cells were seeded at a density of 125 000 cells/well, in a 6 well plate and in a 3.5 cm petri dish (Corning) comprising a coverslip. The next day, the cells were treated with siRNAs (see knockdown procedure) for 24 hours and then infected with the different FMNL2 full-length isoform specific lentiviral expression vectors at a MOI of 10. The cells were then left to incubate for another 24 hours before seeding them for an invasion assay, for immunoblotting or for immunofluorescence. The next day, the harvested cells were subjected to SDS-PAGE and immunoblotted to verify FMNL2 knockdown, FMNL2 rescue and FMNL2 overexpression.

The cells for immunofluorescence were fixed with PFA and permeabilized as described previously. Cells were incubated at room temperature with a Rabbit-anti-FMNL2 antibody (FRL2 818) at a 1:100 dilution in 0.03% Triton X-100 plus 5% horse serum in 1X PBS at room temperature. After 1 hour, cells were washed 3 times in 1X PBS and incubated with a secondary antibody, Donkey-anti Rabbit 488 (Jackson Immunoresearch), at a 1:200 dilution, in 0.03% Triton X-100 plus 5% horse serum in 1X PBS at room temperature for 1 hour. The cells were washed 3 times in 1X PBS and once in ddH_2O. They were then mounted on slides with vectasheild mounting media (with DAPI). Visualization was performed with the Zeiss Axio Imager Z1 fluorescence microscope with the 63X objective as described previously. The presence of mCherry allowed us to verify that 90-100% of the A375 cells were infected.

2.14 Transwell invasion assay

6.5mm/8µm transwell inserts (Costar #3422) were coated with 100µl of 1:1 growth factor reduced Matrigel (#356230): DMEM. Transwells were incubated at 37°C for 1h to polymerize. The freshly polymerized transwells were flipped upside down and the underside of the inserts were coated with 50µl of a 1:20 matrigel : DMEM solution. The transwells were placed back into the 37°C incubator for 1h. 7000 A375 cells in 70uL of DMEM (0.5% FBS) were seeded on the underside of the inserts and allowed to adhere for 3 hours at 37^oC. After the 3 hour incubation, the insert was flipped into a 24 well plate containing 600µl of DMEM (0.5% FBS) on the bottom. 200µl of 20% FBS DMEM was carefully added to the top of the insert. Cells were left to invade through the matrigel at 37^oC (5% CO_2) for 72h. (figure 2.2)

After 72h, cells were fixed with CSK buffer (containing 8% paraformaldehyde) for 30 minutes, washed with PBS and then permeabilized with 0.3% Triton X-100 for another 30 minutes. The cells were stained with 50μg/mL of Propidium Iodide (PI) overnight at 4^{o}C. The transwells were then gently washed once in PBS and once in ddH_2O, and then placed onto a 35mm Mat-Tek coverslip culture dish with 15μl Vectashield (Vector Labs). Imaging was accomplished by using the Zeiss Pascal with a 40x 1.30 oil objective. Images were taken for 100 planes (50 planes before the transwell membrane and 50 planes into the matrigel), with the Z step set at Nyquist sampling frequency (~0.5μM/slice).

Figure 2.2: Inverse transwell invasion assay. A375 melanoma cells are carefully seeded on the underside of the transwell inserts where they are left to invade through the matrigel matrix for 72h, towards the 20% FBS DMEM milieu (attractant). Imaging is accomplished with the Zeiss Pascal confocal microscope by taking 50 planes (0.5μm/plane) before the transwell membrane and 50 planes (0.5 μm/plane) into the matrigel

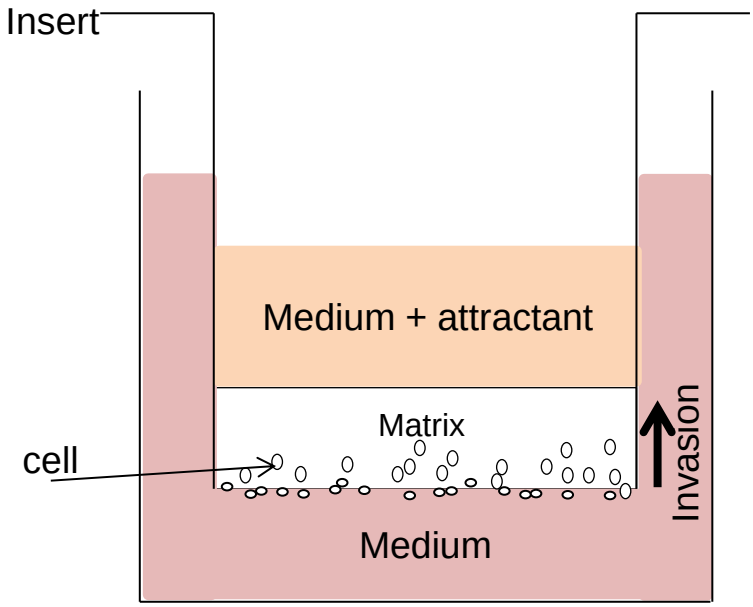
Insert
Medium + attractant
Matrix
cell
Invasion
Medium

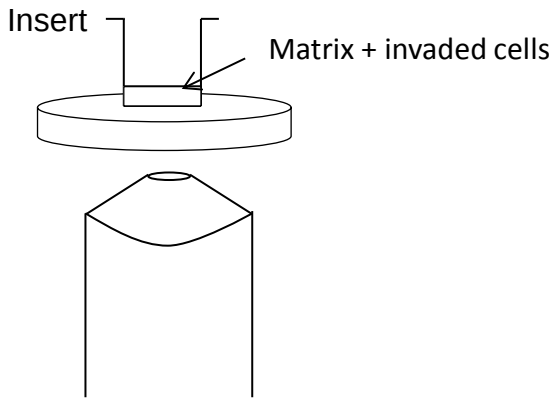
Insert
Matrix + invaded cells
Laser scanning
Confocal microscope

PI
Invasion

Chapter 3

Results

3.0 Results

3.1 Identification of four FMNL2 isoforms in SW620, SW480 and A375 cancer cell lines

Two human FMNL2 isoforms have been reported in the literature: FMNL2 ITM and FMNL2 YHY (Katoh and Katoh 2003) and there are many other predicted splice variants in chimps and mice (Chapter 1). FMNL2 overexpression results in increased invasiveness and metastasis of CRCs (Zhu, Liang, and Ding 2008; Li *et al.* 2010; Zhu *et al.* 2011) and knockdown of FMNL2 expression in two melanoma cell lines inhibits their invasion (Kitzing *et al.* 2010; Block *et al.* 2012). To identify which FMNL2 splice forms are expressed in three human cancer cell lines we performed RT-PCR on total RNA isolated from SW620, SW480 CRCs and A375 melanoma cells. SW480 cells originate from a primary CRC tumor while SW620 cells were later isolated from a lymph node metastasis in the same patient making them an ideal system to study the genetic changes associated with the metastatic switch (Leibovitz *et al.* 1976).

The first RT-PCR reactions were performed using primers based on the FMNL2 ITM and YHY sequence. In addition to the predicted amplicons, we also detected additional specific amplified products. Sequencing of the amplified DNA showed these to be FMNL2 PMR and FMNL2 TQS (figure 3.1a). These results were confirmed using RT-PCR and primers designed to uniquely amplify each splice form (figure 3.1b). The four isoforms were named for the final three amino acids at their C-termini (ITM, PMR, TQS, YHY) (Figure 3.2).

The alternative splicing of FMNL2 mRNA does not affect the region encoding the known conserved functional and regulatory domains. All of the variation occurs in the

Figure 3.1: RT-PCR analysis of FMNL2 isoform expression in SW480, SW620 CRC cells and A375 melanoma cells. 1% agarose gels demonstrating RT-PCR results using cDNA generated from SW480, SW620 CRC cells and A375 melanoma cells RNA. A) All bands have been sequenced to determine the identity of the amplified products: 1- FMNL2 TQS (410bp), 2- FMNL2 PMR (365bp), 3- FMNL2 YHY (345bp) 4- RT-PCR control (plasmid pAW109) (308bp). Sequencing results demonstrates that the different isoforms found in the three cell lines are identical but seem to be expressed at different levels. B) Direct amplification of FMNL2 3' splice variants.

A

SW480
SW620
A375
1
2
3
4
500
400
300
500
400
300
500
400
300

B

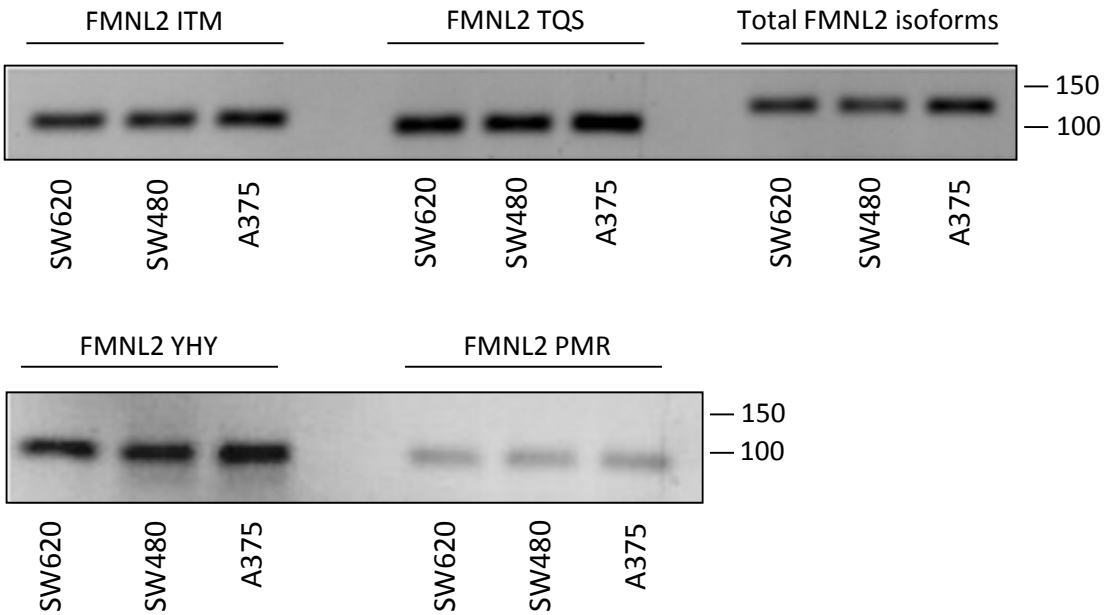
FMNL2 ITM
FMNL2 TQS
Total FMNL2 isoforms
150
100
SW620
SW480
A375
SW620
SW480
A375
SW620
SW480
A375
FMNL2 YHY
FMNL2 PMR
150
100
SW620
SW480
A375
SW620
SW480
A375

Figure 3.2: FMNL2 isoform sequence alignment. FMNL2 isoforms all contain conserved functional and dimerization domains but vary in their C-terminal motif following the DAD domain.

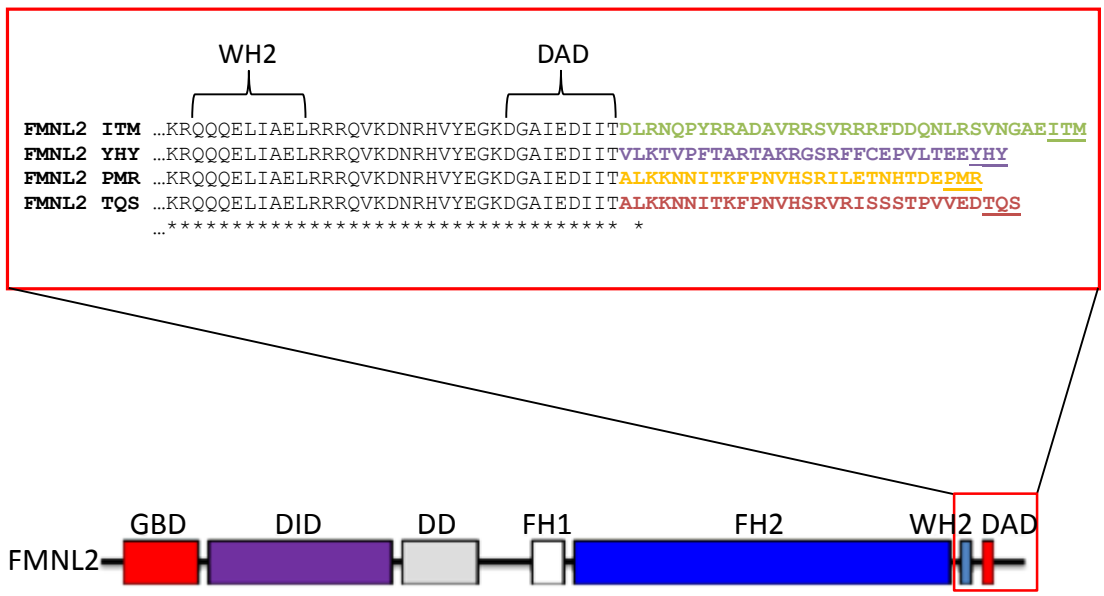
WH2
DAD
FMNL2 ITM …KRQQQELIAELRRRQVKDNRHVYEGKDGAIEDIITDLRNQPYRRADAVRRSVRRRFDDQNLRSVNGAEITM
FMNL2 YHY …KRQQQELIAELRRRQVKDNRHVYEGKDGAIEDIITVLKTVPFTARTAKRGSRFFCEPVLTEEYHY
FMNL2 PMR …KRQQQELIAELRRRQVKDNRHVYEGKDGAIEDIITALKKNNITKFPNVHSRILETNHTDEPMR
FMNL2 TQS …KRQQQELIAELRRRQVKDNRHVYEGKDGAIEDIITALKKNNITKFPNVHSRVRISSSTPVVEDTQS
…********************************** *
GBD
DID
DD
FH1
FH2
WH2 DAD
FMNL2

region C-terminal to the DAD motif and based on analogy to other formins is expected to affect FMNL2 activity as well as autoregulation (Wallar *et al.* 2006; Vaillant *et al.* 2008; Heimsath and Higgs 2012). We also noted in the initial RT-PCR reactions that there may be differential expression of FMNL2 isoforms when comparing invasive and non-invasive cells (figure 3.1a).

3.2 FMNL2 TQS isoform is highly expressed in invasive human cancer cell-lines

FMNL2 has been reported to be overexpressed in many malignant tissues including colon cancers and melanomas (Zhu, Liang, and Ding 2008; Kitzing *et al.* 2010). Our RT-PCR results suggest that there is a variation in isoform expression levels between invasive and non-invasive cancer cell lines (figure 3.1a). Thus, we used qPCR to quantify total FMNL2 expression levels in a variety of cancer cell-lines selected either for their style of invasion or where FMNL2 expression is thought to be elevated (table 3.1). The qPCR results show high expression levels of total FMNL2 mRNA in cancer cell lines using an amoeboid style of invasion (A375, LS174T and WM266.4). Total FMNL2 expression is also increased when comparing non-invasive SW480 to invasive SW620 colorectal cells (figure 3.3a). FMNL2 is not expressed, however, in U2OS cells. Subsequently, we used isoform-specific primers to quantify the levels of each FMNL2 splice variants. In all cases TQS was found to be the major FMNL2 isoform expressed in invasive CRC, melanoma and thyroid cancer cells (figure 3.3b). We were unable to obtain interpretable results with PMR. Nevertheless, the sum of the expression of the individual splice forms compared to the expression level of total FMNL2 suggests that we are not missing any key isoforms in the cancer cell lines. The predominance of TQS

Table 3.1: Human cell lines for qPCR analysis.

Human cell line	Description
A375	Melanoma, amoeboid
A431	Epidermoid carcinoma, mesenchymal
HTB107	Squamous thyroid carcinoma
HUVEC	Endothelial (umbilical vein)
LS174T	CRC, amoeboid
Melanocytes	Epidermis (basal layer)
SW480	CRC, non-invasive
SW620	CRC, metastatic
U2OS	Osteosarcoma
WM266.4	Melanoma, amoeboid

Figure 3.3: Expression of FMNL2 in different cell lines. A) QPCR data showing the absolute expression level of total FMNL2 isoforms in human cell lines. B) QPCR results demonstrating the absolute expression level of FMNL2 isoforms in each cell line. Note the high relative expression of FMNL2 TQS in invasive colorectal carcinoma (SW620) as well as melanoma cell lines WM266.4 and A375. FMNL2 isoforms were detected with the use of isoform specific primers and SYBR green/ROX chemistry using absolute plasmid-based standards. N=3, Error bars represent standard error of the mean (SEM).

A

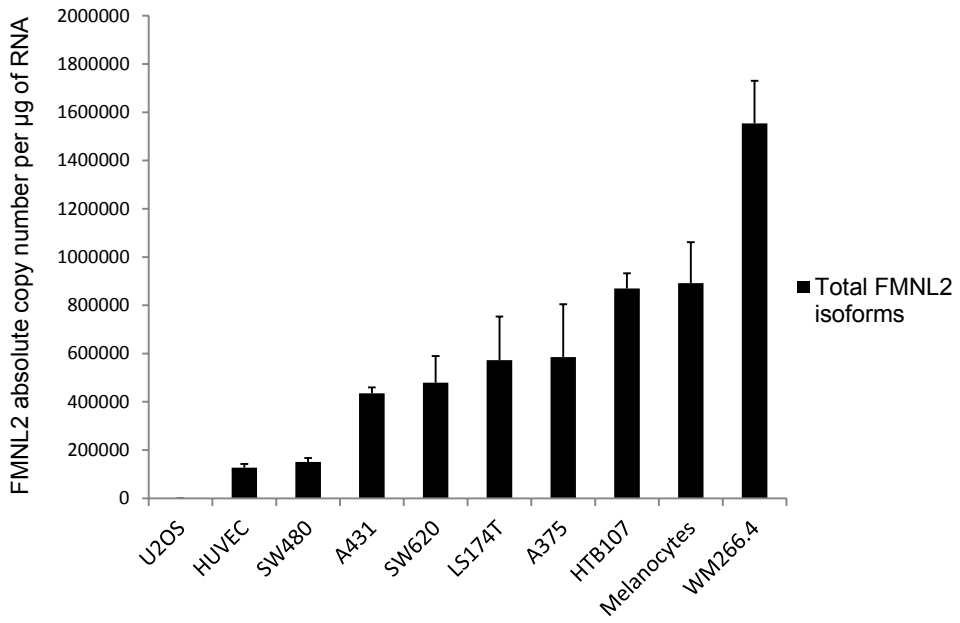
FMNL2 absolute copy number per µg of RNA
2000000
1800000
1600000
1400000
1200000
1000000
800000
600000
400000
200000
0
U2OS
HUVEC
SW480
A431
SW620
LS174T
A375
HTB107
Melanocytes
WM266.4
Total FMNL2 isoforms

B

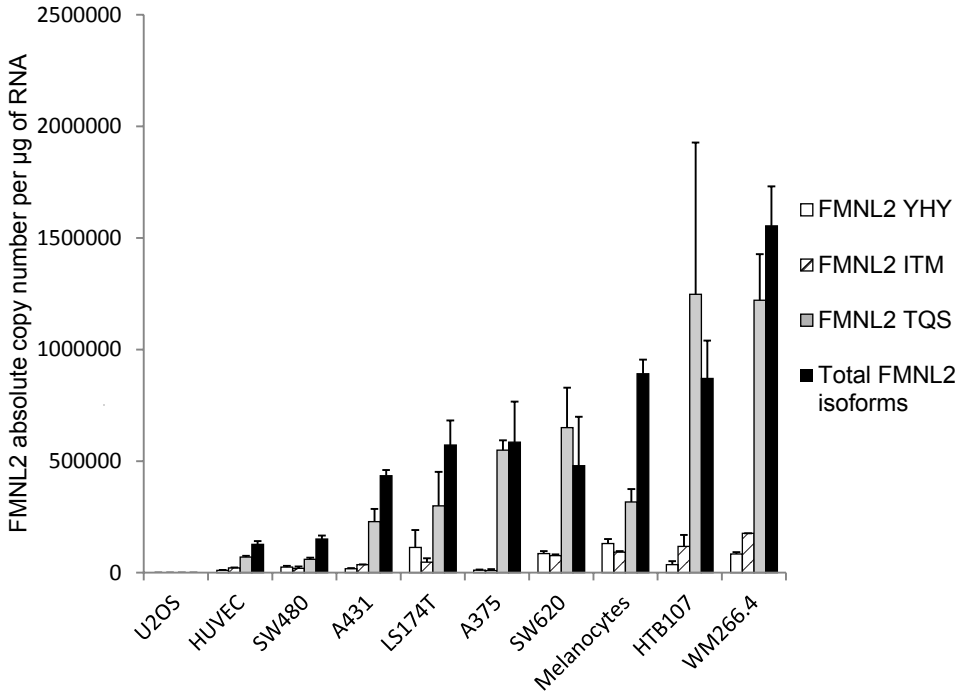
FMNL2 absolute copy number per µg of RNA
2500000
2000000
1500000
1000000
500000
0
U2OS
HUVEC
SW480
A431
LS174T
A375
SW620
Melanocytes
HTB107
WM266.4
FMNL2 YHY
FMNL2 ITM
FMNL2 TQS
Total FMNL2 isoforms

expression also suggests that it may represent an "invasive" isoform of FMNL2 preferentially expressed in highly invasive cells.

3.3 Full length FMNL2 splice variants localize at the plasma membrane

An N-myristoylation site is present at the N-terminus of FMNL1 and this modification targets FMNL1 protein to the plasma membrane (Han *et al.* 2009). FMNL2 contains the same N-myristoylation consensus sequence suggesting that it is similarly modified. Full length (FL) FMNL2 with an N-terminal epitope tag localized to the cytoplasm, however, the N-terminal epitope tag is predicted to disrupt the myristoylation signal (Vaillant *et al.* 2008). In this work, two FL FMNL2 constructs were generated: one with an N-terminal cherry tag and one with a C-terminal cherry tag, to test the effects on FMNL2 subcellular localization. Thus, we transiently transfected NIH 3T3 cells with both FMNL2 constructs and assessed their subcellular localization by immunofluorescence. In this case, the N-terminally tagged FL construct localized in the cytoplasm, consistent with what was previously reported. In contrast, a FL FMNL2 C-terminally cherry tagged protein accumulated at the plasma membrane (figure 3.4) suggesting that FMNL2 is also targeted to the plasma membrane by N-myristoylation. To further explore this model, we tested the effects of truncation at the N-terminal and C-terminal domains on subcellular localization of the FMNL2 protein. We transfected NIH 3T3 cells with a C-terminal cherry tagged FMNL2 140-503 AA derivative and a C-terminal cherry tagged FMNL2 1-503 AA derivative. We found that the 140-503 derivative was primarily cytoplasmic while the 1-503 construct was efficiently targeted to the plasma membrane (figure 3.4).

Figure 3.4: N-terminal tags on FMNL2 interfere with membrane targeting. N-terminal derivatives of FMNL2 as well as full-length FMNL2 isoforms were expressed by transfection in NIH 3T3 cells. Proteins were tagged with C-terminal cherry (*red*) in exception of full-length FMNL2 N-terminally tagged with cherry (*red*); actin was visualized with fluorescein phalloidin (*green*) and nucleus with DAPI (*blue*). FMNL2 derivative 1-503 and C-terminally tagged full-length FMNL2 localize to the plasma membrane. FMNL2 derivative 140-503 as well as the N-terminally tagged full-length FMNL2 are both contained in the cytoplasm and are unable to target the plasma membrane. Scale bar = 20μm.

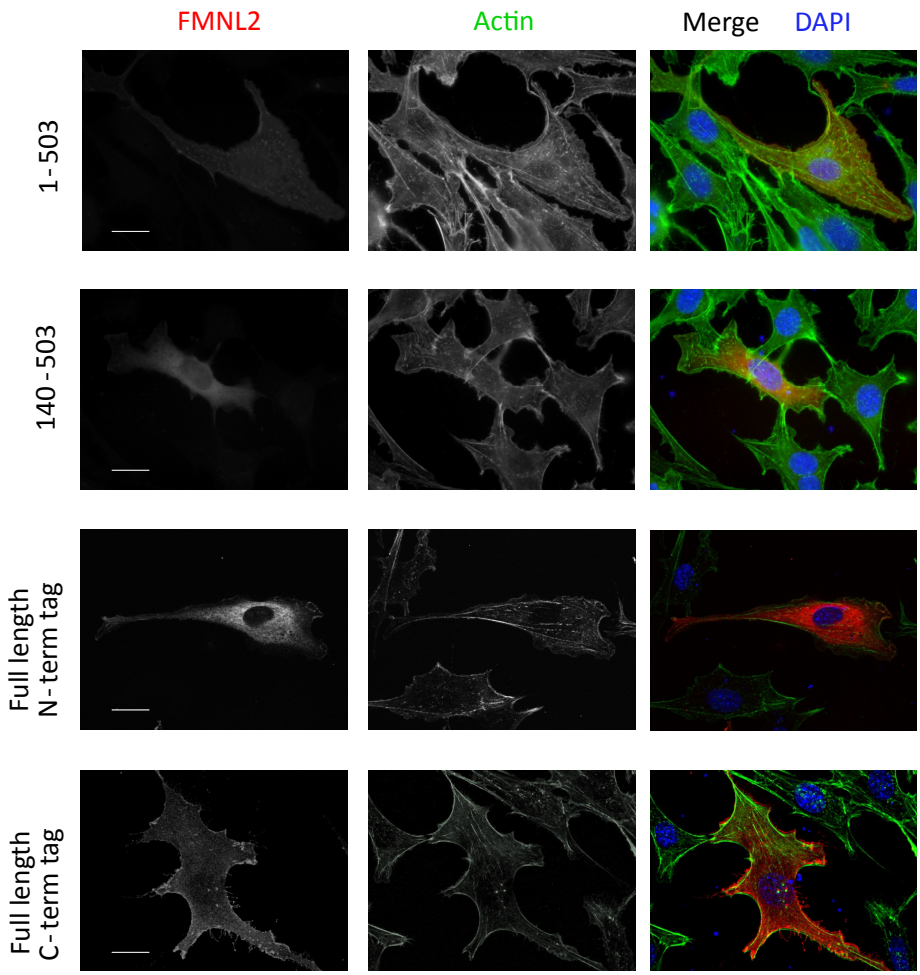
FMNL2
Actin
Merge
DAPI
1-503
140-503
Full length N-term tag
Full length C-term tag

Figure 3.5: Subcellular localization of FMNL2 isoforms. Full-length FMNL2 isoforms were expressed by transfection in NIH 3T3 cells. Proteins were tagged with C-terminal cherry (*red*); actin was visualized with fluorescein phalloidin (*green*) and nucleus with DAPI (*blue*). FMNL2 isoforms localize throughout the cytoplasm and shows apparent membrane targeting. Scale bar = 20μm.

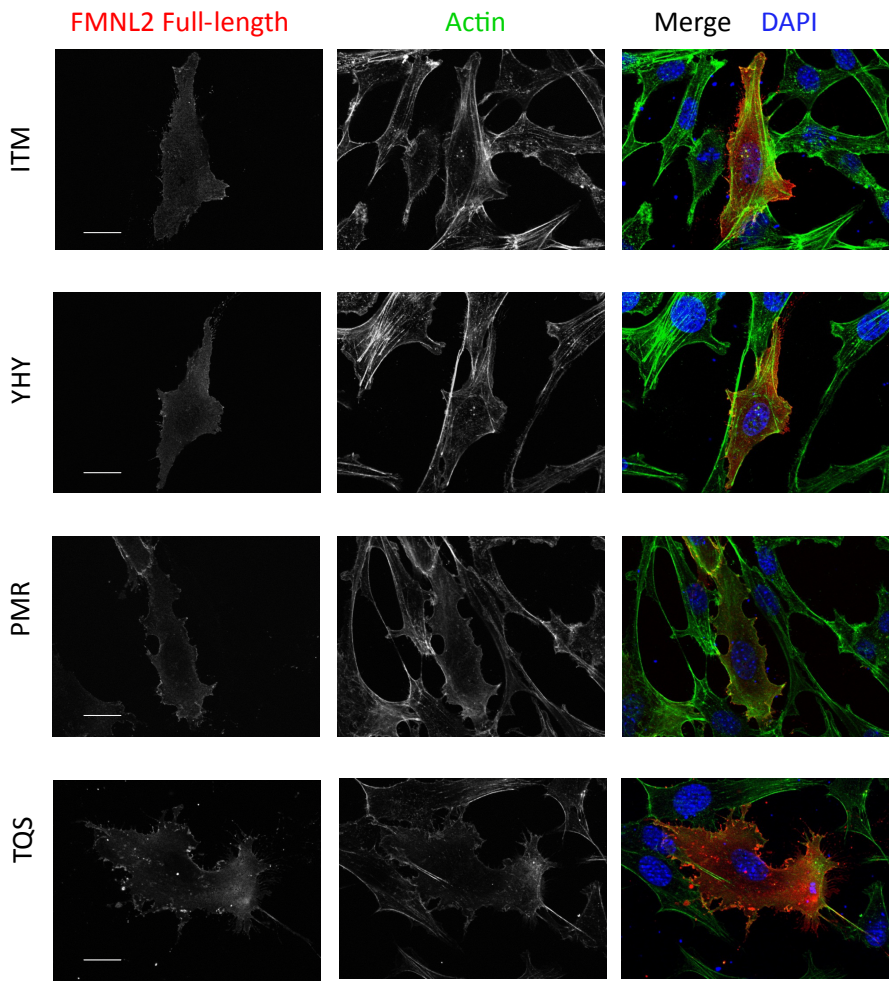
FMNL2 Full-length
Actin
Merge
DAPI
ITM
YHY
PMR
TQS

In similar experiments we transiently transfected C-terminal cherry tagged FL constructs of each FMNL2 splice variant in NIH 3T3 fibroblast cells and assessed their subcellular localization and effects on actin stress fiber formation. As expected, each of the FL FMNL2 isoform derivatives are autoinhibited and do not induce stress fiber formation. In addition, consistent with their modification by N-myristoylation, each of the FMNL2 isoforms accumulated at the plasma membrane (See left panels at figure 3.5).

3.4 Active derivatives of FMNL2 isoforms induce stress fiber formation

To compare activity of each isoform we generated constitutively active (CA) versions of FMNL2 consisting of FH1, FH2, WH2, DAD domains as well as the alternative C-terminal region. Each active FMNL2 derivative was transiently transfected in NIH 3T3 cells and their subcellular localization and the effects on stress fiber formation were visualized by immunofluorescence. A CA derivative of FMNL2 lacking the C-terminal domain following the DAD (FH1-1045) was also transfected to test the effect on stress fiber formation. In this assay, each CA splice variant was distributed throughout the cytoplasm and was able to induce stress fiber formation to a similar level (Figure 3.6 a,b).

3.5 FMNL2 isoforms differ in activity and regulation

As with other formins, FMNL2 protein is able to induce actin polymerization and stress fiber formation (Vaillant *et al.* 2008). A quantitative readout of the effects on actin polymerization *in vivo* can be obtained using an SRF reporter gene assay. Briefly, the SRF reporter is activated by the depletion of monomeric G-actin and serves as a rapid

Figure 3.6: Stress fiber induction by C-terminal derivatives of FMNL2 isoforms. A) C-terminal derivatives of FMNL2 isoforms were expressed by transfection in NIH 3T3 cells. Proteins were tagged with N-terminal myc and visualized with primary antibody Rabbit anti-Myc conjugated to secondary antibody Donkey anti-Rabbit 594 (*red*); actin was visualized with fluorescein phalloidin (*green*) and nucleus with DAPI (*blue*). Scale bar = 20μm. B) Quantification of stress fiber formation. All FMNL2 isoforms induce stress fiber formation at a similar extent. N=3, with more than 100 cells counted per sample. Error bars represents SEM.

A

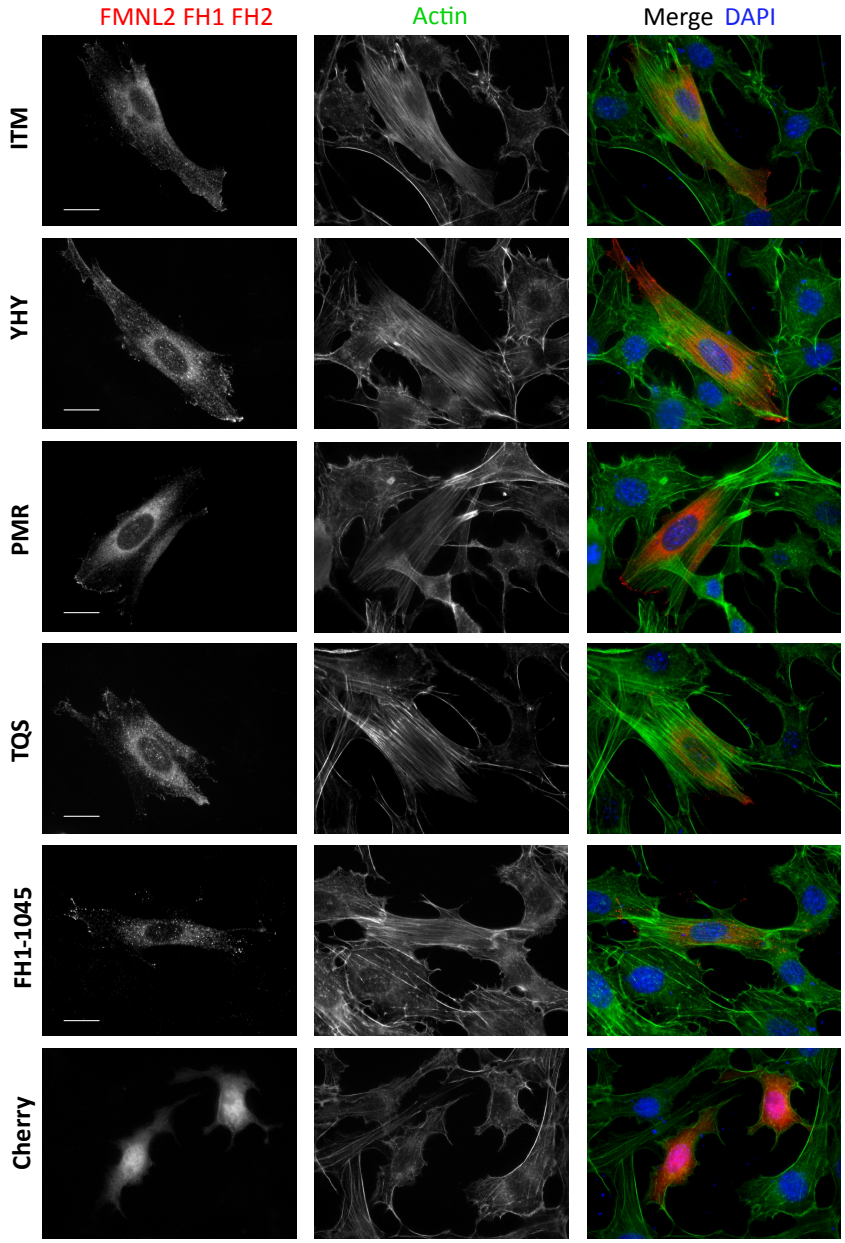
FMNL2 FH1 FH2
Actin
Merge DAPI
ITM
YHY
PMR
TQS
FH1-1045
Cherry

B

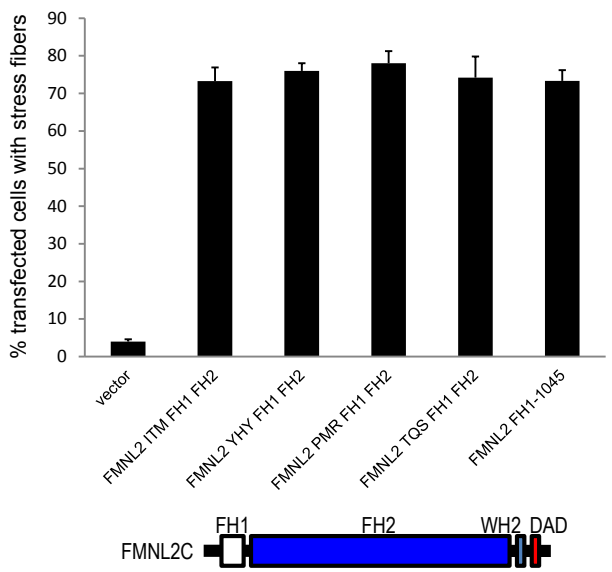
% transfected cells with stress fibers
90
80
70
60
50
40
30
20
10
0
vector
FMNL2 ITM FH1 FH2
FMNL2 YHY FH1 FH2
FMNL2 PMR FH1 FH2
FMNL2 TQS FH1 FH2
FMNL2 FH1-1045
FMNL2C
FH1
FH2
WH2
DAD

cell-based method to indirectly measure F-actin assembly (Sotiropoulos *et al.* 1999; Copeland and Treisman 2002). Full length and FH1FH2 derivatives of each FMNL2 isoform were expressed by transient transfection in NIH 3T3 cells and their ability to activate a serum response factor reporter gene was measured. As expected, none of the full-length FMNL2 isoforms promoted robust SRF activation. However, FL FMNL2 PMR was more active than the other splice forms, suggesting that it is not effectively auto-inhibited (Figure 3.7a). In contrast with the FL derivatives, all of the FH1FH2 constructs induced potent activation of the SRF reporter with FMNL2 TQS more active than the other isoforms (Figure 3.7b).

We also compared the ability of each isoform to induce microtubule acetylation, another FH2-dependent activity. In this assay, Myc-tagged CA derivatives of each FMNL2 isoform were expressed by transient transfection in NIH 3T3 cells and their ability to promote microtubule acetylation was assessed by immunofluorescence (figure 3.8a). Expression of each CA FMNL2 isoform increased acetylation relative to the empty vector control. mDia1 served as a positive control (Thurston *et al.* 2012). There was no statistical differences between TQS and ITM, but both are more effective than YHY and PMR (figure 3.8b)

3.6 FMNL2 knockdown, rescue and overexpression affects A375 melanoma cell morphology

To investigate the effects of FMNL2 expression on cell morphology in A375 cells, we observed the effects of total isoform FMNL2 knockdown, as well as specific isoform rescue and overexpression, on A375 melanoma cell morphology. A knockdown

Figure 3.7: FMNL2 TQS is a potent activator of the SRF pathway. NIH 3T3 fibroblasts were transiently transfected with an SRF luciferase reporter gene and a FMNL2 full length or FH1 FH2 derivative isoform construct. A) Activation of the MRTF/SRF pathway by full-length FMNL2 isoforms. Note that PMR is partially defective in autoregulation. B) Activation of the MRTF/SRF pathway by C-terminal derivatives of each FMNL2 isoform. FMNL2 FH1 FH2 derivative isoforms induced stress fiber formation at a similar level but seem to vary in their ability to induce activation of the SRF reporter gene. Luciferase activity is expressed relative to the SRFVP16 positive control. N=3, Error bars represent SEM.

A

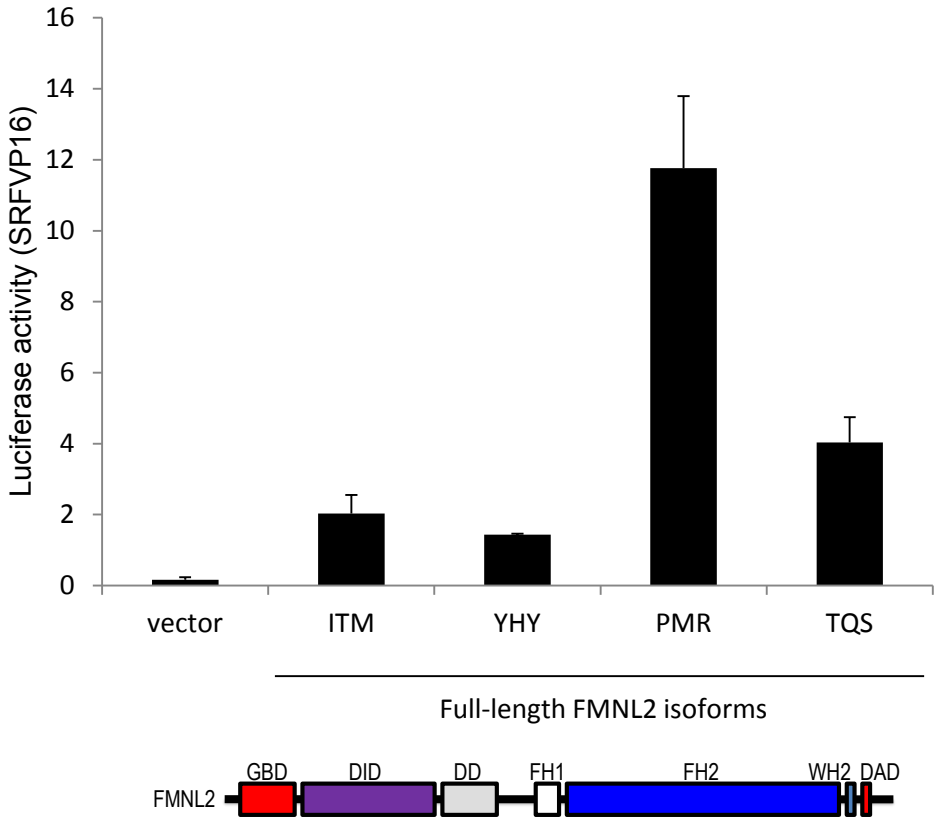
Luciferase activity (SRFVP16)
16
14
12
10
8
6
4
2
0
vector
ITM
YHY
PMR
TQS
Full-length FMNL2 isoforms
FMNL2
GBD
DID
DD
FH1
FH2
WH2
DAD

B

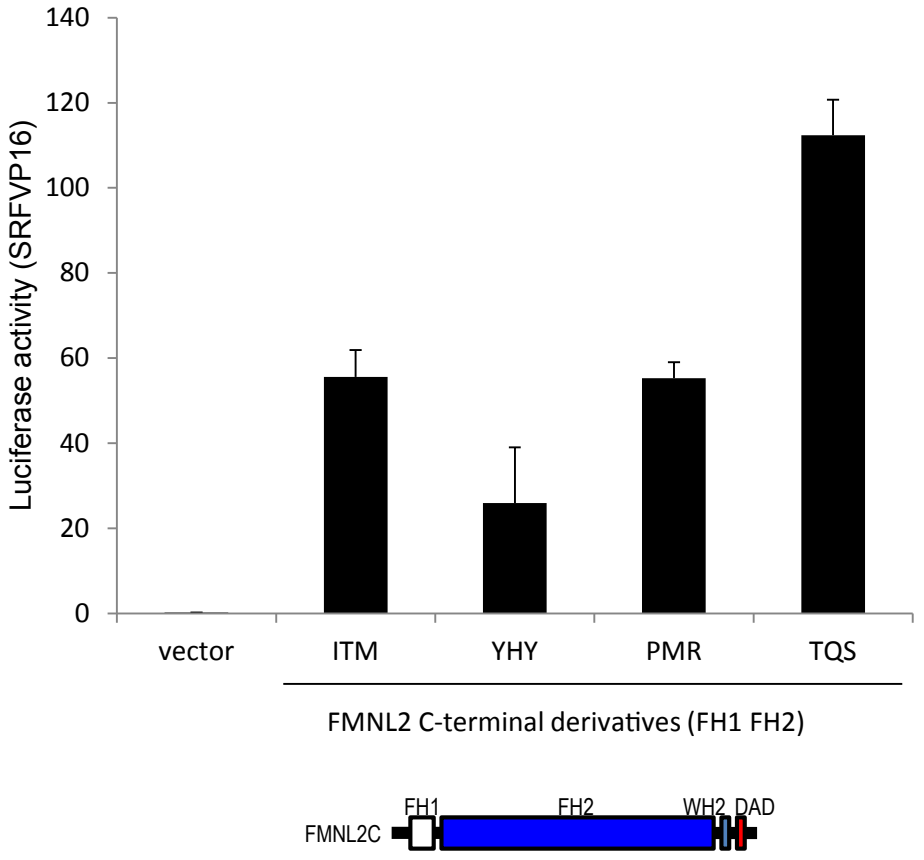
Luciferase activity (SRFVP16)
140
120
100
80
60
40
20
0
vector
ITM
YHY
PMR
TQS
FMNL2 C-terminal derivatives (FH1 FH2)
FMNL2C
FH1
FH2
WH2
DAD

Figure 3.8: C-terminal derivatives of FMNL2 isoforms induce microtubule acetylation. A) Overexpressed N-terminal myc tagged FMNL2 and mDia1 C-terminal derivatives were visualized with the primary antibody Rabbit anti-Myc conjugated to secondary antibody Donkey anti-Rabbit 594 (*red*). Acetylated microtubules were detected using anti Mouse acetyl-alpha-tubulin antibody conjugated to secondary antibody Donkey anti-Mouse 488 (*green*) and nucleus with DAPI (*blue*). B) FMNL2 isoform derivatives differ in their ability to induce microtubule acetylation. Percentage of cells expressing FMNL2 derivatives or controls, displaying increased microtubule acetylation. There is a significant difference ($P \leq 0.05$) between all samples except YHY vs PMR or ITM vs TQS. N=3, with more than 100 cells counted per sample, Error bars represent SEM.

A

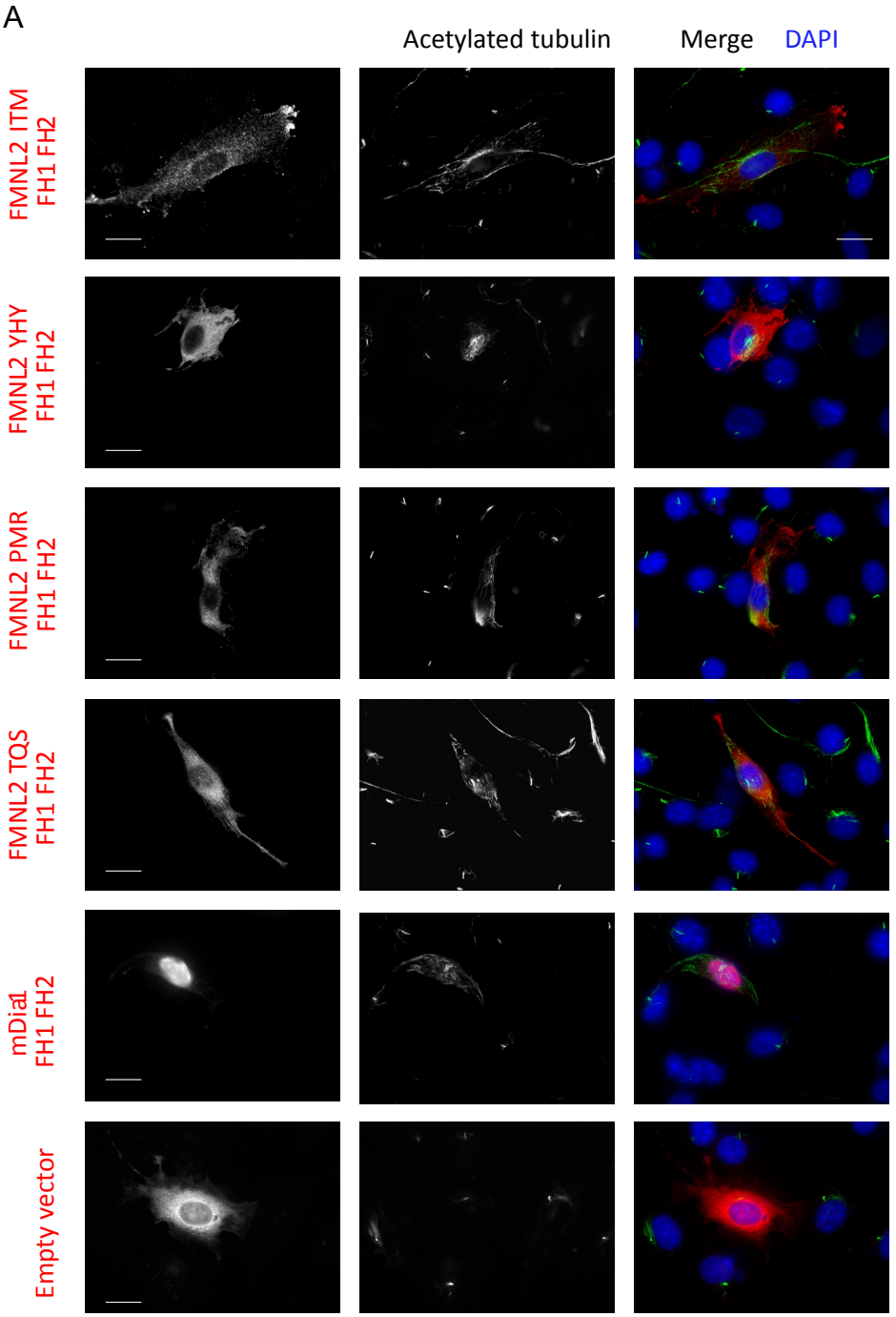
Acetylated tubulin
Merge
DAPI
FMNL2 ITM FH1 FH2
FMNL2 YHY FH1 FH2
FMNL2 PMR FH1 FH2
FMNL2 TQS FH1 FH2
mDia1 FH1 FH2
Empty vector

B

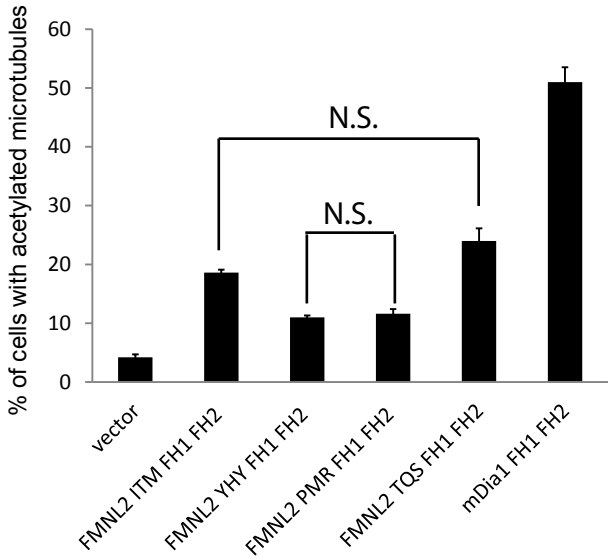
% of cells with acetylated microtubules
60
50
40
30
20
10
0
N.S.
N.S.
vector
FMNL2 ITM FH1 FH2
FMNL2 YHY FH1 FH2
FMNL2 PMR FH1 FH2
FMNL2 TQS FH1 FH2
mDia1 FH1 FH2

of FMNL2 in A375 melanoma cells was performed using a siRNA duplex that targets the 3'UTR of all endogenous FMNL2 isoforms and will not affect the expression of FMNL2 from our various vectors. A375 melanoma cells were transfected with specific siRNA duplexes targeting FMNL2 or scrambled control siRNA for 24 hours then were infected with an empty lentiviral vector independently expressing cherry (*red*) and left for another 24 hours. The level of FMNL2 knockdown was determined by immunoblotting with an anti-FMNL2 antibody. A quantified western blot confirms FMNL2 knockdown in the A375 melanoma cells (90% FMNL2 knockdown compared to control). The efficiency of FMNL2 knockdown was moderately affected by lentiviral infection (figure 3.9a).

FMNL2 expression was visualized by immunofluorescence using an anti-FH2 FMNL2 antibody (*green*). The FMNL2 depleted cells are smaller and more condensed compared to the scrambled transfected and untreated control cells (figure 3.9b). To compare FMNL2 isoform specific activity, we infected FMNL2 knockdown and control A375 melanoma cells with lentiviral vectors expressing each of the FMNL2 isoforms. The A375 cells treated with siRNA and infected were divided into separate plates for immunofluorescence as well as for immunoblotting and for the invasion assay described in section 3.9. Infected cells were detected by mCherry expression mediated by an Internal Ribosome Entry Site (IRES) on the same transcript as FMNL2 (figure 3.10a, *red*). FMNL2 rescue cells and control cells were visualized by immunofluorescence using an FMNL2 specific antibody (figure 3.10a, *green*). Interestingly, expression of each of the FMNL2 isoforms affects A375 cell morphology in both knockdown and control cells. FMNL2 expressing A375 cells are considerably larger and have increased plasma membrane protrusions compared to untreated control (figure 3.10a).

Figure 3.9: FMNL2 knockdown affects A375 melanoma cell morphology. A) siRNA FMNL2 and siRNA scramble treated A375 cells were infected with an empty lentiviral vector independently expressing cherry. These cells were subjected to SDS-PAGE and immunoblotted to detect FMNL2 expression levels. A combination of FMNL2 knockdown, rescue, up regulation and endogenous expression levels (combination of samples from figure 3.9b and 3.10b) can be observed by immunoblot at appendix 2. B) Equivalent samples of treated and untreated cells from (A) are assessed by immunofluorescence. Infected cells are visualized with an empty lentiviral vector independently expressing cherry (*red*). FMNL2 was visualized using a rabbit anti-FMNL2 specific antibody (*green*) and the nucleus was stained with DAPI (*blue*). Scale bar = 20μm, N=3.

A

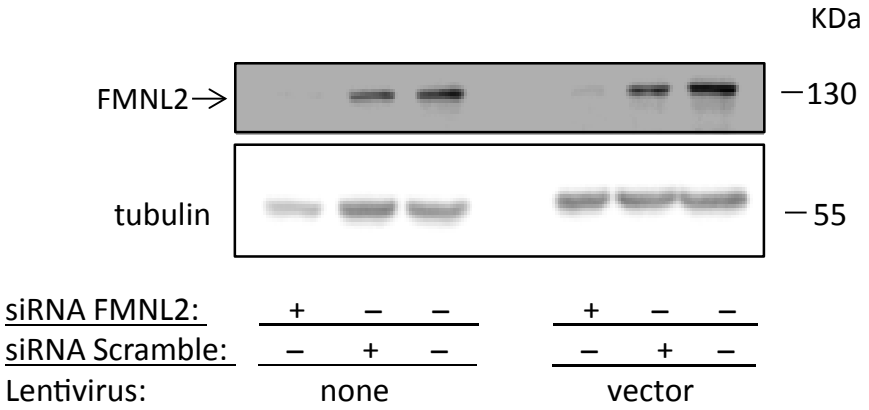
KDa
FMNL2
130
tubulin
55
siRNA FMNL2: + – – + – –
siRNA Scramble: – + – – + –
Lentivirus: none vector

B

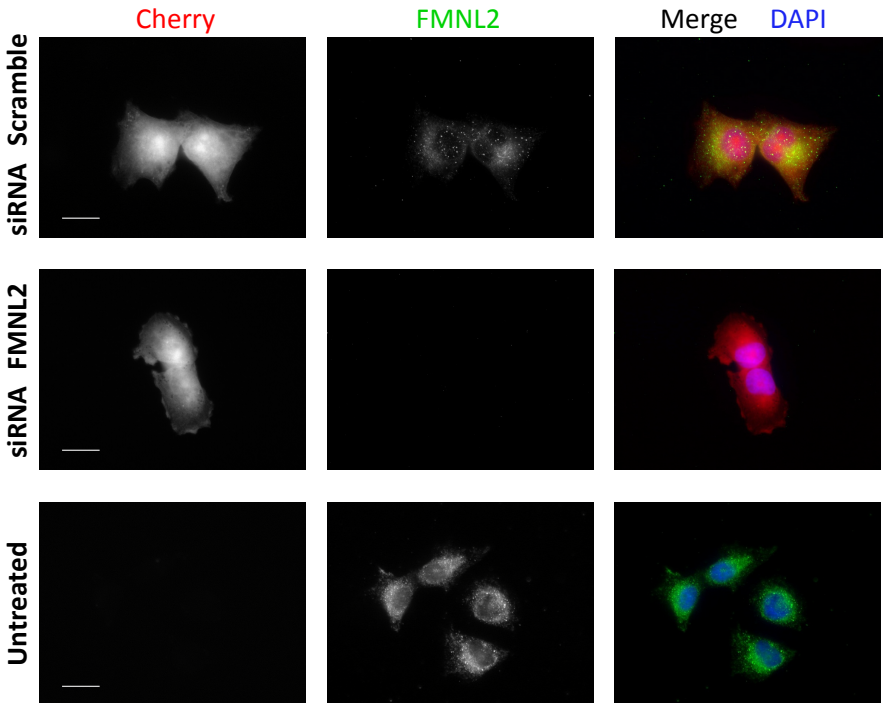
Cherry
FMNL2
Merge
DAPI
siRNA Scramble
siRNA FMNL2
Untreated

Figure 3.10: FMNL2 rescue and overexpression affects A375 melanoma cell morphology. A) siRNA FMNL2 and siRNA scramble treated A375 cells were infected with FMNL2 isoform specific lentiviral vectors independently expressing cherry (*red*). FMNL2 was visualized using a rabbit anti-FMNL2 specific antibody conjugated to a Donkey-anti Rabbit 488 antibody (*green*) and the nucleus was stained with DAPI (*blue*). Scale bar = 20μm. Note the increased size of the A375 melanoma cells when rescued or overexpressed with FMNL2 splice forms in comparison to the untreated cells. B) Equivalent samples of treated and untreated cell lysates from (A) were subjected to SDS-PAGE and immunoblotted to detect FMNL2 expression levels. A combination of FMNL2 knockdown, rescue, up regulation and endogenous expression levels (combination of samples from figure 3.9b and 3.10b) can be observed by immunoblot at appendix 2.

A

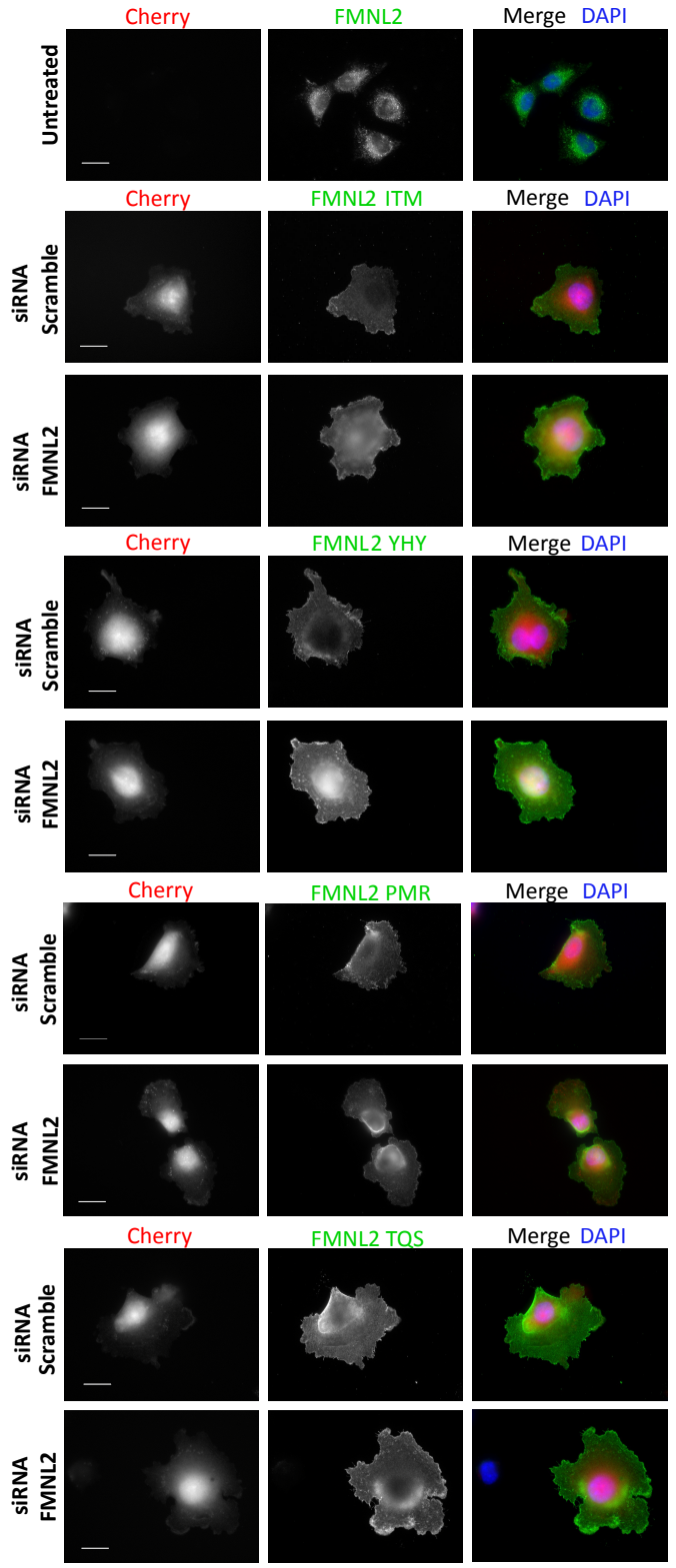
Cherry
FMNL2
Merge DAPI
Untreated
Cherry
FMNL2 ITM
Merge DAPI
siRNA Scramble
siRNA FMNL2
Cherry
FMNL2 YHY
Merge DAPI
siRNA Scramble
siRNA FMNL2
Cherry
FMNL2 PMR
Merge DAPI
siRNA Scramble
siRNA FMNL2
Cherry
FMNL2 TQS
Merge DAPI
siRNA Scramble
siRNA FMNL2

B

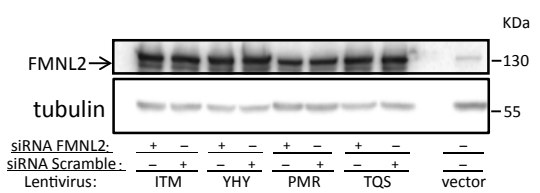
KDa
FMNL2
130
tubulin
55
siRNA FMNL2:
siRNA Scramble:
Lentivirus:
ITM
YHY
PMR
TQS
vector

Immunoblotting results confirm FMNL2 rescue and overexpression in the A375 melanoma cells compared to untreated control (Figure 3.10b). A combination of FMNL2 knockdown, rescue, up regulation and endogenous expression levels (combination of samples from figure 3.9b and 3.10b) can be observed by immunoblot at appendix 2 (figure 5.2).

3.7 FMNL2 knockdown inhibits A375 melanoma cell migration

FMNL2 depletion decreases invasive cell migration of MDA-MB-435 melanoma cells (Kitzing *et al.* 2010). To determine if FMNL2 plays a role in A375 melanoma cell motility, we performed a scratch wound cell migration assay. In this assay, A375 melanoma cells were seeded in an ibidi culture–insert, composed of two chambers, separated by a median. The removal of the insert creates a "wound". Migration of the cells was followed by live-cell imaging and still frames from selected time points are presented. When comparing knockdown and control cells at 0, 20 and 40 hour time points, it is clear that cell migration is inhibited in FMNL2 knockdown cells (figure 3.11a). Thus, FMNL2 activity is required in A375 cells for 2-D cell migration. However, even though a 2D migration assay suggests that FMNL2 is implicated in cell motility, it is not sufficient to determine its role in amoeboid style 3-D invasion.

3.8 FMNL2 knockdown reduces melanoma amoeboid style invasion

Knockdown of FMNL2 expression in MDA-MB-435 melanoma cell lines strongly inhibits amoeboid 3-D motility (Kitzing *et al.* 2010). To determine if FMNL2 is required by other cells that use amoeboid invasion, we knocked it down in WM266.4 and

Figure 3.11: FMNL2 knockdown inhibits A375 melanoma cell migration. A) A wound healing assay was performed using ibidi inserts and visualized by live contrast imaging. siRNA FMNL2 and siRNA scramble treated A375 cells migrated for 0, 20, and 40 hours. B) Equivalent samples of cell lysates from (A) were subjected to SDS-PAGE and immunoblotted to detect FMNL2 expression levels with a rabbit anti-FMNL2 specific antibody.

A

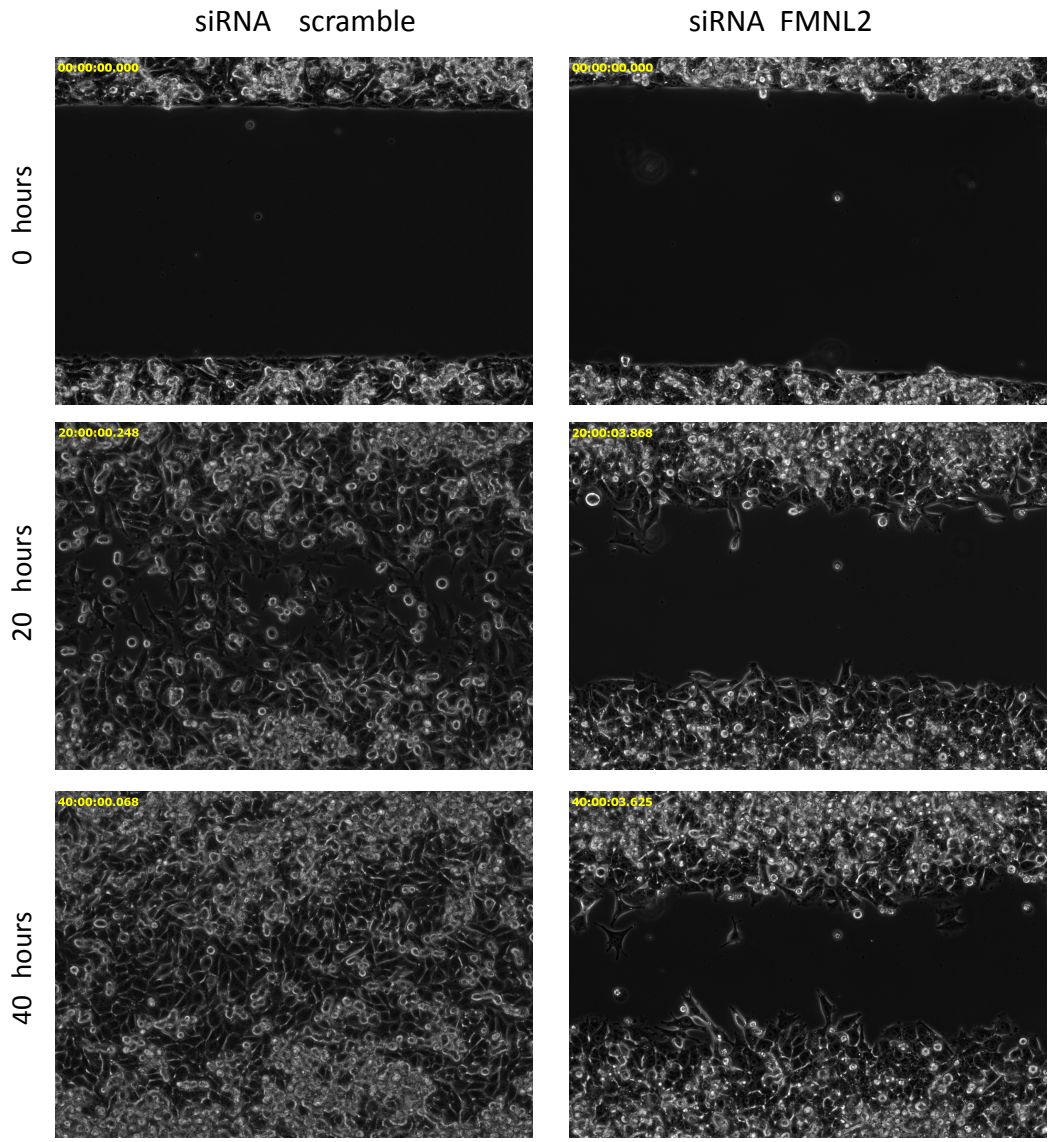
siRNA scramble
siRNA FMNL2
0 hours
20 hours
40 hours
00:00:00.000
00:00:00.000
20:00:00.248
20:00:03.868
40:00:00.068
40:00:03.625

B

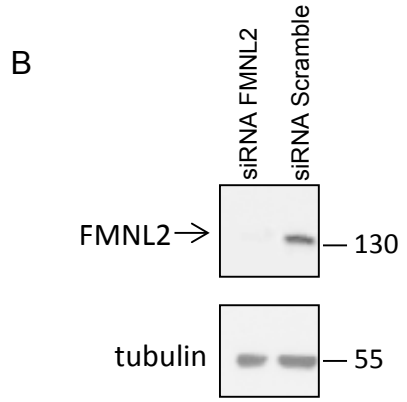
siRNA FMNL2
siRNA Scramble
FMNL2
130
tubulin
55

A375 cells. siRNA FMNL2 and siRNA scramble treated A375 and WM266.4 cells were seeded on the underside of a transwell insert and were allowed to invade through a matrigel matrix for 72h. The number of invading cells was assessed and quantified by confocal microscopy. For both WM266.4 and A375 cells, knockdown of FMNL2 expression inhibited their ability to invade into the matrigel matrix (figure 3.12a and 3.13a). A section through the z-axis projection also shows that siRNA scramble treated A375 and WM266.4 cells invaded further through the matrigel then the FMNL2 depleted cells (figure 3.12b and 3.13b). Western blot quantification reports that FMNL2 knockdown in WM266.4 (approximately 60% knockdown compare to endogenous control) (figure 3.12c) is not as efficient as knockdown in the A375 (90% knockdown compare to endogenous control) (figure 3.13c).

3.9 FMNL2 isoforms rescue and potentiate A375 melanoma cell amoeboid style invasion

FMNL2 TQS is the predominant isoform expressed in the A375 cell line (figure 3.3b) and FMNL2 depleted A375 cells are unable to invade into matrigel in a Boyden chamber assay (figure 3.13). We next wanted to compare the relative ability of each isoform to rescue invasion in FMNL2 knocked-down A375 cells. A375 cells were transfected with FMNL2 siRNA or scrambled control duplex and subsequently infected with lentiviral vectors expressing each of the FMNL2 isoforms. The cells were then seeded on the underside of a transwell for the invasion assay as before. Empty lentiviral vector served as a control. All 4 isoforms were able to rescue invasion, however, the relative efficiency varied in this assay. The most effective isoform was TQS

Figure 3.12: FMNL2 knockdown decreases WM266.4 melanoma amoeboid style invasion. Quantification from confocal stacks of cells invaded into matrigel matrix for 72h. A) Percent WM266.4 cells treated with siRNA FMNL2 and siRNA scramble invaded passed 14 μm into the matrix. B) Confocal stacks z-axis visualization of invaded WM266.4 cells (stained with PI) through the matrigel. C) Equivalent samples of cell lysates from (A) were subjected to SDS-PAGE and immunoblotted to detect FMNL2 expression levels with a rabbit anti-FMNL2 specific antibody.

A

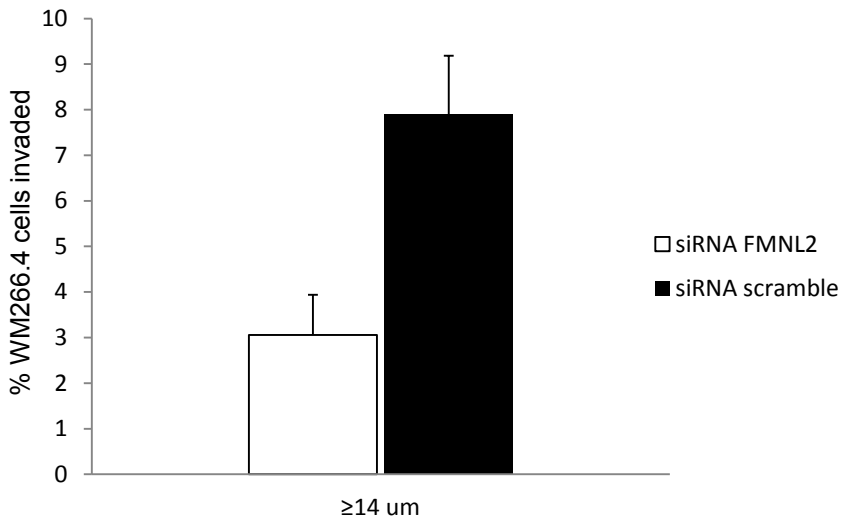
10
9
8
7
6
5
4
3
2
1
0
% WM266.4 cells invaded
≥14 um
siRNA FMNL2
siRNA scramble

B

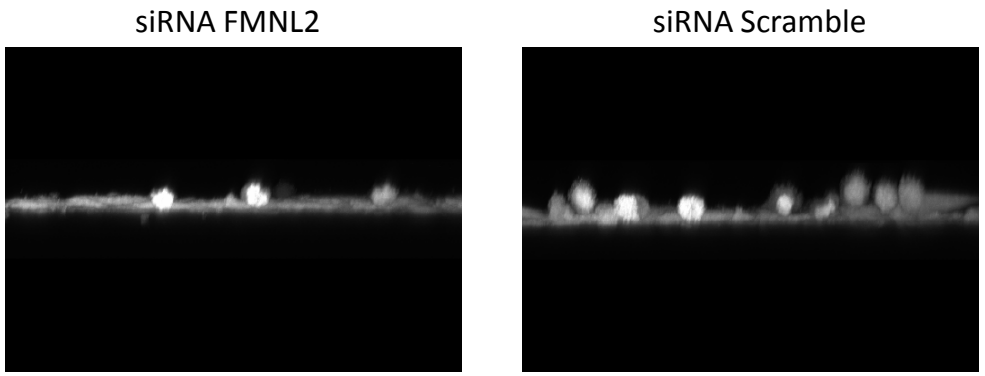
siRNA FMNL2
siRNA Scramble

C

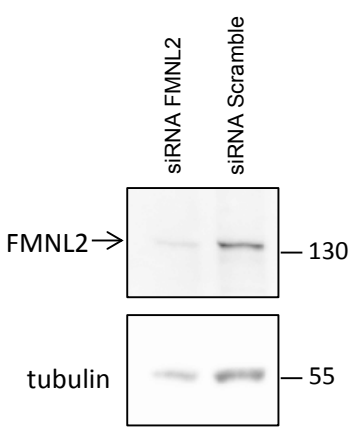
siRNA FMNL2
siRNA Scramble
FMNL2
130
tubulin
55

Figure 3.13: FMNL2 knockdown decreases A375 melanoma amoeboid style invasion. Quantification from confocal stacks of cells invaded into matrigel matrix for 72h. A) A375 cells treated with siRNA FMNL2 and siRNA scramble invaded passed 14 μm into the matrix. B) Confocal stacks z-axis visualization of invaded A375 cells (stained with PI) through the matrigel. C) Equivalent samples of cell lysates from (A) were subjected to SDS-PAGE and immunoblotted to detect FMNL2 expression levels with a rabbit anti-FMNL2 specific antibody.

A

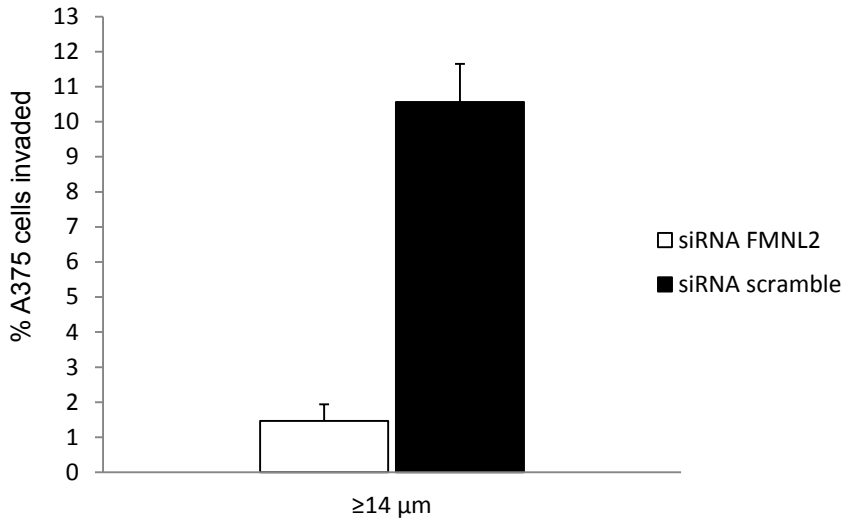
% A375 cells invaded
13
12
11
10
9
8
7
6
5
4
3
2
1
0
≥14 µm
siRNA FMNL2
siRNA scramble

B

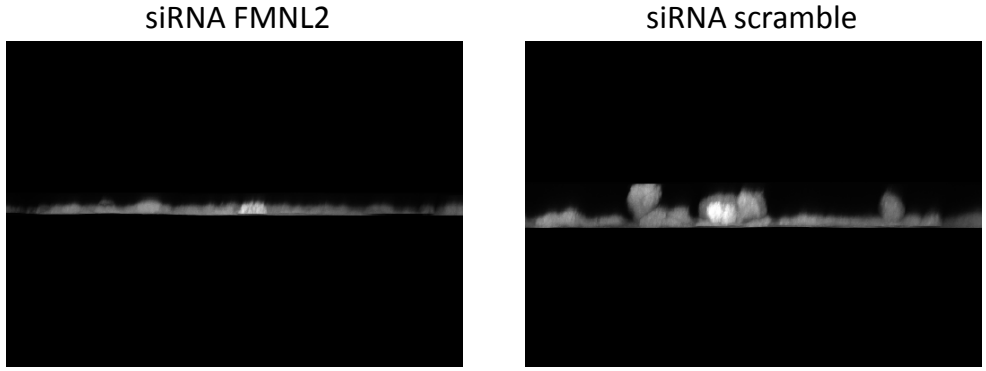
siRNA FMNL2
siRNA scramble

C

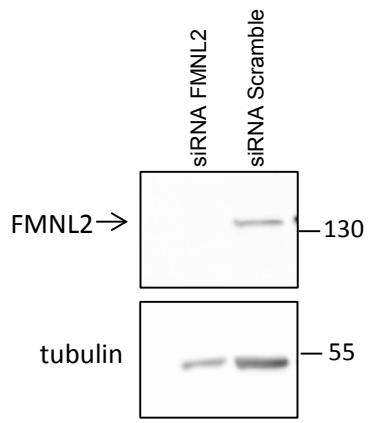
siRNA FMNL2
siRNA Scramble
FMNL2
130
tubulin
55

Figure 3.14: FMNL2 isoforms rescue and potentiate A375 invasion. A) Quantification from confocal stacks of cells invaded past 14 μm into matrigel matrix for 72h. A375 cells were treated with siRNA FMNL2 or siRNA scramble followed by an infection with FMNL2 isoform specific lentiviral expression vectors. B) Confocal stacks z-axis visualization of invaded A375 cells (stained with PI) through the matrigel. N=3

A

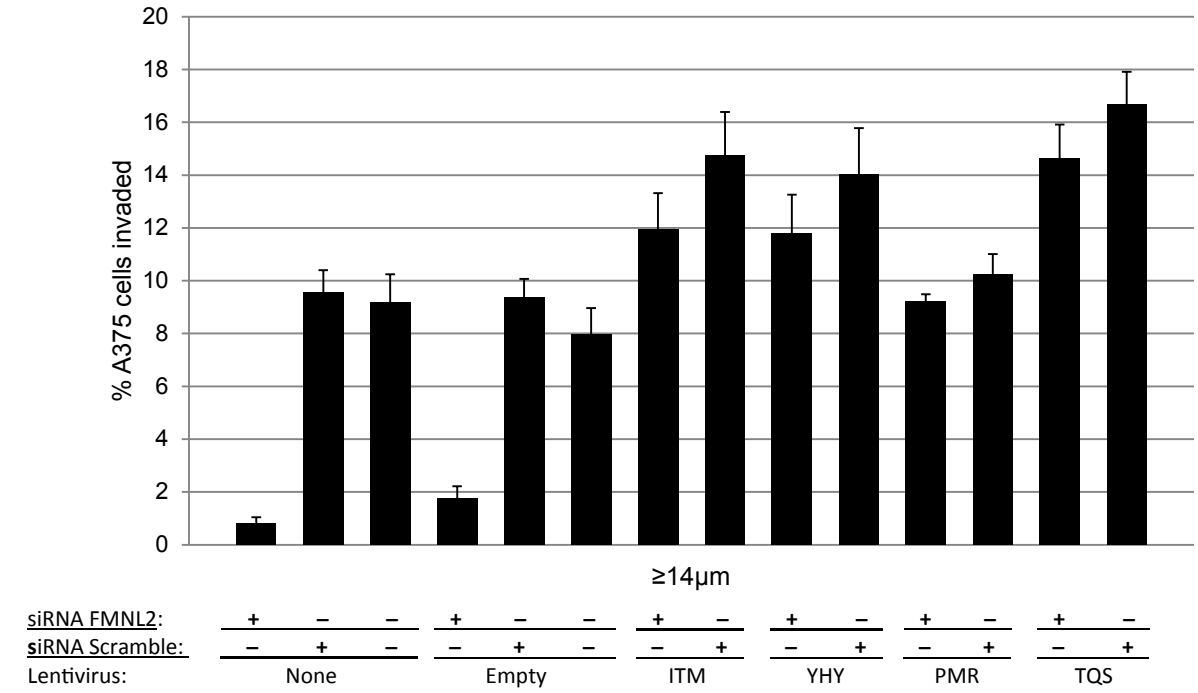
20
18
16
14
12
10
8
6
4
2
0
% A375 cells invaded
≥14μm
siRNA FMNL2: + – – + – – + – + – + – + –
siRNA Scramble: – + – – + – – + – + – + – +
Lentivirus: None Empty ITM YHY PMR TQS

B

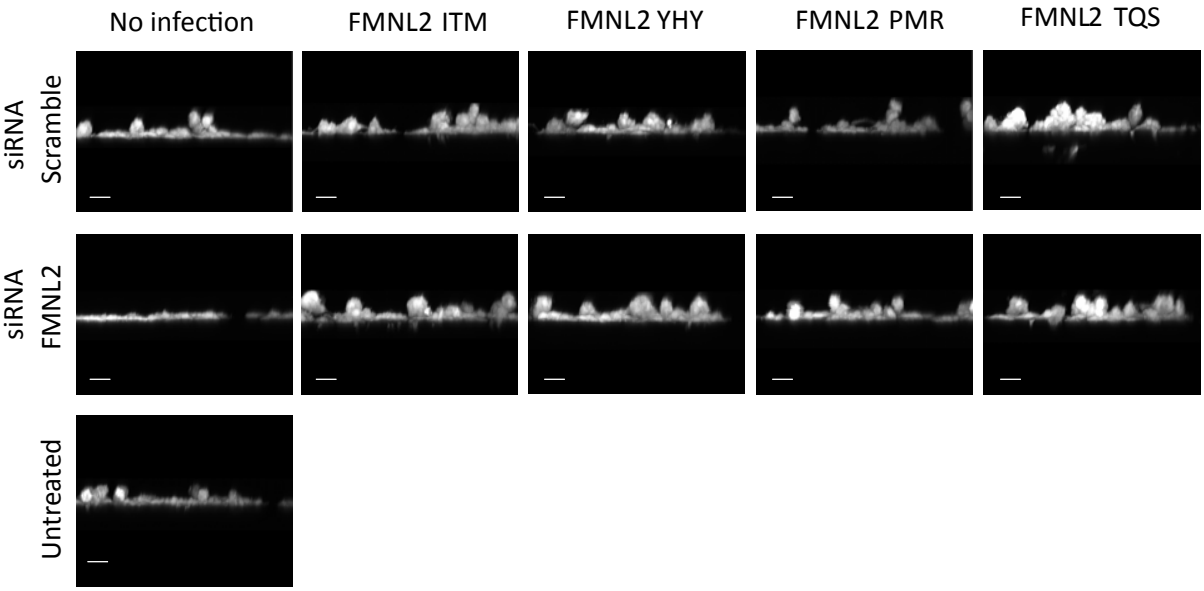
No infection
FMNL2 ITM
FMNL2 YHY
FMNL2 PMR
FMNL2 TQS
siRNA Scramble
siRNA FMNL2
Untreated

which more than doubled the number of invading cells when compared to uninfected or vector infected control cells. YHY and ITM were also able to potentiate invasion beyond control levels (figure 3.14a). The least effective isoform was PMR which potentiated invasion to the same level as control cells. These effects are readily visible in representative confocal z-axis images of the invading cells (figure 3.14b). FMNL2 knockdown, rescue, up regulation and endogenous expression levels can be observed by immunoblot at appendix 2. These preliminary data suggests that there are isoform specific differences in the ability to potentiate invasion. However, we noted that the levels of expression obtained with the lentiviral vectors is higher than the endogenous level of FMNL2 in A375 cells which may interfere with the interpretation of the results. Therefore future work will require generating a new vector with a level of expression that more closely matches the endogenous situation.

Chapter 4

Discussion

4.0 Discussion

4.1 Depletion of FMNL2 in melanoma cell lines inhibits amoeboid style motility

Kitzing *et al*. have recently reported the importance of FMNL2 protein as a specific RhoC effector required in MDA-MB-435 melanoma cells for amoeboid style invasion. We wished to build on these results and determine if FMNL2 is more broadly required in melanoma cell-lines for invasion as well as determine if FMNL2 plays a general role in 3-D amoeboid motility. A scratch wound assay demonstrated that knocking down FMNL2 in A375 cells greatly decreases cell migration, confirming that FMNL2 plays an important role in cell motility. These results were recently confirmed in B16-F1 melanoma cells where FMNL2 depletion also inhibits cell motility (Block *et al.* 2012).

It should be noted that motility on a 2D substrate does not necessarily reflect the 3D situation. For example, invasive A375 melanomas have a more elongated morphology when migrating on a 2D surface, but will be rounded when invading a 3D gel (Sahai and Marshall 2003). Thus, even though a 2D migration assay suggests that FMNL2 is implicated in cell motility, it is not sufficient to evaluate its role in amoeboid style movement.

Accordingly, we used Boyden chamber invasion assays to assess the requirement for FMNL2 activity in 3-D invasion in A375 and WM266.4 melanoma cells. FMNL2 depletion in each cell line strongly decreased invasion compared to the control. Invasion was reduced considerably more in A375 cells than the WM266.4 cells, probably due to knockdown efficiency. Taking into consideration our results, and others, it suggests that

FMNL2 is likely required both for invasion by melanoma cells as well as in cell lines that use an amoeboid style of invasion.

Previous studies of FMNL2 have focused on one isoform designated here as FMNL2 ITM (Katoh and Katoh 2003). However, there are multiple FMNL2 isoforms described in the database and it is not apparent which of these may be relevant to cancer cell motility. This is an important consideration as previous studies have identified specific "invasive" isoforms of other actin-binding proteins which are key regulators of cell invasion and metastasis (Philippar *et al.* 2008; Han *et al.* 2009). In this work, we identified four FMNL2 isoforms expressed in a variety of cancer cell lines, but only one, FMNL2 TQS, that was up-regulated in invasive cells. Our results suggest that the expressed FMNL2 isoforms differ in their auto-regulation and ability to regulate cytoskeletal dynamics.

4.2 FMNL2 splice variants

4.2.1 FMNL2 TQS is preferentially expressed in invasive cancer cell lines

Two human FMNL2 splice forms (FMNL2 ITM and YHY) have been previously reported in the literature (Katoh and Katoh 2003) and a number of additional isoforms are predicted in the chimp and mouse genomes. In this work, I have identified four FMNL2 isoforms (ITM, PMR, TQS and YHY) expressed in three selected human cancer cell lines: invasive SW620, non-invasive SW480 CRCs and invasive A375 melanoma cells.

FMNL2 expression is up regulated in many malignant cell lines, including colorectal cancers, glioblastomas, melanomas and possibly many more (Human Protein Atlas, www.proteinatlas.org) (Parsons *et al.* 2008; Zhu, Liang, and Ding 2008; Kitzing *et*

al. 2010; Li *et al.* 2010). The qPCR data presented here confirms these results and demonstrates that FMNL2 is up regulated in an array of invasive cell lines: SW620 CRC cells, LS174T CRCs, HTB107 thyroid cancer cells and amoeboid style invasion melanoma cell lines (WM266.4 and A375). It will be of interest to determine if FMNL2 is required for invasion in other tumors such as thyroid cancer.

Our qPCR results also show that a specific FMNL2 isoform, TQS, is preferentially expressed in invasive cancer cell lines. It is the major FMNL2 isoform expressed in invasive SW620s and in the invasive cell lines A375, LS174T and WM266.4. We have confirmed the qPCR data by immunoblotting using an antibody directed against the FH2 domain of FMNL2 that recognize all FMNL2 isoforms as well as antibodies recognizing TQS and ITM specifically (see figure 4.1, FMNL2 YHY and PMR specific antibodies are currently being purified). The preferential expression of TQS in these cell lines suggests that it may represent an "invasive" FMNL2 isoform.

We also noted that FMNL2 expression in primary melanocytes is higher than in other non-invasive or non-transformed cell lines (e.g. HUVECs or SW480). It is interesting to speculate that FMNL2 may play a crucial role in the Rho- and actin-dependent formation of the long dendrites formed by melanocytes to deliver melanosomes to surrounding keratinocytes (Scott 2002; Li *et al.* 2011; Bonaventure *et al.* 2013)

Although it is clear that TQS is the predominant isoform in invasive cells, we were not able to obtain reliable qPCR data for FMNL2 PMR. Nonetheless, it is unlikely that PMR makes a significant contribution to total FMNL2 activity as in most cases the expression of the individual splice forms matches the measured level of total FMNL2.

One exception is in the case of the primary melanocytes where the individual isoforms do not account for the total of FMNL2 expression. Further analysis will be required to determine if this "missing" isoform is PMR or one of the other predicted FMNL2 isoforms

4.3 Functional characterisation of FMNL2 isoforms

4.3.1 FMNL2 isoforms vary in their regulation and activity

Each FMNL2 splice variant is identical save for the region encoding the C-terminus of each protein. This region of the protein is likely to affect both FMNL2 function and regulation. For example, the C-terminus of the closely related protein FMNL3, plays a critical role in binding the barbed end and stabilizing the actin filament nucleus (Heimsath and Higgs 2012; Thompson *et al.* 2013). Furthermore, it has been suggested that basic residues in this region of the protein play a role in DRF autoregulation (Wallar *et al.* 2006; Vaillant *et al.* 2008). This data is supported by cell based assay results from our work, suggesting that the FMNL2 splice forms differ in their regulation and activity.

Prior studies from our lab report that a common function of formins is regulating microtubule dynamics and that the FH2 domain should be thought of as a dual-function domain able to regulate both actin and microtubule networks (Bartolini *et al.* 2008; Thurston *et al.* 2012). FMNL2 was reported as being a low acetylated microtubule inducer (Thurston *et al.* 2012), hence, we tested to see if the isoforms differed in their ability to promote microtubule acetylation. Expression of each FMNL2 isoform increase

Figure 4.1: FMNL2 TQS, ITM and total isoforms' expression levels in different cell lines. QPCR data is confirmed by western blotting with antibodies that recognize all FMNL2 isoforms (targets the FH2 domain) or specific to TQS and ITM. α tubulin serves as a control. n = 1. The immunoblotting assay was completed by Allan Heibein.

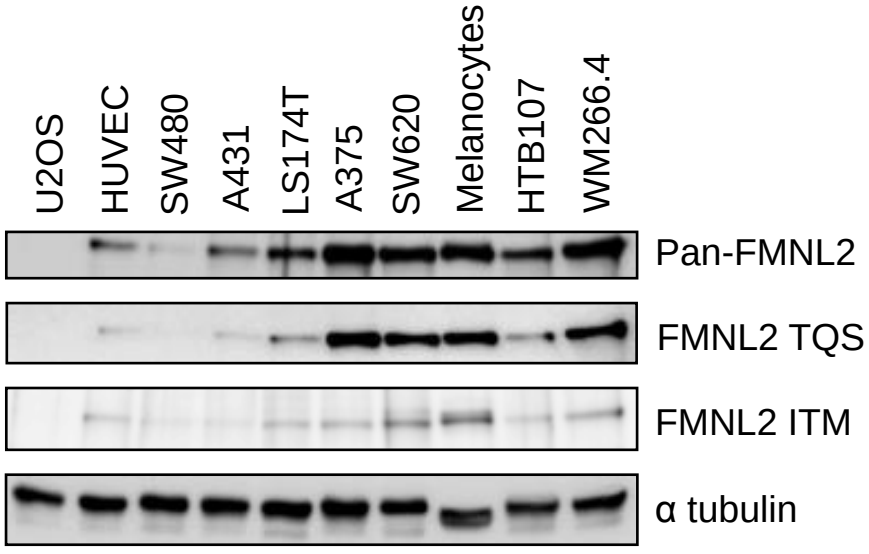
U2OS
HUVEC
SW480
A431
LS174T
A375
SW620
Melanocytes
HTB107
WM266.4
Pan-FMNL2
FMNL2 TQS
FMNL2 ITM
α tubulin

acetylation relative to the empty vector control, even though all of the isoforms may be considered as "weak" acetylators compared to mDia1. The FMNL2 TQS derivative was the most effective at inducing microtubule acetylation compared to the other splice forms. There was no significant difference between TQS and ITM in this assay, but both were better inducers of acetylation than YHY and PMR.

A second cell based assay used to compare FMNL2 isoform's effect on actin dynamics was the SRF reporter gene assay. The SRF reporter is activated in response to depletion of cellular stores of G-actin and is an indirect measure of F-actin accumulation. All constitutively active FMNL2 isoform constructs induced robust activation of the SRF reporter. Yet, there were definite isoform specific differences. More importantly, FMNL2 TQS was considerably more active than the other three isoforms suggesting that it has a more potent effect on actin dynamics than the others. This same assay was also used to measure FMNL2 auto-inhibition. As expected, FL derivatives of TQS, ITM and YHY were essentially inactive, however, FMNL2 PMR expression activated the reporter at a higher level suggesting this isoform is relatively deficient in auto-inhibition. A variety of FMNL2 derivatives have been generated for future studies that will compare directly the effects of each isoform on actin dynamics *in vitro* (see table 5.2 - appendix 3).

4.3.2 Full length FMNL2 splice variants localize to the plasma membrane

FL FMNL2 ITM with an N-terminal epitope tag is distributed throughout the cytoplasm (Vaillant *et al.* 2008). However, it has been suggested that FMNL2 may be subject to lipid modification at its N-terminus that would target it to the plasma membrane. Indeed, N-terminal myristoylation targets the related protein FMNL1 to

accumulate at the membrane bilayer (Han *et al.* 2009) and the N-myristoylation site in FMNL1 is conserved in FMNL2 and FMNL3 proteins. We compared subcellular localisation of FMNL2 constructs with N and C-terminal tags to determine if FMNL2 can also be membrane targeted. We found that an N-terminal tag on FL FMNL2 construct or the deletion of amino acids at the N-terminal domain (140-503 FMNL2 construct) blocks FMNL2's targeting to the cell periphery. However, a C-terminally tagged FL FMNL2 construct or an FMNL2 N-terminal derivative (1-503 FMNL2 construct) accumulates at the plasma membrane, consistent with N-myristoylation at glycine 2. More recently it has been reported that membrane localization by FMNL2 is inhibited by N-myristoylation inhibitors or when glycine 2 is replaced with alanine (Moriya *et al.* 2012). Our results are consistent with N-myristoylation targeting each of the FMNL2 isoforms to the plasma membrane.

4.4. FMNL2 isoforms effect on cell motility

4.4.1 FMNL2 knockdown and overexpression affects A375 melanoma cell morphology

Knockdown of FMNL2 expression in A375 melanoma cells altered cellular morphology; the FMNL2-depleted cells are smaller and more condensed compared to controls. In the reciprocal experiment A375 cells overexpressing each of the FMNL2 isoforms are noticeably larger and have increased plasma membrane protrusions, reminiscent of changes associated with EMT. A key element for cells to invade is the dissociation of individual cells from the epithelial cell sheets. In order to do so, cancer cells adopt EMT (Thiery *et al.* 2009). Previous reports suggested that FMNL2 plays a

role in EMT in human CRC cells (Li *et al.* 2010). Similar to our observations, the loss of FMNL2 in CRCs induced a small compacted cobblestone shape and other changes associated with mesenchymal to epithelial transition (MET) (the reverse process of EMT) (Li *et al.* 2010). Thus, our results are consistent with FMNL2 having a more general role as an effector of EMT.

4.4.2 FMNL2 TQS drives plasma membrane extension

As stated earlier, there is often little correlation between the results of 2D and 3D migration assays. Recently, it was proposed that actin polymerization and lamellipodia protrusions induced by growth factor stimulation on a 2D substrate can predict cell motility in a 3D environment (Meyer *et al*. 2012). Therefore a similar assay was performed. Since FMNL2 TQS was the predominant isoform in the selected melanoma cell lines (LS174T, A375 and WM266.4), we sought to determine its effect on protrusion formation by live cell imaging. Briefly, FL FMNL2 TQS and Lifeact GFP were expressed by transient transfection in A375 melanoma cancer cells; empty vector served as control. The cells were incubated in low serum media (0.5% FBS in DMEM) and then stimulated with 10% serum. The effects on membrane extension were monitored by live cell imaging on a Deltavision system; selected time points are presented (figure 4.2). In control cells, serum starvation inhibits membrane blebbing and filopodia production, both of which are stimulated by the addition of 10% FCS. In contrast we found that cells expressing FMNL2 TQS were not affected by serum starvation and formed filopodia and membrane protrusions at a similar rate to the serum-stimulated control or TQS expressing cells (Figure 4.2). These preliminary results would suggest that FMNL2 overexpression

is sufficient to make membrane protrusion growth factor independent in A375 cells. This would be consistent with a recent study showing that FMNL2 accumulates at filopodia and lamellipodia tips in B16-F1 melanoma cells and that knockdown of FMNL2 expression in these cells decreased lamellipodia protrusions and cell migration efficiency (Block *et al.* 2012).

4.4.3 FMNL2 isoforms rescue and potentiate A375 melanoma cell amoeboid style invasion

Recent studies have identified specific isoforms of actin-binding proteins as key regulators of actin dynamics implicated in cell invasion and metastasis (Philippar *et al.* 2008). For example, an "invasive" splice variant of the Ena/VASP family member Mena ($Mena^{INV}$) has been described to be highly efficient in driving membrane protrusion and tumor cell metastases (Philippar *et al.* 2008). Therefore, we were interested in comparing the ability of each of the FMNL2 isoforms to rescue amoeboid style invasion in FMNL2 knockdown A375 cells. In our initial experiment each isoform was able to rescue invasion, however, the relative efficiency of rescue varied. The most effective isoform was TQS which more than doubled the number of invading cells when compared to uninfected or vector infected control cells. ITM and YHY expression also increased invasion beyond control levels, but not to the same extent as TQS. The least effective isoform was PMR which rescued invasion to control levels.

Figure 4.2: FMNL2 TQS up regulation drives plasma membrane bleb-like protrusions in a growth factor-depleted 2D milieu. Full-length FMNL2 TQS and Lifact GFP were collectively expressed by transfection in A375 melanoma cancer cells in starving media (0.5% FBS in DMEM). An empty vector was transfected with Lifact GFP as a control. Transfected A375 cells are detected by Lifact GFP at a wavelength of 528nm. Movement and morphology alterations of the stimulated or starved cell were followed by live-cell imaging and still frames from selected time points (2 and 4 minutes) are presented. Note the formation and bleb-like protrusions, in both starved and stimulated FMNL2 TQS transfected cells. The A375 cells transfected with the empty vector only show bleb-like protrusions once stimulated with serum. N=1, Scale bar = 30μm. This work was done in collaboration with Dr Trinkle-Mulcahy.

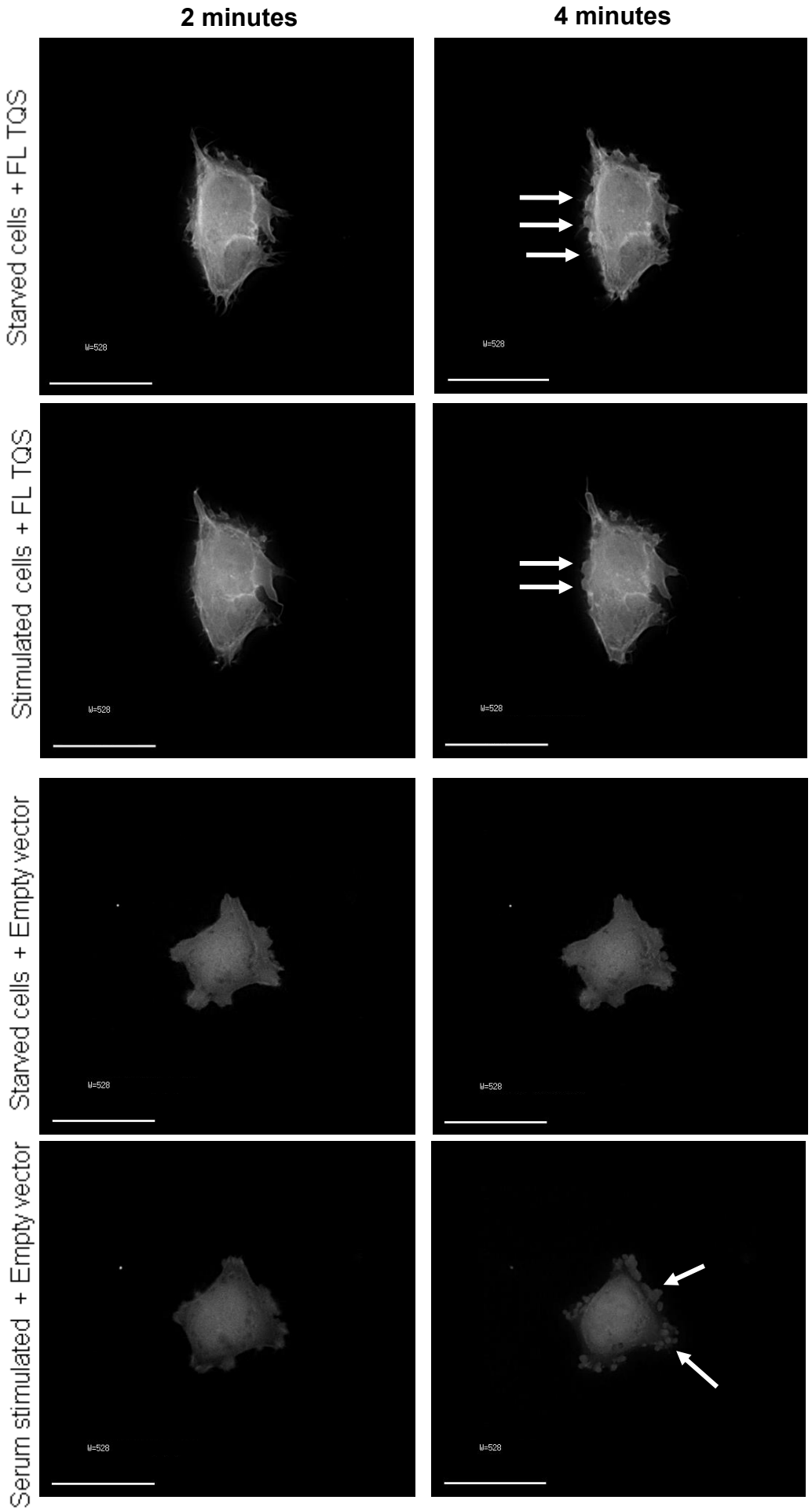
2 minutes
4 minutes
Starved cells + FL TQS
Stimulated cells + FL TQS
Starved cells + Empty vector
Serum stimulated + Empty vector

One concern about the interpretation of these results is the high levels of expression obtained with the lentiviral vector which may mask a more obvious difference between isoforms. Despite this caveat, our preliminary data strongly suggests that there is a real difference in the ability of each isoform to potentiate invasion. Future work will be required to generate an expression system that more closely replicates the endogenous level of FMNL2 expression in these cells.

4.5 Future directions

The work presented in this thesis shows that FMNL2 is required for melanoma cell invasion and that the TQS isoform is preferentially expressed in an array of invasive cancer cell lines including CRCs and thyroid cancer. We would like to extend these assays using our isoform specific FMNL2 antibodies to determine if TQS is also preferentially expressed in relevant patient samples.

It will be of interest to determine if FMNL2 expression is sufficient to render non-invasive cells invasive. This could be easily tested in non-invasive SW480 cells to determine if FMNL2 expression is sufficient to make them invasive as determined in a Boyden Chamber Assay. Xenograft experiments could also be performed with a weakly metastatic cell line and determine which FMNL2 isoform is sufficient to potentiate metastasis.

Ultimately the goal of these studies is the creation of an isoform specific FMNL2 inhibitor. The first small molecule formin inhibitors have been described; SMIFH2 is able to inhibit the activity of all FH2 domains tested to date (Blanchoin and Boujemaa-

Paterski 2009). A second inhibitor was recently described targeting formins Dia1 and Dia2 specifically (Gauvin *et al.* 2009)

4.6 Conclusion

Invasion and metastasis of tumor cells have been a very difficult hallmark of cancer to overcome. Formins such as FMNL2 have been directly linked to cancer due to their up regulation in many malignant cell lines and their relation with cancer cell motility. In this work four FMNL2 isoforms have been identified in CRC and melanoma cells; two of which have not yet been published (PMR and TQS). We report that these splice variants are altered in their regulation and activity. Also, our data shows that FMNL2 isoforms are expressed at different levels in different cell lines. Interestingly, we have found that a specific isoform, FMNL2 TQS, was preferably expressed in invasive and amoeboid cell lines. We then demonstrated that FMNL2 depletion in melanoma amoeboid cell lines strongly inhibits cell migration and invasion. Each FMNL2 isoform is able to rescue invasion; TQS seem to be the most efficient. Our data suggests that FMNL2 TQS might in fact be an “invasive” isoform, thus, it would become a great target against cancer cell amoeboid style invasion.

Appendix 1

Table 5.1: FMNL2 constructs generated for the different experiments in this work.

Construct	Tag	Restriction sites
FMNL2 ITM FL pEF plink2	Cherry (C-term)	Nco1-Spe1
FMNL2 YHY FL pEF plink2	Cherry (C-term)	Nco1-Spe1
FMNL2 PMR FL pEF plink2	Cherry (C-term)	Nco1-Spe1
FMNL2 TQS FL pEF plink2	Cherry (C-term)	Nco1-Spe1
FMNL2 1-503 pEF Plink2	Cherry (C-term)	Nco1-Spe1
FMNL2 140-503 pEF Plink2	Cherry (C-term)	Nco1-Spe1
FMNL2 ITM FH1FH2 PEFN NBRSS	Myc	Nco1-Spe1
FMNL2 YHY FH1FH2 PEFN NBRSS	Myc	Nco1-Spe1
FMNL2 PMR FH1FH2 PEFN NBRSS	Myc	Nco1-Spe1
FMNL2 TQS FH1FH2 PEFN NBRSS	Myc	Nco1-Spe1
FMNL2 ITM FH1FH2 PEFN NBRSS	Cherry (N-term)	Nco1-Spe1
FMNL2 YHY FH1FH2 PEFN NBRSS	Cherry (N-term)	Nco1-Spe1
FMNL2 PMR FH1FH2 PEFN NBRSS	Cherry (N-term)	Nco1-Spe1
FMNL2 TQS FH1FH2 PEFN NBRSS	Cherry (N-term)	Nco1-Spe1
FMNL2 ITM FL pLVX-IRES + ribosome binding site (lentivirus construct)	Cherry (individual promoter)	Xho1-Not1
FMNL2 YHY FL pLVX-IRES + ribosome binding site (lentivirus construct)	Cherry (individual promoter)	Xho1-Not1
FMNL2 TQS FL pLVX-IRES + ribosome binding site (lentivirus construct)	Cherry (individual promoter)	Xho1-Not1
FMNL2 PMR FL pLVX-IRES + ribosome binding site (lentivirus construct)	Cherry (individual promoter)	Spe1-Not1

Appendix 2

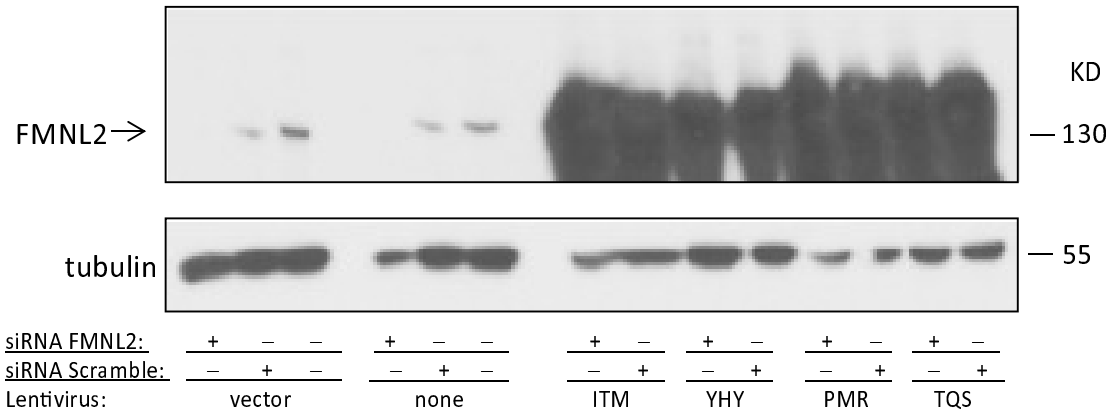

Figure 5.1: FMNL2 expression levels in A375 melanoma cells after knockdown, rescue and overexpression. A375 cells were treated with siRNA FMNL2 or siRNA scramble followed by an infection with FMNL2 isoform specific lentiviral expression vectors or empty lentiviral expression vector. Note that these cells were split and seeded for the immunofluorescence assay described at section 3.6 as well as the invasion assay described at section 3.9. Cell lysates were subjected to SDS-PAGE and immunoblotted to detect FMNL2 expression levels with a rabbit anti-FMNL2 specific antibody.

Appendix 3

Table 5.2: FMNL2 isoform derivative constructs generated for our collaborator (Dr. Higgs).

Construct	Tag	Restriction sites
FMNL2 ITM FH1FH2 pGEX6pt NBRSS	GST + TEV	Sal1-Not1
FMNL2 YHY FH1FH2 pGEX6pt NBRSS	GST + TEV	Sal1-Not1
FMNL2 PMR FH1FH2 pGEX6pt NBRSS	GST + TEV	Sal1-Not1
FMNL2 TQS FH1FH2 pGEX6pt NBRSS	GST + TEV	Sal1-Not1
FMNL2 ITM FH2 pGEX6pt NBRSS	GST + TEV	Nco1-Sal1
FMNL2 YHY FH2 pGEX6pt NBRSS	GST + TEV	Nco1-Sal1
FMNL2 PMR FH2 pGEX6pt NBRSS	GST + TEV	Nco1-Sal1
FMNL2 TQS FH2 pGEX6pt NBRSS	GST + TEV	Nco1-Sal1
FMNL2 ITM + cys WH2 DAD pGEX6pt NBRSS	GST + TEV	Nco1-Sal1
FMNL2 YHY + cys WH2 DAD pGEX6pt NBRSS	GST + TEV	Nco1-Sal1
FMNL2 PMR + cys WH2 DAD pGEX6pt NBRSS	GST + TEV	Nco1-Sal1
FMNL2 TQS + cys WH2 DAD pGEX6pt NBRSS	GST + TEV	Nco1-Sal1

References

Bachmann, C., Fischer, L., Walter, U., and Reinhard, M. 1999. The EVH2 Domain of the Vasodilator-stimulated Phosphoprotein Mediates Tetramerization, F-actin Binding, and Actin Bundle Formation. *Journal of Biological Chemistry*, *274:* 23549–23557

Bächner, D., Sedlacek, Z., Korn, B., Hameister, H., and Poustka, A. 1995. Expression patterns of two human genes coding for different rab GDP-dissociation inhibitors (GDIs), extremely conserved proteins involved in cellular transport. *Human Molecular Genetics 4*: 701–708

Bartolini, F., and Gundersen, G. G. 2010. Formins and microtubules. *Molecular Cell Research*, *1803:* 164–173

Bartolini, Francesca, Moseley, J. B., Schmoranzer, J., Cassimeris, L., Goode, B. L. and Gundersen, G. G. 2008. The formin mDia2 stabilizes microtubules independently of its actin nucleation activity. *The Journal of Cell Biology*, *181:* 523–536

Blanchoin, L. and Boujemaa-Paterski, R. 2009. Inhibitors Target Actin Nucleators. *Chemistry and Biology*, *16:* 1125–1126

Block, J., Breitsprecher, D., Kühn, S., Winterhoff, M., Kage, F., Geffers, R., Rottner, K. 2012. FMNL2 Drives Actin-Based Protrusion and Migration Downstream of Cdc42. *Current Biology*, *22:* 1005–1012

Bloodgood, R. A. 2010. Sensory reception is an attribute of both primary cilia and motile cilia. *Journal of Cell Science*, *123:* 505–509

Bonaventure, J., Domingues, M. J. and Larue, L. 2013. Cellular and molecular mechanisms controlling the migration of melanocytes and melanoma cells. *Pigment Cell and Melanoma Research*, *26*: 316–325

Bravo-Cordero, J. J., Hodgson, L. and Condeelis, J. 2012. Directed cell invasion and migration during metastasis. *Current Opinion in Cell Biology*, *24*: 277–283

Breitsprecher, D., Kiesewetter, A. K., Linkner, J., Urbanke, C., Resch, G. P., Small, J. V. and Faix, J. 2008. Clustering of VASP actively drives processive, WH2 domain-mediated actin filament elongation. *The EMBO Journal*, *27*: 2943–2954

Buccione, R., Caldieri, G. and Ayala, I. 2009. Invadopodia: specialized tumor cell structures for the focal degradation of the extracellular matrix. *Cancer and Metastasis Reviews*, *28*: 137–149

Bussell, K. 2005. Inspired filaments. *Nature Reviews Molecular Cell Biology*, *6*: 92–92

Campellone, K. G. and Welch, M. D. 2010. A nucleator arms race: cellular control of actin assembly. *Nature Reviews Molecular Cell Biology*, *11*: 237–251

Chan, D. C., Bedford, M. T. and Leder, P. 1996. Formin binding proteins bear WWP/WW domains that bind proline-rich peptides and functionally resemble SH3 domains. *The EMBO Journal*, *15*: 1045–1054

Charras, G. and Paluch, E. 2008. Blebs lead the way: how to migrate without lamellipodia. *Nature Reviews Molecular Cell Biology*, *9*: 730–736

Charras, G. t. 2008. A short history of blebbing. *Journal of Microscopy*, *231*: 466–478

Chen, Z., Borek, D., Padrick, S. B., Gomez, T. S., Metlagel, Z., Ismail, A. M, Rosen, M. K. 2010. Structure and control of the actin regulatory WAVE complex. *Nature*, *468*: 533–538

Chesarone, M. A., DuPage, A. G. and Goode, B. L. 2010. Unleashing formins to remodel the actin and microtubule cytoskeletons. *Nature Reviews Molecular Cell Biology*, *11:* 62–74

Copeland, J. W., Copeland, S. J. and Treisman, R. 2004. Homo-oligomerization Is Essential for F-actin Assembly by the Formin Family FH2 Domain. *Journal of Biological Chemistry*, *279*: 50250–50256

Copeland, J. W. and Treisman, R. 2002. The Diaphanous-related Formin mDia1 Controls Serum Response Factor Activity through its Effects on Actin Polymerization. *Molecular Biology of the Cell*, *13*: 4088–4099

Cunningham, C. C., Gorlin, J. B., Kwiatkowski, D. J., Hartwig, J. H., Janmey, P. A., Byers, H. R. and Stossel, T. P. 1992. Actin-binding protein requirement for cortical stability and efficient locomotion. *Science*, *255*: 325–327

Delorme, V., Machacek, M., DerMardirossian, C., Anderson, K. L., Wittmann, T., Hanein, D., Bokoch, G. M. 2007. Cofilin Activity Downstream of Pak1 Regulates Cell Protrusion Efficiency by Organizing Lamellipodium and Lamella Actin Networks. *Developmental Cell*, *13*: 646–662

Dentler, W. L. 1981. Microtubule-Membrane Interactions in Cilia and Flagella. *International Review of Cytology*, 72: 1–47

Desai, A. and Mitchison, T. J. 1997. Microtubule Polymerization Dynamics. *Annual Review of Cell and Developmental Biology*, *13*: 83–117

DeWard, A. D., Eisenmann, K. M., Matheson, S. F. and Alberts, A. S. 2010. The role of formins in human disease. *Molecular Cell Research*, *1803*: 226–233

Doherty, G. J. and McMahon, H. T. 2008. Mediation, Modulation and Consequences of Membrane-Cytoskeleton Interactions. *Annual Review of Biophysics*, *37*: 65–95

Esue, O., Harris, E. S., Higgs, H. N. and Wirtz, D. 2008. The Filamentous Actin Cross-Linking/Bundling Activity of Mammalian Formins. *Journal of Molecular Biology*, *384*: 324–334

Favaro, P. M. B., Traina, F., Vassallo, J., Brousset, P., Delsol, G., Costa, F. F. and Saad, S. T. O. 2006. High expression of FMNL1 protein in T non-Hodgkin's lymphomas. *Leukemia Research*, *30*: 735–738

Friedl, P. and Wolf, K. 2003. Tumour-cell invasion and migration: diversity and escape mechanisms. *Nature Reviews Cancer*, *3*: 362–374

Gauvin, T. J., Fukui, J., Peterson, J. R. and Higgs, H. N. 2009. Isoform-Selective Chemical Inhibition of mDia-Mediated Actin Assembly. *Biochemistry*, *48*: 9327–9329

Gettemans, J., Van Impe, K., Delanote, V., Hubert, T., Vandekerckhove, J. and De Corte, V. 2005. Nuclear Actin-Binding Proteins as Modulators of Gene Transcription. *Traffic*, *6*: 847–857

Goicoechea, S. M., Bednarski, B., Stack, C., Cowan, D. W., Volmar, K., Thorne, L., Otey, C. A. 2010. Isoform-Specific Upregulation of Palladin in Human and Murine Pancreas Tumors. *PLoS ONE, 5:* 10347

Goldschmidt-Clermont, P. J., Furman, M. I., Wachsstock, D., Safer, D., Nachmias, V. T. and Pollard, T. D. 1992. The control of actin nucleotide exchange by thymosin beta 4 and profilin. A potential regulatory mechanism for actin polymerization in cells. *Molecular Biology of the Cell*, *3*: 1015–1024

Goode, B. L. and Eck, M. J. 2007. Mechanism and Function of Formins in the Control of Actin Assembly. *Annual Review of Biochemistry*, *76*: 593–627

Gupton, S. L. and Gertler, F. B. 2007. Filopodia: The Fingers That Do the Walking. *Science Signaling*, 400: 5

Hager, M. H., Morley, S., Bielenberg, D. R., Gao, S., Morello, M., Holcomb, I. N., Freeman, M. R. 2012. DIAPH3 governs the cellular transition to the amoeboid tumour phenotype. *EMBO Molecular Medicine*, *4*: 743–760

Han, Y., Eppinger, E., Schuster, I. G., Weigand, L. U., Liang, X., Kremmer, E., Krackhardt, A. M. 2009. Formin-like 1 (FMNL1) Is Regulated by N-terminal Myristoylation and Induces Polarized Membrane Blebbing. *Journal of Biological Chemistry*, *284*: 33409–33417

Hanahan, D. and Weinberg, R. 2000. The Hallmarks of Cancer. *Cell*, *100*: 57–70

Hanahan, D. and Weinberg, R. A. 2011. Hallmarks of Cancer: The Next Generation. *Cell*, *144*: 646–674

Harris, E. S., Gauvin, T. J., Heimsath, E. G. and Higgs, H. N. 2010. Assembly of filopodia by the formin FRL2 (FMNL3). *Cytoskeleton*, *67*: 755–772

Harris, E. S., Li, F. and Higgs, H. N. 2004. The Mouse Formin, FRLα, Slows Actin Filament Barbed End Elongation, Competes with Capping Protein, Accelerates Polymerization

from Monomers, and Severs Filaments. *Journal of Biological Chemistry*, *279*: 20076–20087

Harris, E. S., Rouiller, I., Hanein, D. and Higgs, H. N. 2006. Mechanistic Differences in Actin Bundling Activity of Two Mammalian Formins, FRL1 and mDia2. *Journal of Biological Chemistry*, *281*: 14383–14392

Heimsath, E. G. and Higgs, H. N. 2012. The C Terminus of Formin FMNL3 Accelerates Actin Polymerization and Contains a WH2 Domain-like Sequence That Binds Both Monomers and Filament Barbed Ends. *Journal of Biological Chemistry*, *287*: 3087–3098

Higgs, H. N. 2005. Formin proteins: a domain-based approach. *Trends in Biochemical Sciences*, *30*: 342–353

Ishikawa, R., Sakamoto, T., Ando, T., Higashi-Fujime, S. and Kohama, K. 2003. Polarized actin bundles formed by human fascin-1: their sliding and disassembly on myosin II and myosin V in vitro. *Journal of Neurochemistry*, *87*: 676–685

Ishizaki, T., Morishima, Y., Okamoto, M., Furuyashiki, T., Kato, T. and Narumiya, S. 2001. Coordination of microtubules and the actin cytoskeleton by the Rho effector mDia1. *Nature Cell Biology*, *3*: 8–14

Katoh, K., Kano, Y., Amano, M., Onishi, H., Kaibuchi, K. and Fujiwara, K. 2001. Rho-Kinase–Mediated Contraction of Isolated Stress Fibers. *The Journal of Cell Biology*, *153*: 569–584

Katoh, M. and Katoh, M. 2003. Identification and characterization of human FMNL1, FMNL2 and FMNL3 genes in silico. *International journal of oncology*, *22*: 1161–1168

Kitzing, T. M., Wang, Y., Pertz, O., Copeland, J. W. and Grosse, R. 2010. Formin-like 2 drives amoeboid invasive cell motility downstream of RhoC. *Oncogene*, *29*: 2441–2448

Kitzing, Thomas M., Sahadevan, A. S., Brandt, D. T., Knieling, H., Hannemann, S., Fackler, O. T., Grosse, R. 2007. Positive feedback between Dia1, LARG and RhoA regulates cell morphology and invasion. *Genes and Development*, *21*: 1478–1483

Korn, E. D., Carlier, M. F. and Pantaloni, D. 1987. Actin polymerization and ATP hydrolysis. *Science*, *238*: 638–644

Kovar, D. R. 2006. Molecular details of formin-mediated actin assembly. *Current Opinion in Cell Biology*, *18*: 11–17

Kovar, D. R., Harris, E. S., Mahaffy, R., Higgs, H. N. and Pollard, T. D. 2006. Control of the Assembly of ATP- and ADP-Actin by Formins and Profilin. *Cell*, *124:* 423–435

Kovar, D. R. and Pollard, T. D. 2004. Progressing actin: Formin as a processive elongation machine. *Nature Cell Biology*, *6*: 1158–1159

Krause, M., Dent, E. W., Bear, J. E., Loureiro, J. J. and Gertler, F. B. 2003. ENA/VASP PROTEINS: Regulators of the Actin Cytoskeleton and Cell Migration. *Annual Review of Cell and Developmental Biology*, *19*: 541–564

Lämmermann, T. and Sixt, M. 2009. Mechanical modes of "amoeboid" cell migration. *Current Opinion in Cell Biology*, *21*: 636–644

Lazarides, E. and Burridge, K. 1975. α-Actinin: Immunofluorescent localization of a muscle structural protein in nonmuscle cells. *Cell*, *6*: 289–298

Leibovitz, A., Stinson, J. C., McCombs, W. B., McCoy, C. E., Mazur, K. C. and Mabry, N. D. 1976. Classification of Human Colorectal Adenocarcinoma Cell Lines. *Cancer Research*, *36*: 4562–4569

Leung, D. W. and Rosen, M. K. 2005. The nucleotide switch in Cdc42 modulates coupling between the GTPase-binding and allosteric equilibria of Wiskott–Aldrich syndrome protein. *Proceedings of the National Academy of Sciences of the United States of America*, *102*: 5685–5690

Li, A., Ma, Y., Yu, X., Mort, R. L., Lindsay, C. R., Stevenson, D., Machesky, L. M. 2011. Rac1 Drives Melanoblast Organization during Mouse Development by Orchestrating Pseudopod- Driven Motility and Cell-Cycle Progression. *Developmental Cell*, *21*: 722–734

Li, F. and Higgs, H. N. 2003. The Mouse Formin mDia1 Is a Potent Actin Nucleation Factor Regulated by Autoinhibition. *Current Biology*, *13*: 1335–1340

Li, Y., Zhu, X., Zeng, Y., Wang, J., Zhang, X., Ding, Y. and Liang, L. 2010. FMNL2 Enhances Invasion of Colorectal Carcinoma by Inducing Epithelial-Mesenchymal Transition. *Molecular Cancer Research*, *8*: 1579–1590

Liang, L., Guan, J., Zeng, Y., Wang, J., Li, X., Zhang, X. and Ding, Y. (2011). Down-regulation of formin-like 2 predicts poor prognosis in hepatocellular carcinoma. *Human Pathology*, *42*(11), 1603–1612. doi:10.1016/j.humpath.2010.08.025

Lizárraga, F., Poincloux, R., Romao, M., Montagnac, G., Dez, G. L., Bonne, I., Chavrier, P. 2009. Diaphanous-Related Formins Are Required for Invadopodia Formation and Invasion of Breast Tumor Cells. *Cancer Research*, *69*: 2792–2800

Machesky, L. M. and Li, A. 2010. Fascin. *Communicative and Integrative Biology*, *3*: 263–270

Maekawa, M., Ishizaki, T., Boku, S., Watanabe, N., Fujita, A., Iwamatsu, A., Narumiya, S. 1999. Signaling from Rho to the Actin Cytoskeleton Through Protein Kinases ROCK and LIM-kinase. *Science*, *285*: 895–898

Mallavarapu, A. and Mitchison, T. 1999. Regulated Actin Cytoskeleton Assembly at Filopodium Tips Controls Their Extension and Retraction. *The Journal of Cell Biology*, *146*: 1097–1106

Matsudaira, P. 1994. Actin crosslinking proteins at the leading edge. *Seminars in Cell Biology*, *5*: 165–174

Matsudalra, P. 1991. Modular organization of actin crosslinking proteins. *Trends in Biochemical Sciences*, *16*: 87–92

McGough, A., Pope, B., Chiu, W. and Weeds, A. 1997. Cofilin Changes the Twist of F-Actin: Implications for Actin Filament Dynamics and Cellular Function. *The Journal of Cell Biology*, *138*: 771–781

Mejillano, M. R., Kojima, S., Applewhite, D. A., Gertler, F. B., Svitkina, T. M. and Borisy, G. G. 2004. Lamellipodial Versus Filopodial Mode of the Actin Nanomachinery: Pivotal Role of the Filament Barbed End. *Cell*, *118*: 363–373

Mellor, H. 2010. The role of formins in filopodia formation. *Biochimica et Biophysica Acta (BBA) - Molecular Cell Research*, *1803*: 191–200

Michelot, A., Guérin, C., Huang, S., Ingouff, M., Richard, S., Rodiuc, N., Blanchoin, L. 2005. The Formin Homology 1 Domain Modulates the Actin Nucleation and Bundling Activity of Arabidopsis FORMIN1. *The Plant Cell Online*, *17*: 2296–2313

Miyoshi, J. and Yoshimi, T. 2008. Structural and Functional Associations of Apical Junctions with Cytoskeleton. Biochimica Et Biophysica Acta (BBA) - *Biomembranes*, 1778: 670–691

Moriya, K., Yamamoto, T., Takamitsu, E., Matsunaga, Y., Kimoto, M., Fukushige, D., Utsumi, T. 2012. Protein N-Myristoylation Is Required for Cellular Morphological Changes Induced by Two Formin Family Proteins, FMNL2 and FMNL3. *Bioscience, Biotechnology, and Biochemistry*, *76*: 1201–1209.

Moseley, J. B., Sagot, I., Manning, A. L., Xu, Y., Eck, M. J., Pellman, D. and Goode, B. L. 2004. A Conserved Mechanism for Bni1- and mDia1-induced Actin Assembly and Dual Regulation of Bni1 by Bud6 and Profilin. *Molecular Biology of the Cell*, *15*: 896–907

Neuhaus, J.-M., Wanger, M., Keiser, T. and Wegner, A. 1983. Treadmilling of actin. *Journal of Muscle Research and Cell Motility*, *4*: 507–527

Nobes, C. D. and Hall, A. 1995. Rho, Rac, and Cdc42 GTPases regulate the assembly of multimolecular focal complexes associated with actin stress fibers, lamellipodia, and filopodia. *Cell*, *81*: 53–62

Nürnberg, A., Kitzing, T. and Grosse, R. 2011. Nucleating actin for invasion. *Nature Reviews Cancer*, *11*: 177–187

Olson, M. F. and Sahai, E. 2009. The actin cytoskeleton in cancer cell motility. *Clinical and Experimental Metastasis*, *26*: 273–287

Otomo, T., Tomchick, D. R., Otomo, C., Panchal, S. C., Machius, M. and Rosen, M. K. 2005. Structural basis of actin filament nucleation and processive capping by a formin homology 2 domain. *Nature*, *433*: 488–494

Otto, J. J. 1994. Actin-bundling proteins. *Current Opinion in Cell Biology*, *6*: 105–109

Paavilainen, V. O., Bertling, E., Falck, S. and Lappalainen, P. 2004. Regulation of cytoskeletal dynamics by actin-monomer-binding proteins. *Trends in Cell Biology*, *14*: 386–394

Palazzo, A. F., Cook, T. A., Alberts, A. S. and Gundersen, G. G. 2001. mDia mediates Rho-regulated formation and orientation of stable microtubules. *Nature Cell Biology*, *3*: 723–729

Paluch, E., Piel, M., Prost, J., Bornens, M. and Sykes, C. 2005. Cortical Actomyosin Breakage Triggers Shape Oscillations in Cells and Cell Fragments. *Biophysical Journal*, *89:* 724–733

Parsons, D. W., Jones, S., Zhang, X., Lin, J. C.-H., Leary, R. J., Angenendt, P., Kinzler, K. W. 2008. An Integrated Genomic Analysis of Human Glioblastoma Multiforme. *Science*, *321*: 1807–1812

Paul, A. and Pollard, T. 2008. The Role of the FH1 Domain and Profilin in Formin-Mediated Actin-Filament Elongation and Nucleation. *Current Biology*, *18*: 9–19

Paul, A. S. and Pollard, T. D. 2009. Review of the mechanism of processive actin filament elongation by formins. *Cell Motility and the Cytoskeleton*, *66*: 606–617

Pellegrin, S. and Mellor, H. 2005. The Rho Family GTPase Rif Induces Filopodia through mDia2. *Current Biology*, *15*: 129–133

Petrie, R. J. and Yamada, K. M. 2012. At the leading edge of three-dimensional cell migration. *Journal of Cell Science*, *125*: 5917–5926

Philippar, U., Roussos, E. T., Oser, M., Yamaguchi, H., Kim, H.-D., Giampieri, S., Gertler, F. B. 2008. A Mena Invasion Isoform Potentiates EGF-Induced Carcinoma Cell Invasion and Metastasis. *Developmental Cell*, *15*: 813–828

Pollard, T. D. 1984. Polymerization of ADP-actin. *The Journal of Cell Biology*, *99*: 769–777

Pollard, Thomas D and Borisy, G. G. 2003. Cellular Motility Driven by Assembly and Disassembly of Actin Filaments. *Cell*, *112*: 453–465

Pring, M., Evangelista, M., Boone, C., Yang, C. and Zigmond, S. H. 2003. Mechanism of Formin-Induced Nucleation of Actin Filaments. *Biochemistry*, *42*: 486–496

Pruss, R. M., Mirsky, R., Raff, M. C., Thorpe, R., Dowding, A. J. and Anderton, B. H. 1981. All classes of intermediate filaments share a common antigenic determinant defined by a monoclonal antibody. *Cell*, *27*: 419–428

Pruyne, D., Evangelista, M., Yang, C., Bi, E., Zigmond, S., Bretscher, A. and Boone, C. 2002. Role of Formins in Actin Assembly: Nucleation and Barbed-End Association. *Science*, *297*: 612–615

Pudas, R., Kiema, T.-R., Butler, P. J. G., Stewart, M. and Ylänne, J. 2005. Structural Basis for Vertebrate Filamin Dimerization. *Structure*, *13*: 111–119

Reed, N. A., Cai, D., Blasius, T. L., Jih, G. T., Meyhofer, E., Gaertig, J. and Verhey, K. J. 2006. Microtubule Acetylation Promotes Kinesin-1 Binding and Transport. *Current Biology*, *16*: 2166–2172

Rheenen, J. van, Condeelis, J. and Glogauer, M. 2009. A common cofilin activity cycle in invasive tumor cells and inflammatory cells. *Journal of Cell Science*, *122*: 305–311

Ridley, A. J. 2011. Life at the Leading Edge. *Cell*, *145*: 1012–1022

Ridley, A. J., Schwartz, M. A., Burridge, K., Firtel, R. A., Ginsberg, M. H., Borisy, G., Horwitz, A. R. 2003. Cell Migration: Integrating Signals from Front to Back. *Science*, *302*: 1704–1709

Rodal, A. A., Sokolova, O., Robins, D. B., Daugherty, K. M., Hippenmeyer, S., Riezman, H., Goode, B. L. 2005. Conformational changes in the Arp2/3 complex leading to actin nucleation. *Nature Structural and Molecular Biology*, *12*: 26–31

Rosales-Nieves, A. E., Johndrow, J. E., Keller, L. C., Magie, C. R., Pinto-Santini, D. M. and Parkhurst, S. M. 2006. Coordination of microtubule and microfilament dynamics by Drosophila Rho1, Spire and Cappuccino. *Nature Cell Biology*, *8*: 367–376

Rottner, K., Behrendt, B., Small, J. V. and Wehland, J. 1999. VASP dynamics during lamellipodia protrusion. *Nature Cell Biology*, *1*: 321–322

Russell, R. J., Xia, S.-L., Dickinson, R. B. and Lele, T. P. 2009. Sarcomere Mechanics in Capillary Endothelial Cells. *Biophysical Journal*, *97*: 1578–1585

Sahai, E. and Marshall, C. J. 2002a. RHO–GTPases and cancer. *Nature Reviews Cancer*, *2*: 133–142

Sahai, E. and Marshall, C. J. 2002b. ROCK and Dia have opposing effects on adherens junctions downstream of Rho. *Nature Cell Biology*, *4*: 408–415

Sahai, E. and Marshall, C. J. 2003. Differing modes of tumour cell invasion have distinct requirements for Rho/ROCK signalling and extracellular proteolysis. *Nature Cell Biology*, *5*: 711–719

Schoumacher, M., Goldman, R. D., Louvard, D. and Vignjevic, D. M. 2010. Actin, microtubules, and vimentin intermediate filaments cooperate for elongation of invadopodia. *The Journal of Cell Biology*, *189*: 541–556

Schulze, E. and Kirschner, M. 1987. Dynamic and stable populations of microtubules in cells. *The Journal of Cell Biology*, *104*: 277–288

Scott, G. 2002. Rac and Rho: The Story Behind Melanocyte Dendrite Formation. *Pigment Cell Research*, *15*: 322–330

Small, J. V., Stradal, T., Vignal, E. and Rottner, K. 2002. The lamellipodium: where motility begins. *Trends in Cell Biology*, *12*: 112–120

Sotiropoulos, A., Gineitis, D., Copeland, J. and Treisman, R. 1999. Signal-Regulated Activation of Serum Response Factor Is Mediated by Changes in Actin Dynamics. *Cell*, *98*: 159–169

Staiger, C. J. and Blanchoin, L. 2006. Actin dynamics: old friends with new stories. *Current Opinion in Plant Biology*, *9*: 554–562

Takenawa, T. and Suetsugu, S. (2007). The WASP–WAVE protein network: connecting the membrane to the cytoskeleton. *Nature Reviews Molecular Cell Biology*, *8*: 37–48

Tanji, M., Ishizaki, T., Ebrahimi, S., Tsuboguchi, Y., Sukezane, T., Akagi, T., Narumiya, S. 2010. mDia1 Targets v-Src to the Cell Periphery and Facilitates Cell Transformation, Tumorigenesis, and Invasion. *Molecular and Cellular Biology*, *30*: 4604–4615

Thiery, J. P., Acloque, H., Huang, R. Y. J. and Nieto, M. A. 2009. Epithelial-Mesenchymal Transitions in Development and Disease. *Cell*, *139*: 871–890

Thompson, M. E., Heimsath, E. G., Gauvin, T. J., Higgs, H. N. and Kull, F. J. 2013. FMNL3 FH2–actin structure gives insight into formin-mediated actin nucleation and elongation. *Nature Structural and Molecular Biology*, *20*: 111–118

Thurston, S. F., Kulacz, W. A., Shaikh, S., Lee, J. M. and Copeland, J. W. 2012. The Ability to Induce Microtubule Acetylation Is a General Feature of Formin Proteins. *PLoS ONE*, *7*: 48041

Toivola, D. M., Tao, G.-Z., Habtezion, A., Liao, J. and Omary, M. B. 2005. Cellular integrity plus: organelle-related and protein-targeting functions of intermediate filaments. *Trends in Cell Biology*, *15*: 608–617

Vaillant, D. C., Copeland, S. J., Davis, C., Thurston, S. F., Abdennur, N. and Copeland, J. W. 2008. Interaction of the N- and C-terminal Autoregulatory Domains of FRL2 Does Not Inhibit FRL2 Activity. *Journal of Biological Chemistry*, *283*: 33750–33762

Valastyan, S. and Weinberg, R. A. 2011. Tumor Metastasis: Molecular Insights and Evolving Paradigms. *Cell*, *147*: 275–292

Vega, F. M., Fruhwirth, G., Ng, T. and Ridley, A. J. 2011. RhoA and RhoC have distinct roles in migration and invasion by acting through different targets. *The Journal of Cell Biology*, *193*: 655–665

Vignjevic, D., Kojima, S., Aratyn, Y., Danciu, O., Svitkina, T. and Borisy, G. G. 2006. Role of fascin in filopodial protrusion. *The Journal of Cell Biology*, *174*: 863–875

Wallar, B. J., Stropich, B. N., Schoenherr, J. A., Holman, H. A., Kitchen, S. M. and Alberts, A. S. 2006. The Basic Region of the Diaphanous-autoregulatory Domain (DAD) Is Required for Autoregulatory Interactions with the Diaphanous-related Formin Inhibitory Domain. *Journal of Biological Chemistry*, *281:* 4300–4307

Watanabe, N., Kato, T., Fujita, A., Ishizaki, T. and Narumiya, S. 1999. Cooperation between mDia1 and ROCK in Rho-induced actin reorganization. *Nature Cell Biology*, *1*: 136–143

Watanabe, T., Noritake, J. and Kaibuchi, K. 2005. Regulation of microtubules in cell migration. *Trends in Cell Biology*, *15*: 76–83

Weaver, A. M. 2006. Invadopodia: Specialized Cell Structures for Cancer Invasion. *Clinical and Experimental Metastasis*, *23*: 97–105

Wheeler, A. P. and Ridley, A. J. 2004. Why three Rho proteins? RhoA, RhoB, RhoC, and cell motility. *Experimental Cell Research*, *301*: 43–49

Wolf, K., Mazo, I., Leung, H., Engelke, K., Andrian, U. H. von, Deryugina, E. I., Friedl, P. 2003. Compensation mechanism in tumor cell migration mesenchymal–amoeboid transition after blocking of pericellular proteolysis. *The Journal of Cell Biology*, *160*: 267–277

Wyckoff, J. B., Pinner, S. E., Gschmeissner, S., Condeelis, J. S. and Sahai, E. 2006. ROCK- and Myosin-Dependent Matrix Deformation Enables Protease-Independent Tumor-Cell Invasion In Vivo. *Current Biology*, *16*: 1515–1523

Xu, Y., Moseley, J. B., Sagot, I., Poy, F., Pellman, D., Goode, B. L. and Eck, M. J. 2004. Crystal Structures of a Formin Homology-2 Domain Reveal a Tethered Dimer Architecture. *Cell*, *116*: 711–723

Yamashita, A., Maeda, K. and Maéda, Y. 2003. Crystal structure of CapZ: structural basis for actin filament barbed end capping. *The EMBO Journal*, *22*: 1529–1538

Zaman, M. H., Trapani, L. M., Sieminski, A. L., MacKellar, D., Gong, H., Kamm, R. D., Matsudaira, P. 2006. Migration of tumor cells in 3D matrices is governed by matrix stiffness along with cell-matrix adhesion and proteolysis. *Proceedings of the National Academy of Sciences*, *103*: 10889–10894

Zhu, X., Zeng, Y., Guan, J., Li, Y., Deng, Y., Bian, X., Liang, L. 2011. FMNL2 is a positive regulator of cell motility and metastasis in colorectal carcinoma. *The Journal of Pathology*, *224*: 377–388

Zhu, X.-L., Liang, L. and Ding, Y.-Q. 2008. Overexpression of FMNL2 is closely related to metastasis of colorectal cancer. *International Journal of Colorectal Disease*, *23*: 1041–1047

Zigmond, S. H. 2004. Formin-induced nucleation of actin filaments. *Current Opinion in Cell Biology*, *16*: 99–105

Zigmond, S. H., Evangelista, M., Boone, C., Yang, C., Dar, A. C., Sicheri, F., Pring, M. 2003. Formin Leaky Cap Allows Elongation in the Presence of Tight Capping Proteins. *Current Biology*, *13*: 1820–1823